Title
Metabolite Signaling Mediates Cellular Homeostasis and Proliferation

Author
Krall, Abigail

Publication Date
2018

Peer reviewed|Thesis/dissertation

UNIVERSITY OF CALIFORNIA

Los Angeles

Metabolite Signaling Mediates Cellular Homeostasis and Proliferation

A dissertation submitted in partial satisfaction of the

requirements for the degree Doctor of Philosophy

in Molecular and Medical Pharmacology

by

Abigail Sarah Krall

2018

ABSTRACT OF THE DISSERTATION

Metabolite Signaling Mediates Cellular Homeostasis and Proliferation

by

Abigail Sarah Krall

Doctor of Philosophy in Molecular and Medical Pharmacology

University of California, Los Angeles, 2018

Professor Heather R. Christofk, Chair

Nutrients and metabolites can both positively and negatively regulate cell signaling and anabolic metabolism. These signaling properties suggest that metabolites can influence both proliferation and cellular homeostasis. Here we describe a role for asparagine as an amino acid exchange factor: intracellular asparagine exchanges with extracellular amino acids. We show that intracellular asparagine levels regulate uptake of amino acids, especially serine, arginine, and histidine. Through its exchange factor role, asparagine promotes mTORC1 activity and downstream anabolic metabolism. In addition, we show that asparagine depletion may be sensed through intracellular lactate accumulation. Asparagine depletion impairs trafficking of lactate transporters MCT1 and MCT4 to decrease lactate export. We also provide evidence that lactate binds to and stabilizes ATF4, the transcription factor responsible for asparagine synthetase expression, suggesting that lactate, as a signal of asparagine depletion, is sensed by ATF4 to restore intracellular asparagine. In addition to stimulating ATF4 activity and ASNS expression, we find that lactate inhibits mTORC1 activity in an ATF4-dependent manner. Given

the role of asparagine in amino acid uptake, our data suggest that lactate may be a novel signal to communicate amino acid deficiency to mTORC1. We propose that the cell coordinates anabolism with nutrient availability by linking ATF4 transcriptional activity to mTORC1 inhibition, such that lactate-induced mTORC1 inhibition upon asparagine depletion coincides with ATF4-mediated asparagine regeneration and is relieved upon asparagine restoration. Finally, we hypothesize that lactate signaling may explain why lactate export is a cancer hallmark: cancer cell lactate export both relieves cell-autonomous restrictions on mTORC1-mediated anabolism and enables exploitation of the tumor microenvironment through tumor-generated paracrine lactate signaling.

The dissertation of Abigail Sarah Krall is approved.

Steven J. Bensinger

Thomas G. Graeber

Luisa M. Iruela-Arispe

Owen N. Witte

Heather R. Christofk, Committee Chair

University of California, Los Angeles

2018

Table of Contents

Figures and Tables

Chapter 2

Acknowledgements

Many remarkable individuals contributed to the work presented in this dissertation as well as to my graduate school experience. First, I would like to thank the members of the Christofk lab, past and present, for the helpful scientific discussions, teamwork, and friendship. I feel very fortunate to have worked with such a wonderful group of people.

I would also like thank Shivani Thaker and BJ Sullivan, who have given me continuous support and friendship throughout the years. This experience would not have been the same without them.

I would like to acknowledge and thank Jing Huang and Brett Lomenick. Their thoughtful discussions, advice, and collaboration contributed immensely to the work presented in this dissertation.

To the members of my thesis committee, including Steve Bensinger, Tom Graeber, Luisa Iruela-Arispe, and Owen Witte: thank you for the advice, guidance, and support. I feel honored to have had the opportunity to learn from each of you.

I would like to thank my parents, Michael and Shelley, and my brothers, Jake and Jordan, for the endless support and love, and for being my best friends. I am very grateful.

Lastly, I would like to thank my advisor and mentor, Heather Christofk. Heather's enthusiasm for scientific discovery is contagious and inspiring. She has helped me develop both scientifically and personally. All of the work presented in this dissertation is a result of Heather's

advice, support, and encouragement. It has been an honor to be a member of her laboratory, and I will always be thankful for the opportunity and the experience.

The research presented in this dissertation was performed under the direction of Dr. Heather R. Christofk and was supported by the UCLA Graduate Division Dissertation Year Fellowship awarded to A.S.K.

Chapter 2 is a version of

Krall AS, Xu S, Graeber TG, Braas D, Christofk HR. Asparagine promotes cancer cell proliferation through use as an amino acid exchange factor. *Nat Commun.* 2016 Apr 29;7:11457.

Vita

Education

2007 B.S. Molecular, Cell, and Developmental Biology
University of California, Los Angeles

Publications

1. Flores A, Schell J, **Krall AS**, Jelinek D, Miranda M, Grigorian M, Braas D, White AC, Zhou JL, Graham NA, Graeber T, Seth P, Evseenko D, Coller HA, Rutter J, Christofk HR, Lowry WE. Lactate dehydrogenase activity drives hair follicle stem cell activation. *Nat Cell Biol*. 2017 Sep;19(9):1017-1026.

2. **Krall AS**, Christofk HR. Cell cycle: Division enzyme regulates metabolism. *Nature.* 2017 Jun 15;546(7658):357-358.

3. **Krall AS**, Xu S, Graeber TG, Braas D, Christofk HR. Asparagine promotes cancer cell proliferation through use as an amino acid exchange factor. *Nat Commun.* 2016 Apr 29;7:11457.

4. **Krall AS**, Christofk HR. Rethinking glutamine addiction. *Nat Cell Bio*. 2015. 17(12):1515-7.

5. Domigan CK, Warren CM, Antanesian V, Happel K, Ziyad S, Lee S, **Krall A**, Duan L, Torres-Collado AX, Castellani LW, Elashoff D, Christofk HR, van der Bliek AM, Potente M, Iruela-Arispe ML. *J Cell Sci*. 2015. 128(12):2236-48.

6. Chin RM, Fu X, Pai MY, Vergnes L, Hwang H, Deng G, Diep S, Lomenick B, Meli VS, Monsalve GC, Hu E, Whelan SA, Wang JX, Jung G, Solis GM, Fazlollahi F, Kaweeteerawat C, Quach A, Nili M, **Krall AS**, Godwin HA, Chang HR, Faull KF, Guo F, Jiang M, Trauger SA, Saghatelian A, Braas D, Christofk HR, Clarke CF, Teitell MA, Petrascheck M, Reue K, Jung ME, Frand AR, Huang J. The metabolite α-ketoglutarate extends lifespan by inhibiting ATP synthase and TOR. *Nature*. 2014. 510(7505):397-401.

7. **Krall AS** and Christofk HR. Cancer: A metabolic metamorphosis. *Nature*. 2013. 496(7443):38-40.

8. Vogelauer M*, **Krall AS***, McBrian MA, Li JY., Kurdistani SK. Stimulation of histone deacetylase activity by metabolites of intermediary metabolism. *J. Biol. Chem*. 2012. 287(38):32006-16.
*Authors contributed equally.

Chapter 1

Introduction: Cell signaling, Metabolism, and Cancer

The work in this dissertation will examine the intersection between cell signaling and metabolism – particularly how cellular metabolic status contributes to cell behaviors, including quiescence and proliferation. Below is a brief introduction to signaling-metabolism interconnection and metabolic requirements for cell proliferation. The chapter concludes by highlighting gaps in knowledge that will be addressed in the dissertation.

Most cancer cells exhibit increased glucose consumption and lactate secretion. Glycolysis is the central pathway of glucose metabolism. Through a series of reactions, glucose is converted to pyruvate. In most differentiated tissues, this pyruvate is oxidized in the mitochondria. Cancer cells, however, tend to increase glucose consumption and convert the majority of consumed glucose to lactate - despite the presence of oxygen and the option for more efficient ATP generation through pyruvate oxidation. Increased glucose consumption and lactate secretion is now considered a cancer hallmark and is known as the Warburg effect. Because glycolytic intermediates may be used as substrates for numerous biosynthetic pathways, such as the pentose phosphate and serine synthesis pathways(1), enhanced glucose uptake and flux through glycolysis supports the anabolism required for cell growth and division.

Glutamine and aspartate are limiting for cancer cell proliferation. In addition to increasing glucose metabolism, cancer cells also often exhibit high rates of glutamine consumption to support macromolecular biosynthesis(2). Glutamine fuels the TCA cycle through anaplerosis and contributes to the synthesis of lipids, nucleotides and non-essential amino acids. Although glutamine has been shown to be a prominent carbon source for the TCA cycle in cell culture experiments(2, 3), several lines of evidence suggest that glutamine anaplerosis is not essential for cell proliferation both *in vitro* and *in vivo*, as alternative carbon sources, such as pyruvate and acetate, can also serve as TCA cycle fuels(4-6). Rather, anaplerosis-independent glutamine functions may be limiting for proliferation(6). In addition, aspartate synthesis, which is

critical for nucleotide production, has recently been shown to be limiting for cancer cell growth and may underlie the dependence of proliferating cells on respiration(7, 8).

Cell signaling-metabolism interconnection

Metabolism and cell signaling are intricately interconnected. Cell signaling governs cell behavior by coordinating numerous cellular processes. Cell behavior - such as quiescence, proliferation, differentiation, or migration - depends on the cellular metabolic state. Regulation of metabolism by signaling pathways, therefore, is a way to achieve the appropriate metabolic state to support the intended cell behavior. For example, constitutively-active oncogenic kinases activate both nutrient uptake and metabolism that fuel cell growth(2, 9-12), including aerobic glycolysis and glutamine metabolism, as described above.

Conversely, regulation of signaling pathways by metabolites enables the cell to sense the current metabolic state and adjust cell behavior accordingly. For instance, it enables cells to coordinate anabolism and proliferation with nutrient availability, ensuring that the cell initiates anabolic processes only when resources are abundant. Metabolite sensing by signaling pathways is also critical for cellular homeostasis, both to ensure that the cell limits anabolism to what is needed to sustain basic cellular function and to replenish depleted nutrients.

Cellular metabolic status is sensed by mTOR complex 1 (mTORC1) and activating transcription factor 4 (ATF4). mTORC1 and ATF4, both of which sense intracellular amino acid levels, are the most well-characterized cellular nutrient sensors. mTORC1 is a master metabolic regulator: its activation promotes numerous anabolic processes, including mRNA translation, nucleotide synthesis, and lipid synthesis(13). The complex is activated at the lysosomal membrane by Rheb, downstream of growth factor signaling(14). Amino acids are sensed through direct interactions with signaling components that recruit mTORC1 to the

lysosomal surface(15-19), such that mTORC1 is unable to co-localize with Rheb when amino acids are limiting. The inability of mTORC1 to be activated in the absence of amino acids – despite active growth factor signaling – ensures that anabolism and growth are initiated only when nutrients are abundant.

Conversely, ATF4 transcriptional activity is activated in response to intracellular amino acid depletion. ATF4 is upregulated at the translational level in response to uncharged tRNA molecules. Activation leads to elevated transcription of amino acid transporters and amino acid synthesis enzymes, including asparagine synthetase (ASNS) and serine synthesis pathway enzymes. Amino acid sensing through the ATF4 pathway, therefore, enables amino acid replenishment during conditions of depletion.

Gaps in knowledge addressed by this dissertation

1. Cancer cell lactate export. The Warburg effect is characterized by increased glucose uptake and lactate export. It is now clear how increased glucose uptake supports elevated anabolic metabolism – by providing substrates for biosynthetic pathways. However, it remains unclear how increased lactate secretion impacts anabolic metabolism or cancer progression. Cancer cells export lactate despite the fact that lactate can be catabolized and provide carbons for anabolic metabolism(20, 21). Does intracellular lactate negatively impact cell growth? Does extracellular lactate support cancer cells exploitation of the tumor microenvironment?

2. Asparagine contribution to cancer cell growth. Numerous publications have demonstrated that glutamine and aspartate are limiting for cancer cell growth. Notably, both glutamine and aspartate are obligate substrates for ASNS reaction, raising the possibility that asparagine synthesis contributes to cancer cell glutamine and aspartate dependence. The importance of asparagine for tumor growth has been demonstrated by the effectiveness of

extracellular asparaginase in treating low-ASNS-expressing leukemia. However, the reasons behind cancer cell asparagine dependence are unclear – the only currently known function for asparagine is as a substrate for protein synthesis. Although ATF4 regulates expression of genes involved in multiple amino acid synthesis and transport pathways, asparagine alone rescues the impaired proliferation and autophagy resulting from ATF4 knockdown(22), suggesting that asparagine may globally impact intracellular amino acid levels.

3. Metabolite regulation of cell signaling. Research over the past two decades has focused on the regulation of cell metabolism by signaling pathways(2, 9-12). The reciprocal of this bi-directional relationship has received less attention. As demonstrated by amino acid regulation of mTORC1, metabolites can directly interact with components of cell signaling pathways to impact cellular activities(15-19). However, unlike protein-protein interactions, protein-metabolite interactions are often low-affinity and transient, making their detection difficult and their impact on cell behavior underappreciated.

The work presented in this dissertation identifies novel signaling functions for asparagine and lactate. We demonstrate a role for asparagine in cellular amino acid uptake, which influences anabolic metabolism downstream of mTORC1. We also provide evidence that lactate is a metabolic negative feedback signal that is sensed through direct binding to ATF4.

REFERENCES

1. Ward PS, Thompson CB. Metabolic reprogramming: a cancer hallmark even warburg did not anticipate. Cancer Cell. 2012;21(3):297-308. doi: 10.1016/j.ccr.2012.02.014. PubMed PMID: 22439925; PMCID: PMC3311998.

2. DeBerardinis RJ, Mancuso A, Daikhin E, Nissim I, Yudkoff M, Wehrli S, Thompson CB. Beyond aerobic glycolysis: transformed cells can engage in glutamine metabolism that exceeds the requirement for protein and nucleotide synthesis. Proc Natl Acad Sci U S A.

2007;104(49):19345-50. doi: 10.1073/pnas.0709747104. PubMed PMID: 18032601; PMCID: 2148292.

3. Wise DR, DeBerardinis RJ, Mancuso A, Sayed N, Zhang XY, Pfeiffer HK, Nissim I, Daikhin E, Yudkoff M, McMahon SB, Thompson CB. Myc regulates a transcriptional program that stimulates mitochondrial glutaminolysis and leads to glutamine addiction. Proc Natl Acad Sci U S A. 2008;105(48):18782-7. doi: 10.1073/pnas.0810199105. PubMed PMID: 19033189; PMCID: PMC2596212.

4. Mashimo T, Pichumani K, Vemireddy V, Hatanpaa KJ, Singh DK, Sirasanagandla S, Nannepaga S, Piccirillo SG, Kovacs Z, Foong C, Huang Z, Barnett S, Mickey BE, DeBerardinis RJ, Tu BP, Maher EA, Bachoo RM. Acetate is a bioenergetic substrate for human glioblastoma and brain metastases. Cell. 2014;159(7):1603-14. doi: 10.1016/j.cell.2014.11.025. PubMed PMID: 25525878; PMCID: PMC4374602.

5. Sellers K, Fox MP, Bousamra M, 2nd, Slone SP, Higashi RM, Miller DM, Wang Y, Yan J, Yuneva MO, Deshpande R, Lane AN, Fan TW. Pyruvate carboxylase is critical for non-small-cell lung cancer proliferation. J Clin Invest. 2015;125(2):687-98. doi: 10.1172/JCI72873. PubMed PMID: 25607840; PMCID: PMC4319441.

6. Tardito S, Oudin A, Ahmed SU, Fack F, Keunen O, Zheng L, Miletic H, Sakariassen PO, Weinstock A, Wagner A, Lindsay SL, Hock AK, Barnett SC, Ruppin E, Morkve SH, Lund-Johansen M, Chalmers AJ, Bjerkvig R, Niclou SP, Gottlieb E. Glutamine synthetase activity fuels nucleotide biosynthesis and supports growth of glutamine-restricted glioblastoma. Nat Cell Biol. 2015;17(12):1556-68. doi: 10.1038/ncb3272. PubMed PMID: 26595383; PMCID: PMC4663685.

7. Birsoy K, Wang T, Chen WW, Freinkman E, Abu-Remaileh M, Sabatini DM. An Essential Role of the Mitochondrial Electron Transport Chain in Cell Proliferation Is to Enable Aspartate Synthesis. Cell. 2015;162(3):540-51. doi: 10.1016/j.cell.2015.07.016. PubMed PMID: 26232224; PMCID: PMC4522279.

8. Sullivan LB, Gui DY, Hosios AM, Bush LN, Freinkman E, Vander Heiden MG. Supporting Aspartate Biosynthesis Is an Essential Function of Respiration in Proliferating Cells. Cell. 2015;162(3):552-63. doi: 10.1016/j.cell.2015.07.017. PubMed PMID: 26232225; PMCID: PMC4522278.

9. Elstrom RL, Bauer DE, Buzzai M, Karnauskas R, Harris MH, Plas DR, Zhuang H, Cinalli RM, Alavi A, Rudin CM, Thompson CB. Akt stimulates aerobic glycolysis in cancer cells. Cancer Res. 2004;64(11):3892-9. doi: 10.1158/0008-5472.CAN-03-2904. PubMed PMID: 15172999.

10. Guo D, Hildebrandt IJ, Prins RM, Soto H, Mazzotta MM, Dang J, Czernin J, Shyy JY, Watson AD, Phelps M, Radu CG, Cloughesy TF, Mischel PS. The AMPK agonist AICAR inhibits the growth of EGFRvIII-expressing glioblastomas by inhibiting lipogenesis. Proc Natl Acad Sci U S A.

2009;106(31):12932-7. doi: 10.1073/pnas.0906606106. PubMed PMID: 19625624; PMCID: PMC2714280.

11. Clarke JF, Young PW, Yonezawa K, Kasuga M, Holman GD. Inhibition of the translocation of GLUT1 and GLUT4 in 3T3-L1 cells by the phosphatidylinositol 3-kinase inhibitor, wortmannin. Biochem J. 1994;300 (Pt 3):631-5. PubMed PMID: 8010944; PMCID: PMC1138214.

12. Deprez J, Vertommen D, Alessi DR, Hue L, Rider MH. Phosphorylation and activation of heart 6-phosphofructo-2-kinase by protein kinase B and other protein kinases of the insulin signaling cascades. J Biol Chem. 1997;272(28):17269-75. PubMed PMID: 9211863.

13. Howell JJ, Ricoult SJ, Ben-Sahra I, Manning BD. A growing role for mTOR in promoting anabolic metabolism. Biochem Soc Trans. 2013;41(4):906-12. doi: 10.1042/BST20130041. PubMed PMID: 23863154.

14. Bar-Peled L, Schweitzer LD, Zoncu R, Sabatini DM. Ragulator is a GEF for the rag GTPases that signal amino acid levels to mTORC1. Cell. 2012;150(6):1196-208. doi: 10.1016/j.cell.2012.07.032. PubMed PMID: 22980980; PMCID: 3517996.

15. Chantranupong L, Scaria SM, Saxton RA, Gygi MP, Shen K, Wyant GA, Wang T, Harper JW, Gygi SP, Sabatini DM. The CASTOR Proteins Are Arginine Sensors for the mTORC1 Pathway. Cell. 2016;165(1):153-64. doi: 10.1016/j.cell.2016.02.035. PubMed PMID: 26972053; PMCID: PMC4808398.

16. Wang S, Tsun ZY, Wolfson RL, Shen K, Wyant GA, Plovanich ME, Yuan ED, Jones TD, Chantranupong L, Comb W, Wang T, Bar-Peled L, Zoncu R, Straub C, Kim C, Park J, Sabatini BL, Sabatini DM. Metabolism. Lysosomal amino acid transporter SLC38A9 signals arginine sufficiency to mTORC1. Science. 2015;347(6218):188-94. doi: 10.1126/science.1257132. PubMed PMID: 25567906; PMCID: PMC4295826.

17. Saxton RA, Chantranupong L, Knockenhauer KE, Schwartz TU, Sabatini DM. Mechanism of arginine sensing by CASTOR1 upstream of mTORC1. Nature. 2016;536(7615):229-33. doi: 10.1038/nature19079. PubMed PMID: 27487210; PMCID: PMC4988899.

18. Saxton RA, Knockenhauer KE, Wolfson RL, Chantranupong L, Pacold ME, Wang T, Schwartz TU, Sabatini DM. Structural basis for leucine sensing by the Sestrin2-mTORC1 pathway. Science. 2016;351(6268):53-8. doi: 10.1126/science.aad2087. PubMed PMID: 26586190; PMCID: PMC4698039.

19. Wolfson RL, Chantranupong L, Saxton RA, Shen K, Scaria SM, Cantor JR, Sabatini DM. Sestrin2 is a leucine sensor for the mTORC1 pathway. Science. 2016;351(6268):43-8. doi: 10.1126/science.aab2674. PubMed PMID: 26449471; PMCID: PMC4698017.

20. Faubert B, Li KY, Cai L, Hensley CT, Kim J, Zacharias LG, Yang C, Do QN, Doucette S, Burguete D, Li H, Huet G, Yuan Q, Wigal T, Butt Y, Ni M, Torrealba J, Oliver D, Lenkinski RE, Malloy CR, Wachsmann JW, Young JD, Kernstine K, DeBerardinis RJ. Lactate Metabolism in Human Lung Tumors. Cell. 2017;171(2):358-71 e9. doi: 10.1016/j.cell.2017.09.019. PubMed PMID: 28985563; PMCID: PMC5684706.

21. Hui S, Ghergurovich JM, Morscher RJ, Jang C, Teng X, Lu W, Esparza LA, Reya T, Le Z, Yanxiang Guo J, White E, Rabinowitz JD. Glucose feeds the TCA cycle via circulating lactate. Nature. 2017;551(7678):115-8. doi: 10.1038/nature24057. PubMed PMID: 29045397.

22. Ye J, Kumanova M, Hart LS, Sloane K, Zhang H, De Panis DN, Bobrovnikova-Marjon E, Diehl JA, Ron D, Koumenis C. The GCN2-ATF4 pathway is critical for tumour cell survival and proliferation in response to nutrient deprivation. EMBO J. 2010;29(12):2082-96. doi: 10.1038/emboj.2010.81. PubMed PMID: 20473272; PMCID: 2892366.

Chapter 2

Asparagine Promotes Cancer Cell Proliferation through Use as an Amino Acid Exchange Factor

INTRODUCTION

Many tumor cells exhibit high rates of glutamine consumption to support macromolecular biosynthesis and cell proliferation(1). Glutamine fuels the TCA cycle through anaplerosis and contributes to the synthesis of lipids, nucleotides and non-essential amino acids. However, the full spectrum of glutamine contribution to cancer cell growth remains an area of active investigation. Although glutamine can contribute to synthesis of several amino acids through its catabolism to glutamate, only asparagine requires glutamine for *de novo* synthesis; glutamine is a substrate for asparagine synthetase (ASNS). ASNS activity is unidirectional and ATP-dependent, suggesting that cells synthesize asparagine at the expense of macromolecule synthesis and cellular energy.

The importance of asparagine for tumor growth has been demonstrated by the effectiveness of extracellular asparaginase in treating low-ASNS-expressing leukemia. Notably, the off-target glutaminase (GLS) activity of asparaginase is not required for its anti-tumor effects(2). Although asparaginase is effective as a therapeutic for cancers that obtain the majority of their asparagine from the environment, cancers that are capable of synthesizing asparagine de novo via ASNS are less responsive to asparaginase therapy(3). Moreover, leukemic asparaginase resistance is associated with elevated ASNS expression(4), and ASNS expression in solid tumors correlates with tumor grade and poor prognosis(5). Recently, genetic silencing of ASNS in sarcoma cells combined with depletion of plasma asparagine levels via asparaginase was shown to blunt tumor growth in vivo(6). Thus, cancer cells appear to have high demand for asparagine, and this demand has the potential to be exploited therapeutically.

The nature of ASNS regulation suggests that asparagine may play a role in cellular amino acid homeostasis. ASNS expression is upregulated in response to individual or combined limitation of numerous amino acids, including most essential amino acids(7, 8). Amino acid-starvation-

induced upregulation of ASNS is mediated by activating transcription factor 4 (ATF4), the transcriptional activity of which is activated in response to uncharged tRNAs. Although ATF4 regulates expression of genes involved in multiple amino acid synthesis and transport pathways, asparagine alone rescues the impaired proliferation and autophagy resulting from induced ATF4 knockdown(9), supporting the idea that asparagine globally impacts intracellular amino acid levels. However, the only currently known function for asparagine is as a substrate for protein synthesis. Here we identify a novel role for asparagine as an amino acid exchange factor. We show that asparagine exchanges with extracellular amino acids to regulate mTOR complex 1 (mTORC1) activation, nucleotide synthesis, and proliferation. Our results indicate that glutamine contribution to cancer cell survival and proliferation is, in part, mediated by glutamine-dependent asparagine synthesis.

RESULTS

Glutamine independence confers asparagine dependence

The broad contribution of glutamine carbon and nitrogen to cancer metabolism has led to the development of drugs targeting glutamine metabolism such as CB-839, an orally bioavailable glutaminase (GLS) inhibitor currently undergoing Phase I evaluation for cancer treatment(10-12). We hypothesized that glutamine-dependent cancers may generate resistance to drugs targeting glutamine metabolism by increasing reliance on metabolites downstream of glutamine. To test this hypothesis, we generated both LPS2 liposarcoma cells that grow in the absence of glutamine and SUM159PT breast cancer cells that are resistant to CB-839(10) (Figure 2-1A-B).

Since glutamine is required for *de novo* asparagine synthesis, we examined whether resistance to glutamine withdrawal confers growth dependence on exogenous asparagine. Also, since CB-839-resistant cells down-regulate cellular glutamine consumption (Figure 2-1C), thereby limiting glutamine availability for the ASNS reaction, we examined whether resistance to GLS inhibition

confers growth dependence of exogenous asparagine as well. LPS2 glutamine-independent and SUM159PT CB-839-resistant cells, but not their parental cells, require asparagine in the cell culture medium for proliferation (Figure 2-2). LPS2 glutamine-independent cells increase expression of glutamine synthetase (GS) (Figure 2-1B), likely to fulfill cellular glutamine requirements for nucleotide synthesis and protein synthesis by synthesizing glutamine from glutamate(13). However, the dependence of glutamine-independent cells on exogenous asparagine indicates that GS-derived glutamine is insufficient to fulfill the cellular demand for asparagine and suggests that maintaining intracellular asparagine levels is critical for proliferation. Dependence of glutamine-independent cells on exogenous asparagine for proliferation is consistent with a recent report that exogenous asparagine protects cells from apoptosis upon glutamine deprivation(5).

Given the structural similarity of asparagine and glutamine, we examined whether asparagine could be metabolized like glutamine as a potential resistance mechanism to glutamine deprivation and GLS inhibition. To determine if blocking glutamine metabolism causes cells to catabolize asparagine, we labeled the cell culture medium with either asparagine uniformly labeled on carbon (U-^{13}C-asparagine) or uniformly labeled on nitrogen (U-^{15}N-asparagine). The only detected metabolites labeled with asparagine carbon in the resistant cells are small percentages of aspartate and malate (Figure 2-3A). Asparagine nitrogen is detected in approximately ten percent of purines (Figure 2-3B). However, both the U-^{13}C-asparagine and U-^{15}N-asparagine utilized in these experiments are contaminated with small percentages of labeled aspartate, and the observed label on aspartate, malate, and purines is likely due to this contamination and the increased consumption of aspartate by the resistant cells (Figure 2-3C). These data suggest that asparagine is not widely catabolized in LPS2 glutamine-independent cells, SUM159PT CB-839 resistant cells, or their parental counterparts.

Since cells resistant to glutamine withdrawal and glutaminase inhibition require exogenous asparagine for proliferation but do not seem to catabolize it, we considered that the resistant cells may require exogenous asparagine simply for protein synthesis. To examine this possibility, we tested whether the LPS2 cells resistant to glutamine withdrawal and/or the SUM159PT cells resistant to GLS inhibition consume more ^{13}C-asparagine from the medium than their parental counterparts. All four cell lines (both resistant cells and both parental cells) obtain a majority of their intracellular asparagine from the culture medium, as indicated by the high percentage of ^{13}C-labeled intracellular asparagine when the medium is labeled with U-^{13}C-asparagine (Figure 2-4A). However, asparagine is not depleted from the medium in either the parental or resistant cell lines, and CB-839-resistant cells actually exhibit a net efflux of asparagine rather than influx when grown in the presence of glutamine (Figure 2-4B). These results suggest that dependence of glutamine-independent cells on exogenous asparagine is not solely for the purpose of protein synthesis and suggest that asparagine export may be important for growing cells.

Asparagine levels impact cancer cell proliferation in glutamine-abundant conditions

Since exogenous asparagine is required for proliferation of glutamine-independent cells, we next asked whether intracellular asparagine levels affect cell proliferation in glutamine-abundant conditions. To address this question, we knocked down ASNS using stable expression of short hairpin RNA (shRNA) in a panel of cancer cell lines. All of the cell lines analyzed, when grown in DMEM (which has 4 mM glutamine but lacks asparagine), exhibit reduced proliferation following partial ASNS knockdown when compared to cells expressing a scrambled shRNA (Figure 2-5A-B). However, supplementation of DMEM medium with 0.1 mM asparagine completely rescues proliferation of HeLa cells in which ASNS expression is suppressed by ASNS knockdown (Figure 2-5C). These results indicate that the growth benefit provided by ASNS expression is due to asparagine synthesis, rather than to another aspect of the ASNS

reaction, such as cytoplasmic glutamate production (Figure 2-5D), and suggest that intracellular asparagine levels impact cancer cell proliferation in glutamine-abundant conditions.

Asparagine is an amino acid exchange factor

Intracellular glutamine has the capacity to exchange with extracellular essential amino acids(14) and regulate mTOR activity(14-16). Given that net asparagine influx is not detected, even for cells that require exogenous asparagine for proliferation, we hypothesized that asparagine is imported into the cell only to be exported in exchange for other amino acids. To test whether intracellular asparagine is capable of exchanging with extracellular amino acids, a high intracellular glutamine/asparagine concentration was generated in serum- and amino acid-starved LPS2 cells by a 60 minute pre-load with either 2 mM L-glutamine, 2 mM L-asparagine, or a combination of the two. After washing away the exogenous glutamine and/or asparagine, a glutamine/asparagine-free amino acid mixture (AA medium) was added to the cells for 30 minutes. Glutamine and asparagine export from the cells was evaluated both by examining extracellular glutamine/asparagine levels following the 30 minute AA medium treatment and by measuring intracellular glutamine/asparagine levels before and after AA medium treatment. Confirming previous results(14), glutamine is detected in the medium only upon stimulation with amino acids (Figure 2-6A). Consistent with exchange factor capacity, asparagine is also detected in the medium upon stimulation with amino acids (Figure 2-6B). Moreover, intracellular levels of both glutamine and asparagine are depleted following asparagine/glutamine-free amino acid treatment (Figure 2-6C-D), and absolute quantification of intracellular and exported glutamine/asparagine verified that intracellular depletion is due to export (Figure 2-6E-F). While asparagine and glutamine are exported following amino acid stimulation of pre-loaded LPS2 cells, efflux of glycine, another neutral amino acid, is not detected (Figure 2-7A). Notably, when pre-loaded with a combination of glutamine and asparagine, asparagine but not glutamine export is detected (Figure 2-6A-B). In addition, while a glutamine pre-load is required to

observe glutamine export upon amino acid treatment, intracellular asparagine depletion occurs in response to amino acid treatment even with an asparagine-starved, no pre-load state (Figure 2-7B). These results suggest that LPS2 cells can use asparagine as an amino acid exchange factor and may in fact prefer use of asparagine over glutamine for amino acid exchange.

Knowing that asparagine is capable of exchanging with extracellular amino acids, we next examined whether intracellular asparagine levels regulate amino acid import under normal growth (non-starvation) conditions. Amino acid import is considerably impaired upon ASNS knockdown in non-starved HeLa cells grown in DMEM (Figure 2-8). Import of serine and basic amino acids arginine and histidine is particularly sensitive to ASNS knockdown in DMEM, and supplementing DMEM with 0.1 mM asparagine completely rescues uptake of these amino acids (Figure 2-9). Uptake of other amino acids (leucine, methionine, phenylalanine, tryptophan, and lysine), although impaired by ASNS knockdown, is also impaired by exogenous asparagine supplementation. This may indicate competition with asparagine for a common transporter for import. These results indicate that intracellular asparagine depletion through ASNS knockdown impairs amino acid uptake in cells cultured in complete medium, including 4 mM glutamine, suggesting that amino acid exchange with asparagine occurs under normal growth conditions and is not simply a substitute for glutamine exchange in glutamine-depleted conditions.

Asparagine regulates serine uptake and metabolism

Given the capacity of asparagine for amino acid exchange, we asked whether asparagine has increased capacity to exchange with certain amino acids. Notably, ASNS expression in human tumors strongly correlates with expression of genes involved in serine/glycine synthesis and one-carbon metabolism (Figure 2-10), suggesting that cellular demand for serine and asparagine may be specifically connected. To examine whether asparagine preferentially exchanges with certain amino acids, asparagine-pre-loaded LPS2 parental cells were treated

with non-polar, basic, or serine/threonine (which share a transporter) amino acid sub-categories. Although asparagine export is observed with all three groups, asparagine preferentially exchanges with serine/threonine and non-polar amino acids over basic amino acids following amino acid starvation (Figure 2-11A). In addition, following a five minute amino acid stimulation, intracellular non-polar and basic amino acid levels are approximately 50% higher in asparagine-pre-loaded glutamine-independent LPS2 cells compared with cells that lack a pre-load, while intracellular serine and threonine levels are approximately three-fold higher in asparagine-pre-loaded cells (Figure 2-11B-C).

Because asparagine regulates serine uptake, we asked whether asparagine levels alter serine synthesis or metabolism. To examine this possibility, we determined the impact of ASNS knockdown on serine synthesis pathway gene expression in the absence and presence of exogenous asparagine. ASNS knockdown results in elevated mRNA and protein expression of serine synthesis pathway enzymes, which is prevented by the addition of exogenous asparagine to the medium (Figure 2-12A-B). Consistently, ASNS knockdown results in increased incorporation of glucose carbon into serine and glycine (Figure 2-12C). ASNS knockdown also results increased localization of ATF4 to the promoters of serine synthesis enzyme genes, as indicated by chromatin immunoprecipitation (Figure 2-13A). Moreover, ATF4 knockdown abolishes the increased expression of serine synthesis pathway enzymes upon ASNS knockdown (Figure 2-13B). These data suggest that cells may compensate for decreased intracellular asparagine levels and consequent decreased ability to exchange intracellular asparagine for extracellular serine by transcriptionally upregulating the serine synthesis pathway through ATF4 activation.

Asparagine regulates mTORC1 activation

Amino acids are essential for mTORC1 activation(17, 18), and mTORC1 activity is particularly sensitive to arginine levels(19). Because asparagine functions as an amino acid exchange factor and regulates arginine import, we hypothesized that asparagine levels may influence mTORC1 activity. Pre-loading serum- and amino acid-starved LPS2, HeLa, or A431 cells with asparagine prior to stimulation with amino acids increases mTORC1 activation upon amino acid stimulation, and asparagine and glutamine pre-loading activate mTORC1 with similar kinetics (Figure 2-14). Importantly, asparagine/glutamine pre-load only results in mTOR activation following amino acid stimulation, indicating that it is their exchange factor roles that elicit mTORC1 activation.

Given that cells may obtain asparagine either from the environment or by *de novo* synthesis via ASNS activity, we speculated that ASNS expression levels would determine mTORC1 sensitivity to extracellular asparagine levels. Consistent with this hypothesis, mTORC1 activity in LPS2 cells, which have relatively low ASNS levels and obtain asparagine from the medium (Figure 2-15A), is sensitive to 6 hours of asparagine withdrawal when cultured in medium with serum and 2 mM glutamine (Figure 2-15B). Moreover, the kinetics of mTORC1 activation of serum- and amino acid-starved LPS2 cells are reduced upon stimulation with medium lacking asparagine (Figure 2-15C). While mTORC1 activity recovers after 24 hours of asparagine depletion (Figure 2-15B), simultaneous withdrawal of both asparagine and glutamine prevents recovery after 24 hours of withdrawal (Figure 2-15D), suggesting either that asparagine and glutamine can compensate for each other in the exchange factor role or that ASNS activity increases with prolonged asparagine withdrawal. Not surprisingly, the effect of asparagine withdrawal on mTORC1 activity is more pronounced in glutamine-independent (asparagine-dependent) LPS2 cells than in the parental cell line (Figure 2-15E versus Figure 2-15B).

Together these data suggest that mTORC1 activity in cells with low ASNS expression is sensitive to exogenous asparagine levels.

We next evaluated mTORC1 sensitivity to extracellular glutamine and asparagine levels in cells with high ASNS expression and the capacity to synthesize asparagine *de novo*. HeLa and A431 cells, which have relatively high ASNS levels (Figure 2-15A), are unaffected by asparagine withdrawal when grown in DMEM supplemented with 0.1 mM asparagine prior to withdrawal (Figure 2-16A-C). Unlike LPS2 mTORC1 activity (Figure 2-15B), HeLa and A431 mTORC1 activities are remarkably sensitive to glutamine withdrawal (Figure 2-16A-C). 2 mM asparagine supplementation, however, rescues HeLa and A431 mTORC1 activity upon glutamine withdrawal (Figure 2-16B-C). Asparagine rescue of mTORC1 activity in HeLa and A431 cells suggests either that the added asparagine compensates for the exchange factor role of glutamine or that mTORC1 responsiveness to glutamine is mediated, at least partially, by glutamine-dependent asparagine synthesis, which is not required when exogenous asparagine is provided.

To determine if mTORC1 insensitivity to asparagine withdrawal in HeLa cells is due the ability of the cells to synthesize asparagine *de novo*, we reduced ASNS expression and examined mTORC1 sensitivity to exogenous glutamine and exogenous asparagine. Stable ASNS knockdown in high ASNS-expressing HeLa and A431 cells generates mTORC1 sensitivity to exogenous asparagine and decreases sensitivity to exogenous glutamine (Figure 2-17A-B). In addition, although HeLa mTORC1 activity recovers after 24 hours of glutamine withdrawal (Figure 2-16A), simultaneous withdrawal of glutamine and asparagine prevents or delays complete recovery (Figure 2-17C), suggesting that mTORC1 recovery is due to increased asparagine consumption in the absence of glutamine. Collectively these results suggest that intracellular asparagine levels can influence mTORC1 activity in cultured cancer cell lines, and

the degree to which cellular mTORC1 activity is sensitive to exogenous asparagine depends on the ASNS expression level.

To assess how acute loss of ASNS expression in high-ASNS-expressing HeLa cells affects mTORC1 activation, we examined mTORC1 signaling in HeLa cells with a doxycycline-inducible ASNS shRNA or a doxycycline-inducible scrambled shRNA at early time points post induction of ASNS knockdown. At 48 hours post-induction of ASNS knockdown in asparagine-free DMEM, ASNS knockdown cells exhibit increased autophagy (as indicated by increased LC3-II levels) and reduced mTOR activity (Figure 2-18), consistent with a starved cellular state in the absence of asparagine.

Asparagine levels also influence activation of AMPK, as indicated by increased phosphorylation of AMPKα on Thr172 upon induction of ASNS knockdown (Figure 2-19A-B). Although AMPK activation negatively regulates mTORC1 activity, the timing of AMPK activation is delayed relative to impaired mTORC1 activation upon ASNS knockdown (Figure 2-19A). Moreover, reduced mTORC1 activation is seen to the same extent in ASNS single knockdown and ASNS/AMPKα double knockdown HeLa cells (Figure 2-19B), suggesting that AMPK activation is not primarily responsible for altered mTORC1 activation with varying intracellular asparagine.

Asparagine coordinates protein and nucleotide synthesis

To better understand the physiological importance of intracellular asparagine, we examined the influence of asparagine on protein synthesis, a process that is regulated by mTORC1(20). Since mTORC1 promotes mRNA translation through phosphorylation of eukaryotic initiation factor 4E (eIF4E)-binding protein (4E–BP1), with phosphorylation preventing 4E-BP1 from binding to eIF4E at the 5’ cap of mRNAs and permitting assembly of the translation initiation complex(21), we examined whether ASNS knockdown impacts 4E-BP1 phosphorylation.

Although absolute levels of 4E-BP1 phosphorylated on Ser65 are unaltered, ASNS knockdown leads to elevated levels of unphosphorylated 4E-BP1, resulting in a decreased ratio of phosphorylated-to-unphosphorylated 4E-BP1 (Figure 2-20A) and increased 4E-BP1-eIF4E binding, as indicated by co-immunoprecipitation (Figure 2-20B). The gene encoding 4E-BP1 is an ATF4 target(22, 23), and elevated levels of unphosphorylated 4E-BP1 may be a result of ATF4 activation induced by asparagine depletion (Figure 2-13). Consistent with an increased percentage of the inhibitory form of 4E-BP1, ASNS knockdown reduces the rate of ^{35}S-methionine incorporation into newly synthesized proteins, in a manner that is completely rescued by supplementing the medium with 0.1 mM asparagine (Figure 2-20C). Together, these results are consistent with a model whereby intracellular asparagine levels regulate protein synthesis through modulation of mTORC1 phosphorylation of 4E-BP1.

Because asparagine influences both serine uptake and mTORC1 activity, we examined whether asparagine also affects nucleotide synthesis. Serine is crucial for both purine and thymidine synthesis through its conversion to glycine and donation to the one-carbon unit pool(24). mTORC1 activation promotes nucleotide synthesis by increasing phosphorylation of CAD (carbamoyl-phosphate synthetase 2, aspartate transcarbamoylase, dihydroorotase)(25), which catalyzes the first three steps of *de novo* pyrimidine synthesis, and by increasing translation of phosphoribosyl pyrophosphate (PRPP) synthetase 2 (PRPS2)(26), which synthesizes PRPP, a substrate for the rate limiting enzymes of purine and pyrimidine synthesis as well as for nucleotide salvage pathway enzymes. Reducing intracellular asparagine through ASNS knockdown results in reduced phosphorylation of CAD on serine 1859 and reduced PRPS2 protein levels (Figure 2-21A-B). PRPS1 protein levels (Figure 2-21B) and PRPS1 and PRPS2 mRNA levels (Figure 2-21C), however, are also reduced upon ASNS knockdown, suggesting that mTORC1 translational regulation is not entirely responsible for decreased PRPS levels. Consistent with the observed reduction in CAD phosphorylation, PRPS1/2 levels, and serine

uptake in ASNS knockdown cells, ASNS knockdown results in reduced PRPP levels (Figure 2-22A), decreased serine incorporation into purines (Figure 2-22B), reduced purine levels, and reduced pyrimidine levels (Figure 2-22C). Although both the reduction in serine import and reduced PRPS levels may contribute to reduced nucleotide levels upon ASNS knockdown, rescuing PRPS2 levels through ectopic PRPS2 overexpression is insufficient to rescue nucleotide levels (Figure 2-23A-B). Rescuing serine uptake with cell-permeable serine methyl-ester, on the other hand, rescues some of the nucleoside monophosphate and nucleoside diphosphate levels, but does not rescue levels of nucleoside triphosphates (Figure 2-23C). Through its involvement in both mTORC1 activation and serine uptake, our results collectively suggest that asparagine plays a role in coordinating protein and nucleotide synthesis (Figure 2-24).

DISCUSSION

We present here a previously unrecognized role for asparagine as an amino acid exchange factor. Our results suggest that intracellular asparagine exchanges with extracellular amino acids, especially serine, arginine, and histidine, to promote mTORC1 activation, protein and nucleotide synthesis, and cell proliferation under normal growth non-starvation conditions. During conditions of asparagine depletion, the cells increases ATF4 activity to restore both intracellular asparagine and serine, uptake of which is compromised in the absence of asparagine (Figure 2-25).

Cancer cell asparagine demand contributes to glutamine dependence

Our results suggest that asparagine is an important glutamine-derived metabolite for proliferating cells, and demand for asparagine likely contributes to cancer cell glutamine dependence, especially under cell culture conditions (which sometimes lack asparagine). Cancer cells that have adapted to glutamine independence require exogenous asparagine for

proliferation. Importantly, resistance to glutamine depletion does not occur when cells are cultured in media that lack asparagine, such as DMEM. Although glutamine-independent cells presumably synthesize enough glutamine for protein and purine synthesis via glutamine synthetase, the cells are not able to grow in the absence of exogenous asparagine, indicating that the demand for asparagine in proliferating cells exceeds the amount of asparagine that can be synthesized through the glutamine synthetase/ASNS pathway.

Asparagine versus glutamine in amino acid exchange

Although both asparagine and glutamine are capable of exchanging with amino acids, the extent to which each amino acid acts as an exchange factor under physiological conditions is unclear. Glutamine is the most abundant free amino acid in the blood at a concentration of 0.5 - 0.8 mM (27), and most cell culture media contain 2-4 mM glutamine. Blood asparagine concentration is much lower at 0.05 – 0.1 mM(27), and media asparagine concentration ranges from 0 mM in DMEM to 0.38 mM in RPMI. Moreover, we found that intracellular glutamine levels are 10-100-fold higher than asparagine levels, depending on the cell line and the asparagine concentration in the media. However, although glutamine is more abundant than asparagine, glutamine is extensively metabolized – primarily in the mitochondria by GLS. On the other hand, asparagine is a metabolic dead-end and may therefore be more available for exchange with extracellular amino acids. We show that asparagine is preferentially exported upon amino acid stimulation following pre-loading of cells with an equimolar asparagine/glutamine combination, and that asparagine, unlike glutamine, is exported even without a pre-load. We also show that reducing intracellular asparagine levels via ASNS knockdown decreases amino acid uptake, even in the presence of abundant glutamine. The impact of ASNS expression levels on mTORC1 activation suggests that the influence of glutamine on mTORC1 activity may be in part mediated by glutamine-dependent asparagine synthesis via ASNS.

Asparagine transporters

Although our data suggests asparagine exchanges with extracellular amino acids, it is unclear which transporters are involved in asparagine import and exchange. Glutamine is thought to be imported into the cell through SLC1A5 (or ASCT2) and exchange with extracellular amino acids through the neutral amino acid antiporter SLC7A5 (or LAT1)(14). The structural similarity between glutamine and asparagine suggests that the two amino acids may have similar affinities for transporters. In addition, preloading cells with glutamine or asparagine results in similar intracellular levels of glutamine or asparagine prior to AA medium stimulation (Figure 2-6); however, preloading with both glutamine and asparagine decreases the total intracellular amount of each by about half (Figure 2-6), suggesting potential use of a common transporter for import into the cell. Asparagine exchange with serine and arginine raises the possibility that asparagine uses SLC1A4 and SLC7A1 for its exchange function. Future studies assessing asparagine export upon inhibition of individual amino acid antiporters will further clarify the mechanistic details of asparagine exchange.

Asparagine coordinates anabolic processes

Our data suggest that asparagine plays a role in coordinating protein and nucleotide synthesis (Figure 2-24). The exchange factor role of asparagine influences protein synthesis through amino acid-induced mTORC1 activation and downstream activation of translation initiation factors, such as eIF4E. Asparagine regulation of nucleotide synthesis is likely due to asparagine exchange with extracellular serine. However, our data suggest that asparagine may also influence nucleotide synthesis through modulation of PRPS1/2 levels and/or mTORC1-regulated CAD activity.

Metabolic resistance mechanisms: therapeutic implications

Our results support asparagine as an important contributor to cancer cell growth and suggest strategies for improving efficacy of asparaginase and glutaminase inhibitors as cancer treatments. Our findings that asparagine is an amino acid exchange factor that modulates protein and nucleotide biosynthesis can explain the clinical efficacy of asparaginase in low ASNS-expressing cancers(3). Since cancers evade asparaginase sensitivity by upregulating ASNS expression(4), presumably to recover intracellular asparagine pools via ASNS-catalyzed synthesis from glutamine, coupling asparaginase treatment with a glutamine-low diet may improve efficacy of asparaginase treatment. Additionally, our findings that cancer cells acquire resistance to CB-839-inhibition by becoming auxotrophic for asparagine suggest that coupling glutaminase inhibition with an asparagine-low diet may improve efficacy of glutaminase inhibitors. Collectively, our results suggest that future studies combining drugs targeting asparagine or glutamine metabolism with specialized diets to prevent or delay drug resistance may improve treatment outcomes.

EXPERIMENTAL PROCEDURES

Cell lines and culture conditions. HeLa cells (ATCC) and A431 (provided by Dr. Thomas Graeber, UCLA) were cultured in DMEM supplemented with 10% fetal bovine serum and 1% penicillin-streptomycin, unless otherwise stated. The LPS2 cell line was derived from a liposarcoma tumor sample(28, 29). SUM159PT (provided by Dr. Frank McCormick, UCSF) and LPS2 cells were cultured as described below. Mycoplasma contamination testing was not conducted on cell lines used in this study.

Generation of glutamine-independence and CB-839 resistance. To generate glutamine-independence, LPS2 liposarcoma cells were cultured in a modified DMEM (m-DMEM) containing or lacking glutamine, with media replacement every 48 hours. m-DMEM is

glucose/glutamine/pyruvate-free DMEM (Invitrogen A14430-01) supplemented with 10 mM glucose, 1 mM pyruvate, 0.1 mM alanine, 0.1. mM aspartic acid, 0.1 mM asparagine, 0.1 mM glutamic acid, 2 mM glutamine, 0.3 mM proline, 0.00289 mM thymidine, and 10% dialyzed FBS (Invitrogen). Renewed proliferation in the absence of glutamine was observed approximately 6 weeks post-glutamine withdrawal. To generate resistance to glutaminase inhibitor CB-839 (Calithera Biosciences), SUM159PT breast cancer cells were cultured in pyruvate-free m-DMEM in the presence of 1 uM CB-839 or an equal volume of DMSO, with media replacement every 48 hours. A 10 mM stock solution of CB-839 was prepared in DMSO, and a fresh aliquot was thawed for each media change. Renewed proliferation in the presence of CB-839 was observed approximately 6 weeks after treatment was initiated.

Proliferation assays. Cells were seeded in triplicate in 6-well plates at 5 x 10^4 cells/well. Cells were counted every 24 hours for 72 or 96 hours using a particle counter (Beckman Coulter). For asparagine withdrawal experiments, cells were seeded in complete medium, allowed to adhere to the plate for ~6 hours, followed by replacement with medium containing or lacking asparagine.

Intracellular metabolite extraction and analysis. Cells were seeded in 6-well plates, and metabolites were extracted at 70-80% confluence. When heavy isotope labeling was performed, medium was replaced 24 hours prior to extraction with medium containing the labeled metabolite. Cells were washed with ice-cold 150 mM ammonium acetate, and scraped off the plate in 800 µl ice-cold 50% methanol. 10 nmol norvaline was added as an internal standard, followed by 400 µl chloroform. After vigorous vortexing, the samples were centrifuged at maximum speed, the aqueous layer was transferred to a glass vial, and the metabolites were dried under vacuum. Metabolites were resuspended in 50 µL 70% acetonitrile (ACN) and 5 µL of this solution used for the mass spectrometer-based analysis. The analysis was performed on

a Q Exactive (Thermo Scientific) in polarity-switching mode with positive voltage 4.0 kV and negative voltage 4.0 kV. The mass spectrometer was coupled to an UltiMate 3000RSLC (Thermo Scientific) UHPLC system. Mobile phase A was 5 mM NH4AcO, pH 9.9, B) was ACN, and the separation achieved on a Luna 3mm NH2 100A (150 x 2.0 mm) (Phenomenex) column. The flow was 200 µL / min, and the gradient ran from 15% A to 95% A in 18 min, followed by an isocratic step for 9 min and re-equilibration for 7 min. Metabolites were detected and quantified as area under the curve (AUC) based on retention time and accurate mass (≤ 3 ppm) using the TraceFinder 3.1 (Thermo Scientific) software. Relative amounts of metabolites between various conditions, as well as percentage of labeling, were calculated and corrected for naturally occurring 13C abundance.

Medium metabolite measurements. For medium metabolite measurements, 5 µL medium was mixed with 800 µl ice-cold 50% methanol. 10 nmol norvaline was added as an internal standard, followed by 400 µl chloroform. After vigorous vortexing, the samples were centrifiuged at maximum speed, the aqueous layer was transferred to a glass vial, and the metabolites were dried under vacuum. Metabolites were resuspended in 100 µL 70% acetonitrile (ACN) and 5 µL of this solution used for the mass spectrometer-based analysis, as described above for intracellular metabolites. To look at changes in extracellular amino acid levels over time, the experiment was initiated by the addition of fresh medium to the cells, and blank medium from a cell-free plate was included in the analysis. Data was plotted as percent change from blank medium and normalized by area under the growth curve during the incubation period. To highlight differences in amino acid uptake, experiments in Fig. 3g and Supplementary Fig. 2c were performed with 1/3x Amino Acid DMEM (DMEM diluted 3-fold with 1.8 mM calcium chloride, 0.81 mM magnesium sulfate, 5.33 mM potassium chloride, 110 mM sodium chloride, 0.906 mM sodium phosphate monobasic, 44 mM sodium bicarbonate, 25 mM glucose, 4 mM glutamine, and 1 mM pyruvate). For asparagine and glutamine absolute

quantification, serial dilutions of U-^{13}C-asparagine or U-^{13}C-glutamine at known concentrations were added to sample triplicates prior to chloroform addition. Sample asparagine and glutamine amounts were calculated according to standard curves generated from the ^{13}C standards. Glutamine consumption and glutamate production rates were determined using a Nova Biomedical BioProfile Basic Analyzer and normalized to area under the growth curve.

Amino acid starvation and stimulation. Amino acid starvation was performed as previously described (14). Cells were starved of serum for 16 hours followed by a 3 hour amino acid starvation in D-PBS containing 0.9 mM calcium chloride, 0.5 mM magnesium chloride, 1 g/l glucose, and 20 mM HEPES pH 7.4 (starve medium). For experiments involving glutamine and asparagine pre-loading, serum- and amino acid-starved cells were incubated with 2 mM glutamine, 2 mM asparagine, or 2 mM asparagine and 2 mM glutamine in starve medium for 1 hour at 37°C. Pre-loaded cells were washed twice with PBS to remove residual extracellular glutamine and asparagine prior to amino acid treatment. Amino acid stimulation was performed with AA medium (20 mM HEPES pH 7.4, 1.8 mM calcium chloride, 0.814 mM magnesium sulfate, 5.33 mM KCl, 110.3 mM NaCl, 0.906 mM sodium phosphate monobasic, 44.05 mM sodium bicarbonate, 1 g/l glucose, 0.8 mM leucine, 0.8 mM isoleucine, 0.2 mM methionine, 0.8 mM valine, 0.4 mM phenylalanine, 0.08 mM tryptophan, 02 mM histidine, and 0.8 mM lysine, 0.4 mM arginine, 0.4 mM serine, 0.8 mM threonine,) or glucose/glutamine/pyruvate-free DMEM supplemented with 1 g/l glucose.

Cell lysis and immunoblotting. Cells were lysed in buffer containing 50 mM Tris pH 7.4, 1% Nonidet P-40, 0.25% sodium deoxycholate, 1 mM EDTA, 150 mM NaCl, 1 mM dithiothreitol, 1 mM sodium orthovanadate, 20 mM sodium fluoride, 2 µg/ml aprotinin, 2µg/ml leupeptin and 0.7 µg/ml pepstatin. Western blot analysis was performed using standard protocols, and the following commercial antibodies were used as probes: ASNS (Proteintech 14681-1-AP, 1:1000),

phospho-T389 S6 kinase (Cell Signaling 9234, 1:500), S6 kinase (Cell Signaling 2708, 1:1000), phospho-S235/235 S6 ribosomal protein (Cell Signaling 4858, 1:3000), S6 ribosomal protein (Cell Signaling 2217, 1:1000), LC3A/B (Cell Signaling 4108, 1:1000), PHGDH (Cell Signaling 13428, 1:1000), PSAT1 (Abnova H00029968-A01, 1:500), PSPH (Sigma HPA020376, 1:500), SHMT1 (Abcam ab55736, 1:1000), SHMT2 (Cell Signaling 12762, 1:1000), PRPS2 (Abnova H00005634-A01, 1:1000), 4E-BP1 (Cell Signaling 9452, 1:1000) and α-tubulin (Sigma T6074, 1:10000).

Quantitative Real-Time PCR. RNA was purified with Qiagen RNeasy Kit. 1 µg of total RNA was used to synthesize cDNA using the iScript cDNA Synthesis Kit (Bio-Rad) as per manufacturer's instructions. Quantitative PCR (qPCR) was conducted on the Roche LightCycler 480 using SYBR Green I Master Mix (Roche) and 0.5 µM primers. Relative expression values are normalized to control gene (60S acidic ribosomal protein P0). qPCR was performed with the following primers:

ASNS Fwd: CAGAAGATGGATTTTTGGCTG
ASNS Rev: TGTCCAGGAAGAAAAGGCTC
PHGDH Fwd: GCAAAGAGGAGCTGATAGCG
PHGDH Rev: TTCTCAGCTGCGTTGATGAC
PSAT1 Fwd: TGCCGCACTCAGTGTTGTTAG
PSAT1 Rev: GCAATTCCCGCACAAGATTCT
PSPH Fwd: GAGGACGCGGTGTCAGAAAT
PSPH Rev: GGTTGCTCTGCTATGAGTCTCT
SHMT1 Fwd: CTGGCACAACCCCTCAAAGA
SHMT1 Rev: AGGCAATCAGCTCCAATCCAA
SHMT2 Fwd: CCCTTCTGCAACCTCACGAC
SHMT2 Rev: TGAGCTTATAGGGCATAGACTCG
MTHFD2 Fwd: CTGCGACTTCTCTAATGTCTGC
MTHFD2 Rev: CTCGCCAACCAGGATCACA
ATF4 Fwd: GTCCCTCCAACAACAGCAAG
ATF4 Rev: CTATACCCAACAGGGCATCC
PRPS1 Fwd: CCTGCTATTTCTCGCATCAA
PRPS1 Rev: GTGAGTTCTCCTGATGGCTT
PRPS2 Fwd: CTGGGGCGGATCACATCATC
PRPS2 Rev: CCGCATACAAATTATCCACAGGA

Translation rate. Labeling medium was prepared by adding 20 uCi/ml ^{35}S-methionine (PerkinElmer) to methionine-free DMEM containing 10% dialyzed FBS. Following two PBS washes, cells were labeled for 10 minutes and immediately lysed. 10 ug of lysate was spotted onto Whatman filters (pre-blocked with 0.1% methionine). Filters were added to ice-cold 10% TCA for 20 minutes, boiled in 5% TCA for 15 minutes, and washed in ice-cold 5% TCA and 95% ethanol for 20 minutes each. Scintillation fluid was added to dried filters, and radioactivity was measured. Counts per minute readings were normalized to protein content (Bradford assay).

Chromatin immunoprecipitation and Quantitative Real-Time PCR. $2x10^7$ cells were crosslinked by the addition of 1% formaldehyde-containing medium for 10 minutes, followed by the addition of 140 mM glycine for 5 minutes. Crosslinked cells were lysed in 1% SDS; 50mM Tris-HCl, pH 8; 20mM EDTA and sonicated to produce DNA fragments between 200-600 bp in length. Lysate corresponding to $5x10^6$ cells was immunoprecipitated with anti-ATF4 antibody (Proteintech 10835-1-AP) or normal rabbit IgG (Santa Cruz) as a negative control. Complexes were washed with Wash Buffer A (50mM HEPES, pH 7.9; 0.1% SDS; 1% Triton X-100; 0.1% Sodium Deoxycholate; 1mM EDTA; 140mM NaCl), Wash Buffer B (50mM HEPES, pH 7.9; 0.1% SDS; 1% Triton X-100; 0.1% Sodium Deoxycholate; 1mM EDTA; 500mM NaCl), LiCl Buffer (20mM Tris-HCl, pH 8; 0.5% NP-40; 0.5% Sodium Deoxycholate; 1mM EDTA; 250mM LiCl), and TE Buffer (10mM Tris-HCl, pH 8; 1mM EDTA), and eluted in Elution Buffer (50mM Tris-HCl, pH 8; 1mM EDTA; 1% SDS) followed by TE containing 0.67% SDS for 10 minutes each at 65°C. Crosslinking was reversed overnight at 65°C and samples were treated with RNase A for 60 minutes and Proteinase K for 90 minutes. DNA was purified using the QIAGEN PCR Purification Kit. 2ul of eluted immunoprecipitated DNA and 2ul of eluted 1% input were used for Quantitative Real-Time PCR with the following primers sequences:

ASNS Fwd: TGGTTGGTCCTCGCAGGCAT
ASNS Rev: CGCTTATACCGACCTGGCTCCT
PHGDH Fwd: CGTAAGGCAGCAAACACGTA

PHGDH Rev: CCAGCGATAAACCAAAGGTG
PSAT1 Fwd: GTTTGCATCCCTGCGTGT
PSAT1 Rev: CCGAGCTTCCTCACCAACT

shRNA-mediated knockdown. For stable ASNS knockdown, ASNS shRNA (5'-CCGGGCTGTATGTTCAGAAGCTAAACTCGAGTTTAGCTTCTGAACATACAGCTTTTTG-3') or a non-specific "scrambled" shRNA sequence (CCGGCAACAAGATGAAGAGCACCAACTCGAGTTGGTGCTCTTCATCTTGTTGTTTTT) in the pLKO.1-puro vector (Sigma) were cotransfected in HEK293T cells with expression vectors containing the *gag*/*pol*, *rev* and *vsvg* genes. Lentivirus was harvested 48 hours after transfection and added to subconfluent HeLa, A431, Hs578T, MDAMB231, and HCC70 cells with 4 ug/ml polybrene for 12-16 hours. Cells were selected in 2 ug/ml puromycin for 1 week. For stable ATF4 or AMPKα knockdown, ATF4 shRNA (CCGGGCCAAGCACTTCAAACCTCATCTCGAGATGAGGTTTGAAGTGCTTGGCTTTT), AMPKα shRNA (CCGGTGATTGATGATGAAGCCTTAACTCGAGTTAAGGCTTCATCATCAATCATTTTT) or a non-specific shRNA sequence (CCGGGCGCGATAGCGCTAATAATTTCTCGAGAAATTATTAGCGCTATCGCGCTTTTT) in the pLKO.1-hygro were transfected into HEK293T as above for lentivirus production. Infected HeLa shASNS cells were selected in 150 ug/ml Hygromycin B for 2 weeks.
For inducible ASNS knockdown, shRNA oligonucleotides (shASNS 5'-CACCGCTGTATGTTCAGAAGCTAAATTCAAGAGATTTAGCTTCTGAACATACAGC-3' and 5'-AAAAGCTGTATGTTCAGAAGCTAAATCTCTTGAATTTAGCTTCTGAACATACAGC-3';
and shScramble 5'-CACCGTAGCGACTAAACACATCAATTCAAGAGATTGATGTGTTTAGTCGCTA-3' and 5'-AAAATAGCGACTAAACACATCAATCTCTTGAATTGATGTGTTTAGTCGCTAC-3') were annealed and ligated into pENTR™/H1/TO vector (Invitrogen #K4920-00) following the BLOCK-

iT™ Inducible H1 RNAi Entry Vector Kit manual. Resulting shRNA constructs were recombined into pLentipuro/BLOCK-iT-DEST using Gateway® LR ClonaseII® (Invitrogen #11791-020). pLentipuro/BLOCK-iT-DEST is a modification of pLenti4/BLOCK-iT-DEST (Invitrogen #K4925-00) wherein the SV40 promoter/zeocin resistance cassette was replaced with the human PGK promoter/puromycin resistance gene and the cPPT/WPRE elements were added, and was kindly provided by Dr. Andrew Aplin (Thomas Jefferson University, Kimmel Cancer Center)(30, 31). Recombinant lentiviruses were packaged in 293T cells by co-transfecting 4 μg each of lentivirus plasmid with expression vectors containing the *gag*/*pol*, *rev* and *vsvg* genes. Lentivirus was harvested 48 hours after transfection and added to subconfluent HeLa cells with 4 ug/ml polybrene for 16 hours. Cells were selected in 2 ug/ml puromycin for 1 week. Doxycycline induction of knockdown is control by the Tet repressor (TetR) protein expressed from the pLenti0.3/EF/GW/IVS-Kozak-TetR-P2A-Bsd vector, which was constructed by Dr. Ethan Abel and was kindly provided by Dr. Diane M. Simeone (University of Michigan, Translational Oncology Program). Knockdown was induced with 25 ng/ml doxycycline.

ASNS correlation data. ASNS correlations data (Supplementary Fig. 3a) were based on TCGA mRNA expression data via cBioPortal (http://www.cbioportal.org/).

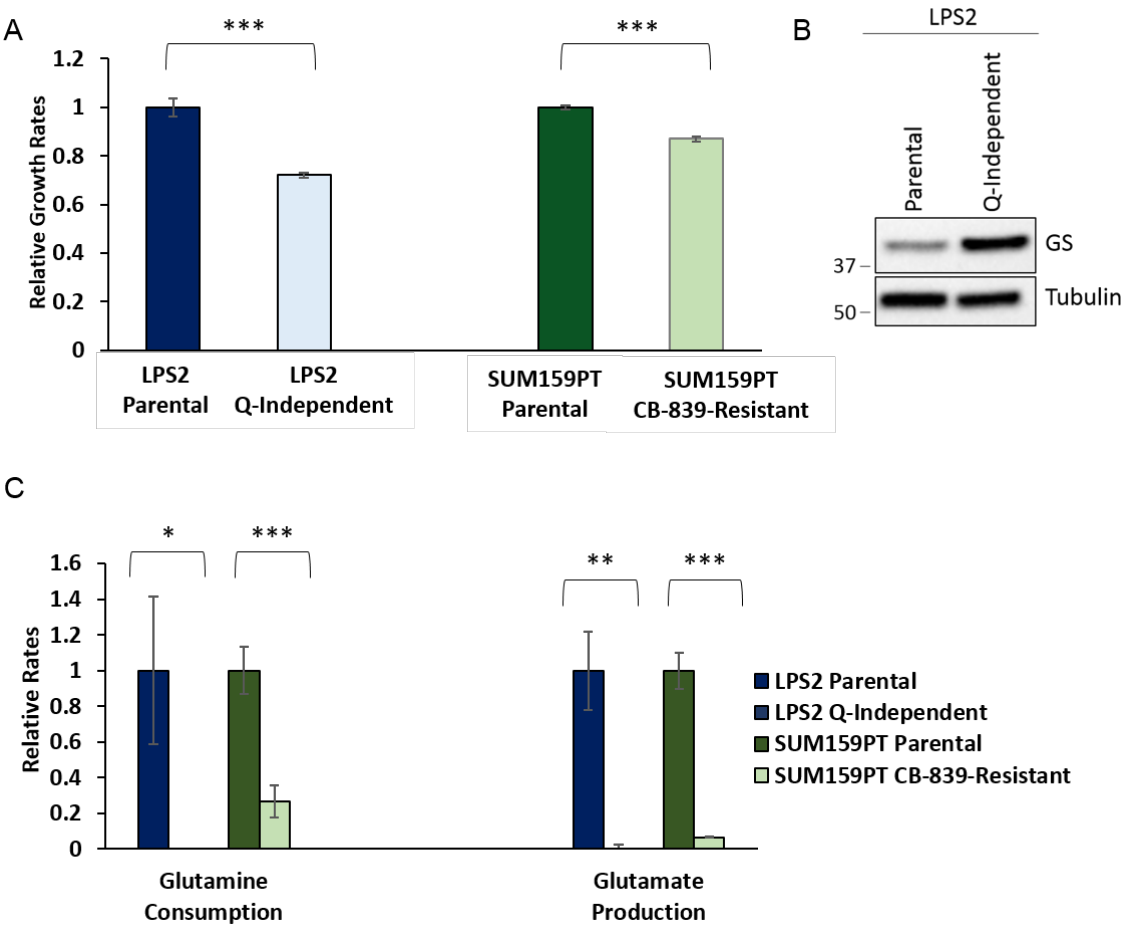

Figure 2-1. **Generation of glutamine-independent and CB-839-resistant cell lines.** (A) Relative growth rates of LPS2 parental, LPS2 glutamine (Q)-independent, SUM159PT parental, and SUM159PT CB-839-resistant cells, normalized to the respective parental cell line. (B) Immunoblot showing levels of glutamine synthetase (GS) and tubulin in parental and glutamine-independent LPS2 cells. (C) Relative glutamine consumption and glutamate production rates for LPS2 parental, LPS2 glutamine (Q)-independent, SUM159PT parental, and SUM159PT CB-839-resistant cells, normalized to the respective parental cell line. *$p < 0.05$; **$p < 0.01$; ***$p < 0.001$.

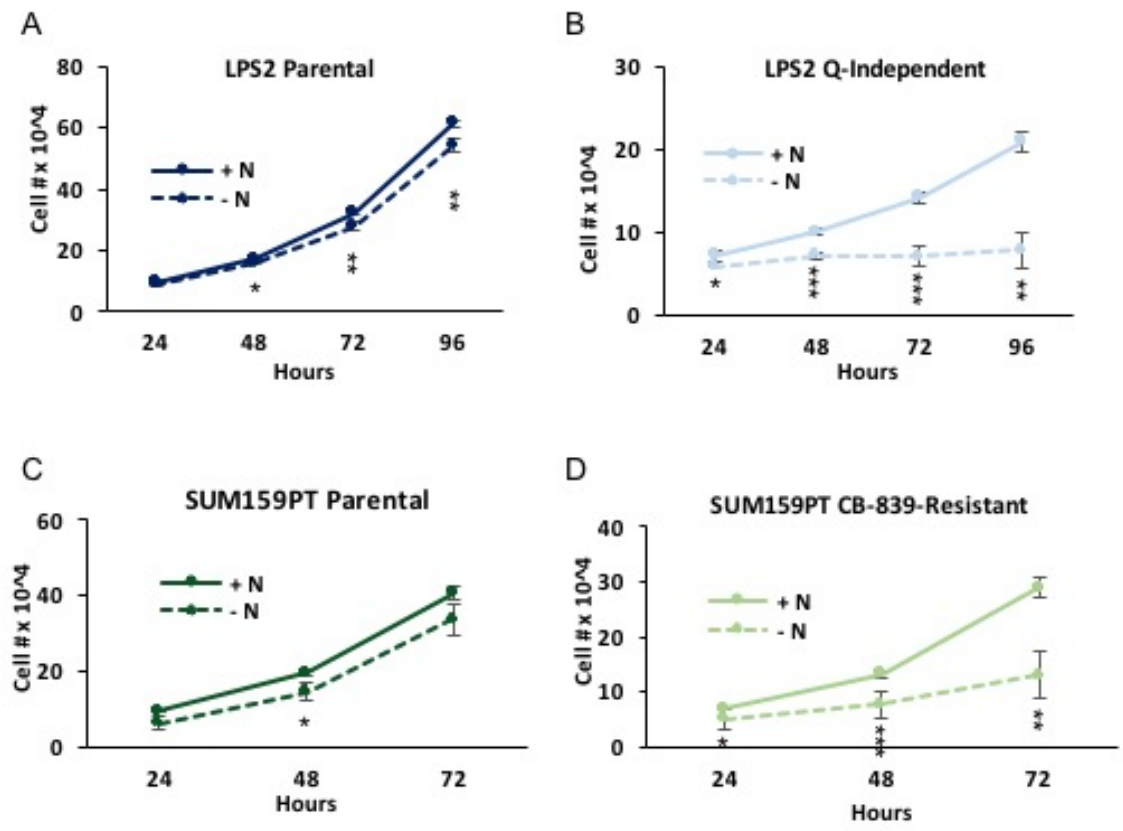

Figure 2-2. **Resistance to glutamine withdrawal or glutaminase inhibition causes cellular asparagine dependence.** (a-d) Proliferation curves of LPS2 parental, LPS2 glutamine (Q)-independent, SUM159PT parental, and SUM159PT CB-839-resistant cells in the presence or absence of 0.1 mM asparagine (N) in the medium. *p < 0.05; **p < 0.01; ***p < 0.001.

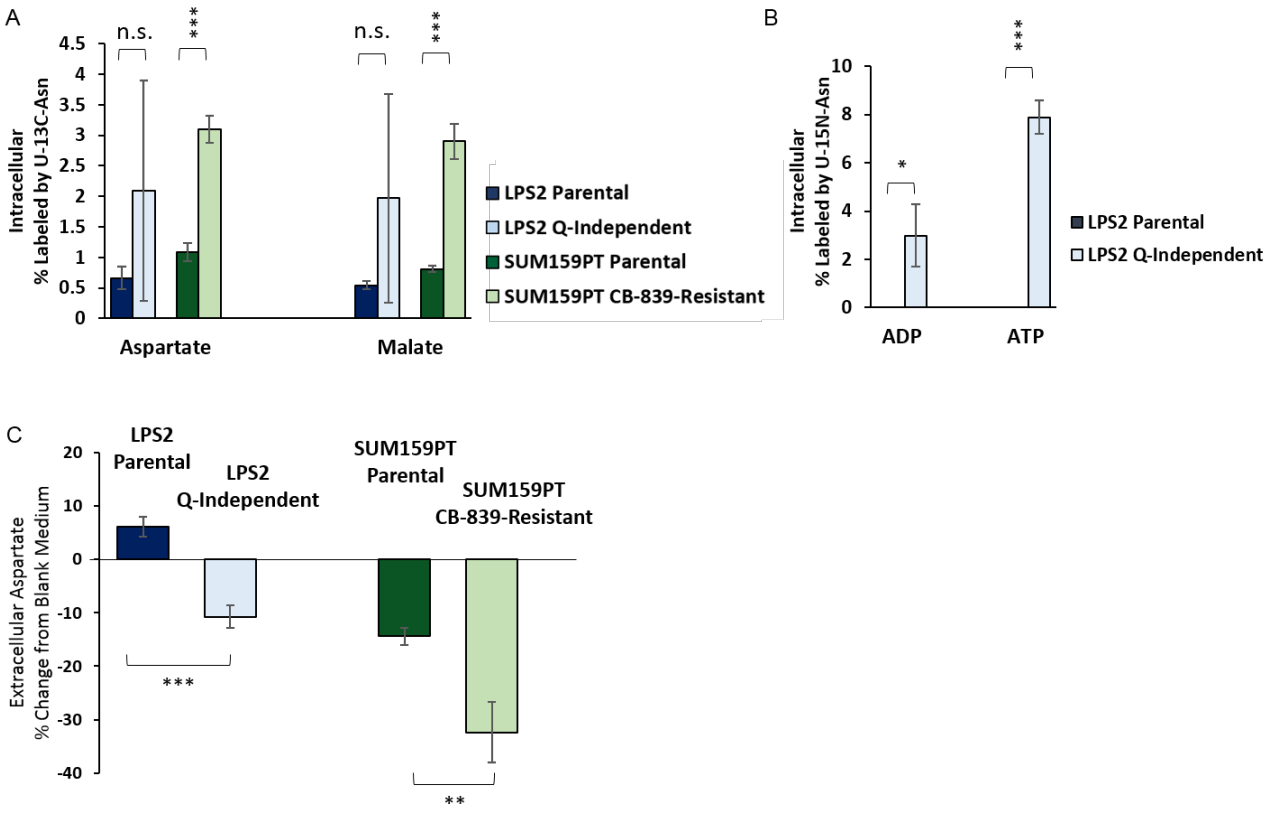

Figure 2-3. **Glutamine-independent and CB-839-resistant cells exhibit minimal asparagine metabolism. (A)** Percentages of intracellular 13C-labeled aspartate and malate in LPS2 parental and glutamine-independent as well as SUM159PT parental and CB-839-resistant cells labeled with U-13C-asparagine in the medium for 24 hours as determined by LC-MS. **(B)** Percentages of intracellular 15N-labeled ADP and ATP in LPS2 parental and glutamine-independent cells labeled with U-15N-asparagine in the medium for 24 hours as determined by LC-MS. **(C)** Changes in extracellular aspartate levels during a 24 hour incubation with the indicated cell line. Values are shown as percent change from aspartate measurements from identical medium incubated on plates lacking cells, with negative bars indicating cellular consumption and positive bars indicating production. Error bars denote standard deviation of the mean. *$p < 0.05$; **$p < 0.01$; ***$p < 0.001$; n.s., not significant.

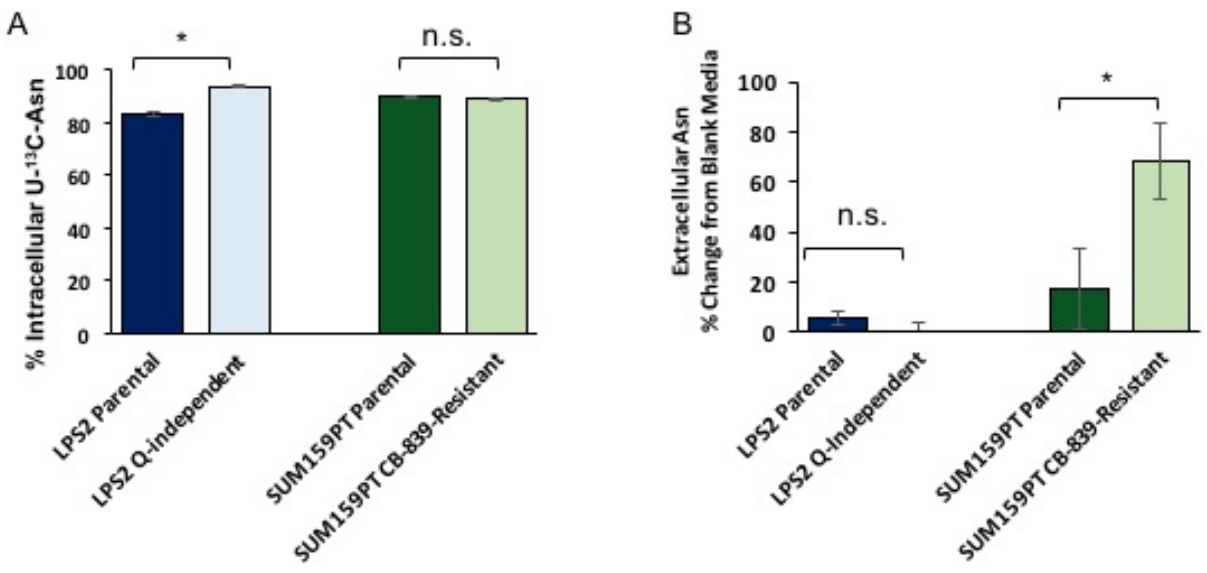

Figure 2-4. **Asparagine is not depleted from the medium of asparagine-dependent cells.** **(A)** Percentages of intracellular 13C-labeled asparagine in LPS2 parental and glutamine-independent as well as SUM159PT parental and CB-839-resistant cells labeled with U-13C-asparagine in the medium for 24 hours, as determined by LC-MS. **(B)** The percent change in medium asparagine levels as determined by LC-MS after 24 hours incubation time for the indicated cells or for medium in an empty tissue culture plate (blank). Error bars denote standard deviation of the mean. *p < 0.05; **p < 0.01; ***p < 0.001; n.s., not significant.

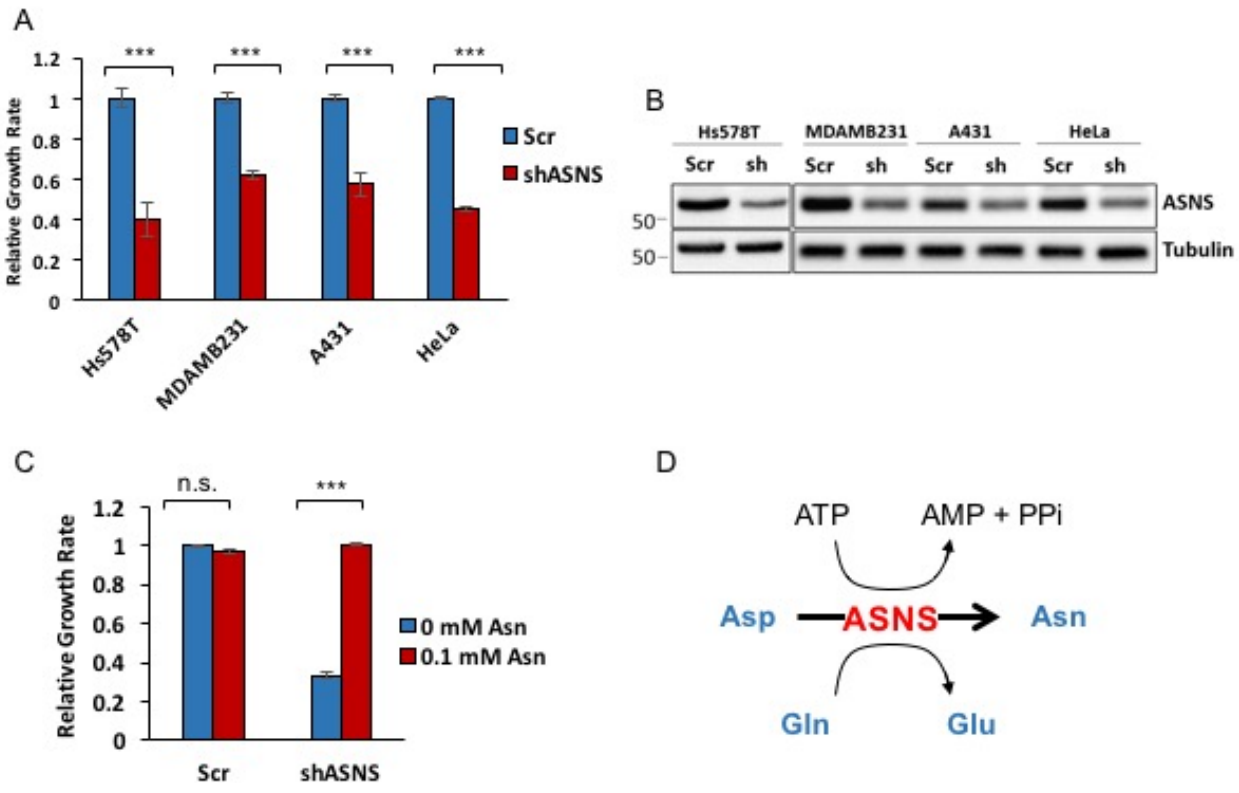

Figure 2-5. **Asparagine levels regulate cell proliferation. (A)** Relative growth rates of cancer cell lines stably expressing scrambled shRNA (Scr) or ASNS shRNA. Growth rates are normalized to the scrambled shRNA control for each cell line. **(B)** Immunoblot showing ASNS protein levels upon stable expression of scrambled (Scr) or ASNS shRNA in cell lines shown in (A). **(C)** Relative growth rates of HeLa cells stably expressing scrambled shRNA (Scr) or ASNS shRNA in the presence or absence of 0.1 mM asparagine. **(D)** Reaction catalyzed by ASNS. Aspartate (Asp) and glutamine (Gln) are converted to asparagine (Asn) and glutamate (Glu). Error bars denote standard deviation of the mean. *p < 0.05; **p < 0.01; ***p < 0.001; n.s., not significant.

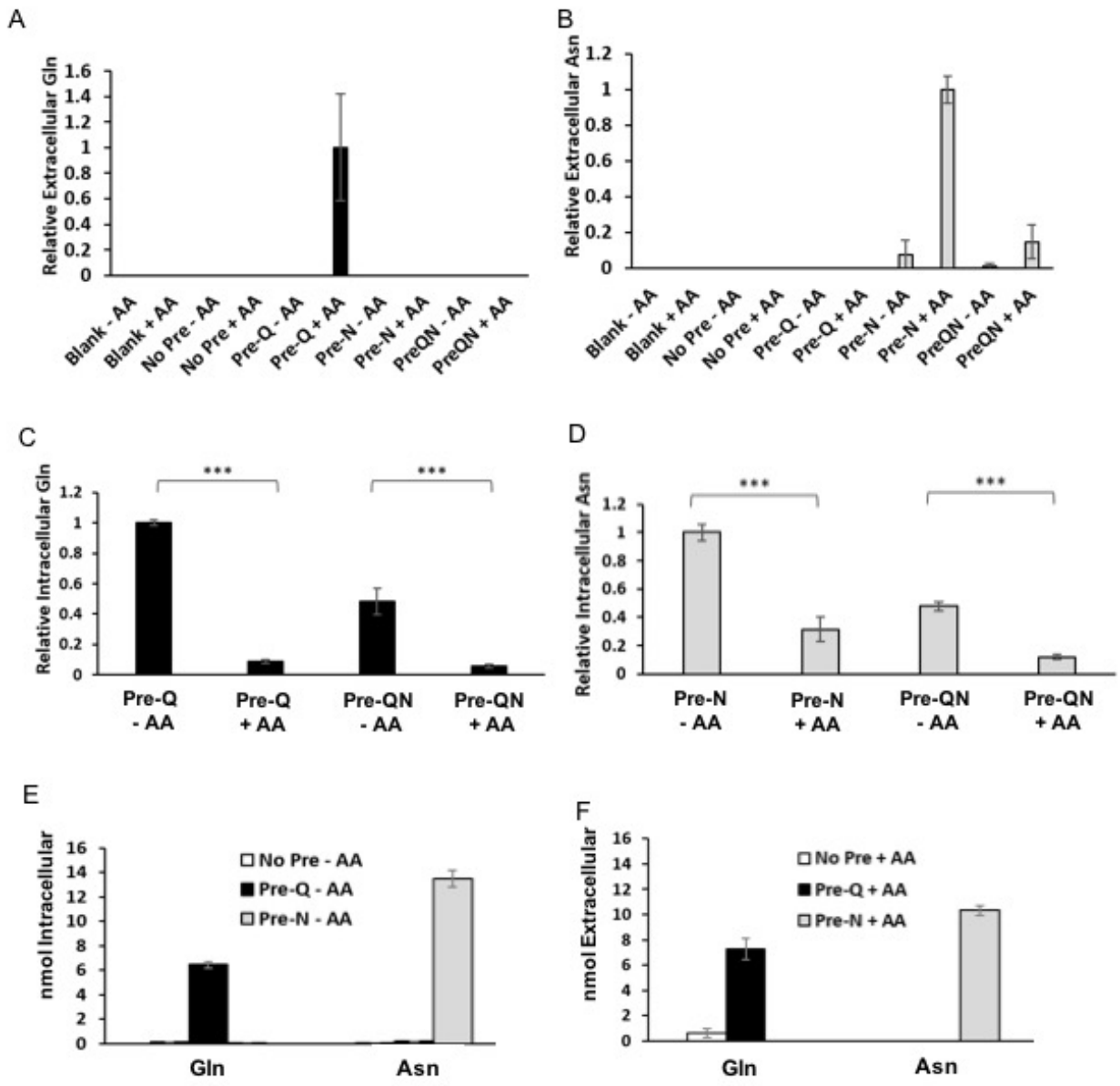
A
Relative Extracellular Gln
1.6
1.4
1.2
1
0.8
0.6
0.4
0.2
0
Blank - AA
Blank + AA
No Pre - AA
No Pre + AA
Pre-Q - AA
Pre-Q + AA
Pre-N - AA
Pre-N + AA
PreQN - AA
PreQN + AA
B
Relative Extracellular Asn
1.2
1
0.8
0.6
0.4
0.2
0
Blank - AA
Blank + AA
No Pre - AA
No Pre + AA
Pre-Q - AA
Pre-Q + AA
Pre-N - AA
Pre-N + AA
PreQN - AA
PreQN + AA
C
Relative Intracellular Gln
***
***
1.2
1
0.8
0.6
0.4
0.2
0
Pre-Q - AA
Pre-Q + AA
Pre-QN - AA
Pre-QN + AA
D
Relative Intracellular Asn
***
***
1.2
1
0.8
0.6
0.4
0.2
0
Pre-N - AA
Pre-N + AA
Pre-QN - AA
Pre-QN + AA
E
nmol Intracellular
16
14
12
10
8
6
4
2
0
No Pre - AA
Pre-Q - AA
Pre-N - AA
Gln
Asn
F
nmol Extracellular
16
14
12
10
8
6
4
2
0
No Pre + AA
Pre-Q + AA
Pre-N + AA
Gln
Asn

Figure 2-6. **Asparagine is an amino acid exchange factor.** Relative glutamine **(A)** and asparagine **(B)** levels in the medium from LPS2 cells, as measured by LC-MS, before and after amino acid (AA) stimulation following preloading of the cells with glutamine (Q) and/or asparagine (N). Serum- and amino acid-starved LPS2 cells were pre-loaded with 2 mM glutamine, 2 mM asparagine, or 2 mM glutamine and 2 mM asparagine for 60 minutes prior to stimulation for 30 minutes with an amino acid mixture (AA medium) lacking glutamine and asparagine. “Blank” indicates measurements from plates lacking cells. “No Pre” indicates measurements from plates of LPS2 cells not preloaded with glutamine or asparagine. Relative intracellular glutamine **(C)** and asparagine **(D)** levels as measured by LC-MS in glutamine and/or asparagine pre-loaded cells before and after amino acid stimulation. **(E)** Absolute quantification of intracellular glutamine and asparagine in pre-loaded cells prior to amino acid stimulation. **(F)** Absolute quantification of extracellular glutamine and asparagine following amino acid stimulation. Error bars denote standard deviation of the mean. *$p < 0.05$; **$p < 0.01$; ***$p < 0.001$.

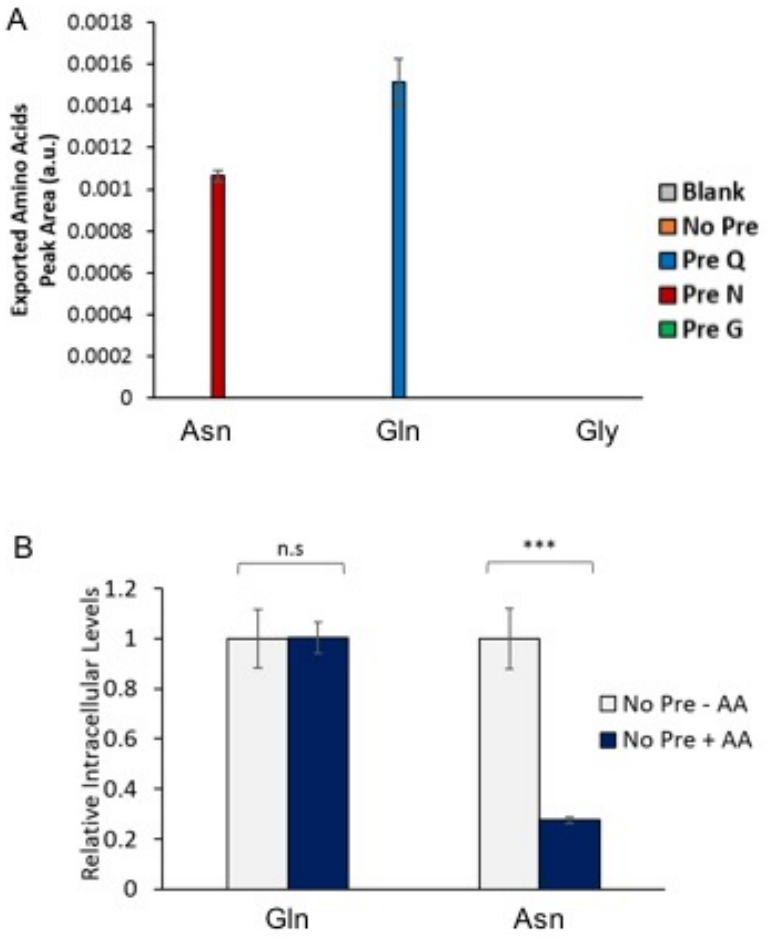

Figure 2-7. **Preferential use of asparagine for amino acid exchange. (A)** Peak area for exported asparagine, glutamine, and glycine following amino acid stimulation of pre-loaded LPS2 cells. Glycine export was not detected. Cells were pre-loaded with 2 mM asparagine, glutamine, or glycine, respectively. **(B)** Relative intracellular glutamine and asparagine levels as measured by LC-MS in serum- and amino acid-starved LPS2 cells before (- AA) and after (+ AA) amino acid stimulation for 30 minutes. "No Pre" indicates lack of glutamine or asparagine pre-load. Error bars denote standard deviation of the mean. *$p < 0.05$; **$p < 0.01$; ***$p < 0.001$.

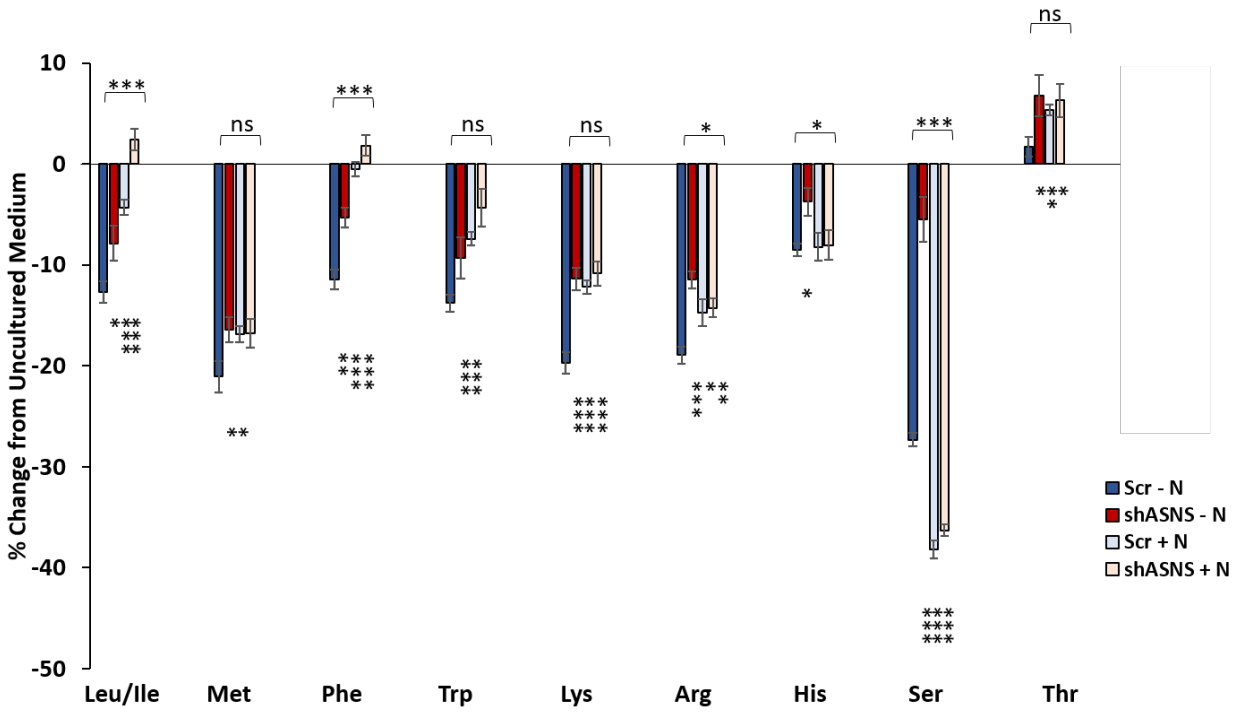

Figure 2-8. **Asparagine promotes amino acid uptake.** Changes in extracellular amino acid levels during a 24 hour incubation with HeLa cells. The 24 hour incubation began 48 hours post-doxycycline-induced expression of a scrambled shRNA (Scr) or ASNS shRNA. Values are shown as percent change from amino acid measurements from identical medium incubated on plates lacking cells, with negative bars indicating cellular consumption and positive bars indicating production. Reduced import of certain amino acids upon asparagine supplementation may indicate competition with asparagine for a common transporter for import. Error bars denote standard error of the mean (n = 6). *p < 0.05; **p < 0.01; ***p < 0.001; ns, not significant.

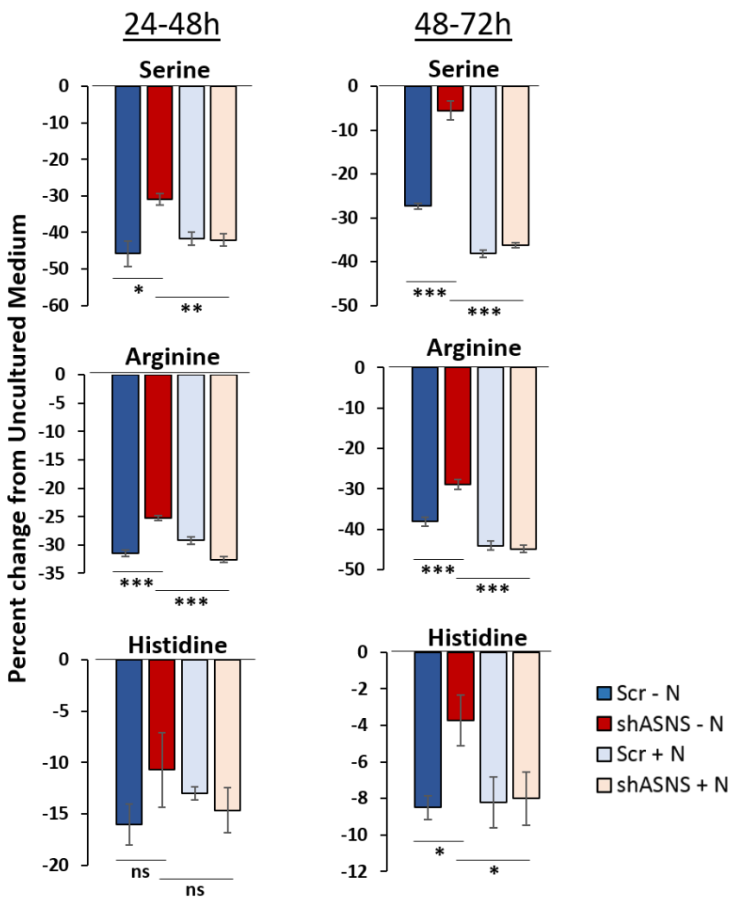

Figure 2-9. **Asparagine regulates serine, arginine, and histidine uptake**. Changes in extracellular amino acid levels during a 24 hour incubation with HeLa cells. The 24 hour incubation began either 24 hours (left panels) or 48 hours (right panels) post-doxycycline-induced expression of a scrambled shRNA (Scr) or ASNS shRNA. Values are shown as percent change from amino acid measurements from identical medium incubated on plates lacking cells, with negative bars indicating cellular consumption and positive bars indicating production. For (a)-(f), error bars denote standard deviation of the mean. For (g), error bars denote standard error of the mean. *p < 0.05; **p < 0.01; ***p < 0.001.

	Gene	Breast	Lung	Pancreas	Colon	Head&Neck	Glioblastoma	Bladder	Thyroid	Sarcoma	Kidney	Melanoma	Liver
Serine Synthesis	PHGDH		0.33	0.66	0.83	0.43	0.31		0.53	0.40			
	PSAT1	0.72	0.50	0.63	0.83	0.76	0.36	0.75	0.85	0.58			
	PSPH		0.47			0.40							
	SHMT1												
	SHMT2	0.39	0.54	0.68		0.38		0.64	0.84				
Glycine/Folate Metabolism	MTHFD1L	0.54			0.58								0.46
	MTHFD2L						0.34						
	MTHFD1						0.39						-0.31
	MTHFD2	0.56	0.62	0.69	0.49	0.73	0.34	0.57	0.81		0.50	0.62	
	MTHFR						-0.39						

Figure 2-10. **ASNS expression correlates with expression of genes involved in serine/glycine metabolism in human tumors.** Listed values are Pearson's correlation coefficients between ASNS mRNA levels and mRNA levels for the listed gene and for the indicated tumor. Blank cells indicate that expression is not substantially correlated with ASNS expression with a Pearson's correlation coefficient greater than 0.3 or less than -0.3. PHGDH, phosphoglycerate dehydrogenase; PSAT1, phosphoserine aminotransferase 1; SHMT1 and SHMT2, serine hydroxymethyltransferase 1 and 2; MTHFD1L, Methylenetetrahydrofolate dehydrogenase 1-like; MTHFD2L, Methylenetetrahydrofolate dehydrogenase 2-like; MTHFD1 and MTFHD2, methylenetetrathydrofolate dehydrogenase 1 and 2; MTHFR, methylenetetrahydrofolate reductase.

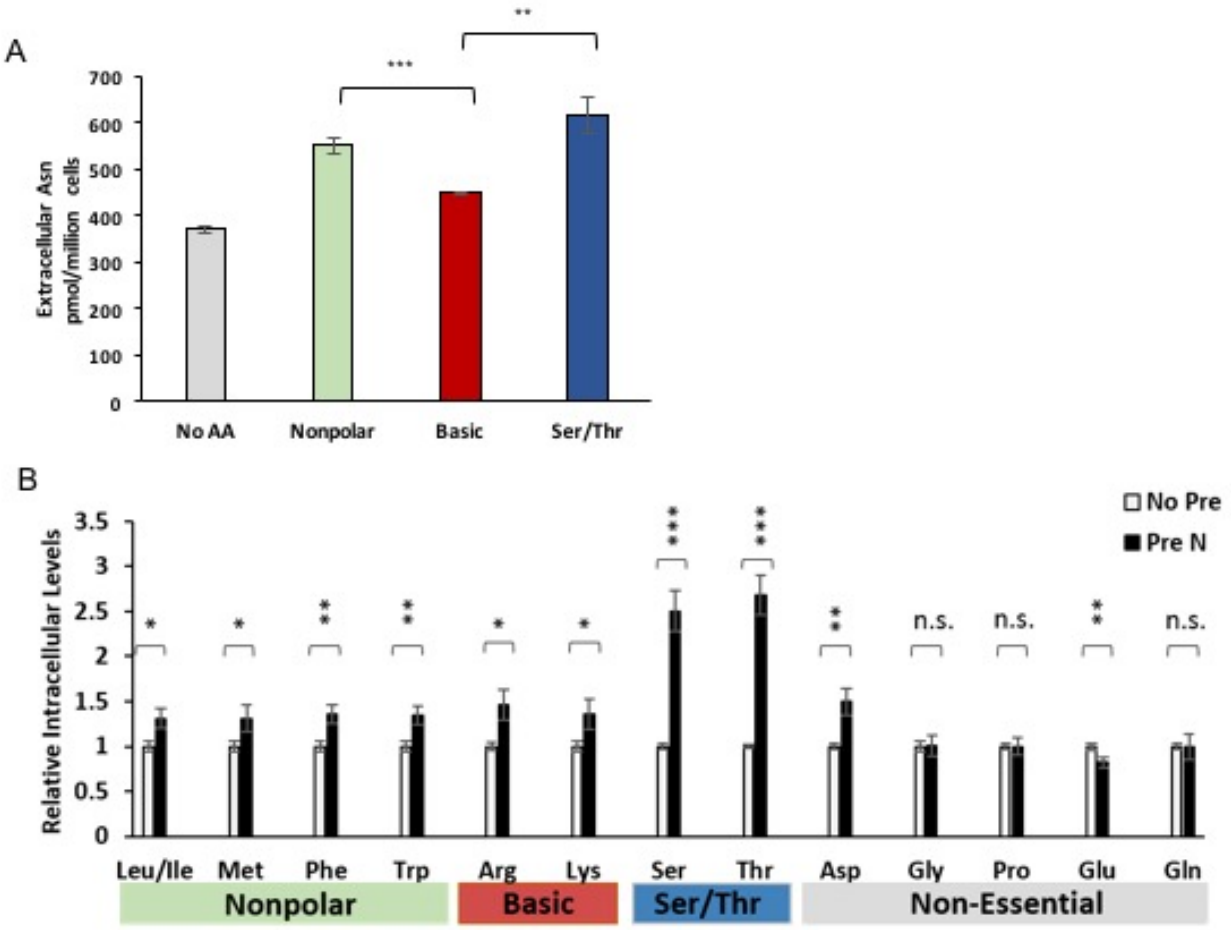

Figure 2-11. **Intracellular asparagine exchanges with extracellular serine. (A)** Asparagine levels in the media, measured by LC-MS, from serum- and amino acid-starved LPS2 cells pre-loaded with asparagine (PreN) and unstimulated (No AA) or stimulated with different amino acid sub-categories: nonpolar, basic, or Ser/Thr. Non-polar amino acids include leucine, isoleucine, methionine, tryptophan, and phenylalanine; basic amino acids include lysine, arginine, and histidine; Ser/Thr includes serine and threonine. **(B)** Relative intracellular amino acid levels in amino acid-starved glutamine-independent LPS2 cells as measured by LC-MS following 5 minute stimulation with complete glutamine-free medium. Prior to stimulation, cells were either pre-loaded with asparagine (Pre N) or starve medium (No Pre). Error bars denote standard deviation of the mean. *p < 0.05; **p < 0.01; ***p < 0.001; n.s., not significant.

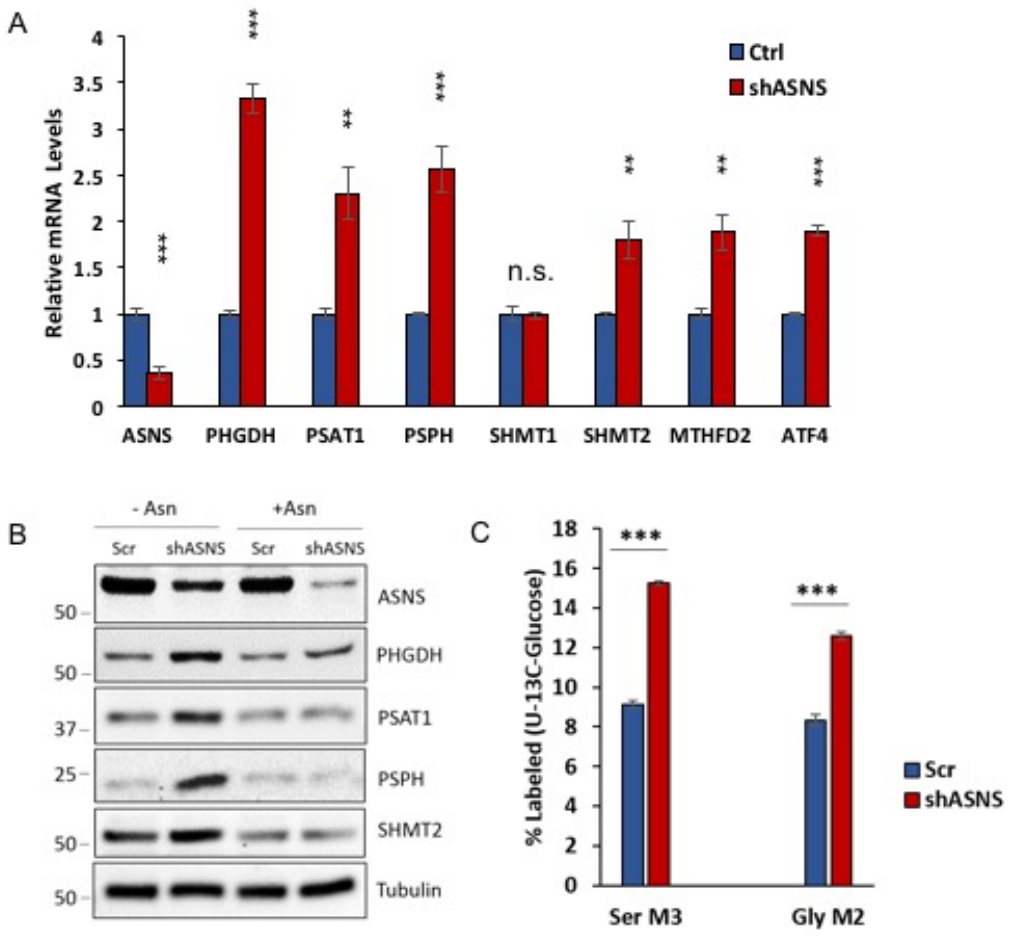

Figure 2-12. **Asparagine levels alter serine metabolism. (A)** Relative mRNA levels of genes involved in serine/glycine metabolism from HeLa cells 48 hours post-doxycycline induction of scrambled shRNA or ASNS shRNA. Quantitative real-time PCR was performed with primers specific to ASNS, PHGDH, PSAT1, PSPH, SHMT1, SHMT2, methylenetetrahydrofolate dehydrogenase 2 (MTHFD2), and activating transcription factor 4 (ATF4). **(B)** Immunoblot showing serine synthesis pathway protein levels in HeLa cells 48 hours post-doxycycline induction of scrambled shRNA or ASNS shRNA expression in the presence or absence of 0.1 mM exogenous asparagine. Percentages of intracellular 13C-labeled serine and glycine in HeLa cells labeled with U-13C-glucose for 24 hours at 24 hours post-induction of scrambled shRNA (Scr) or ASNS shRNA expression, as determined by LC-MS. Error bars denote standard deviation of the mean. *p < 0.05; **p < 0.01; ***p < 0.001; n.s., not significant.

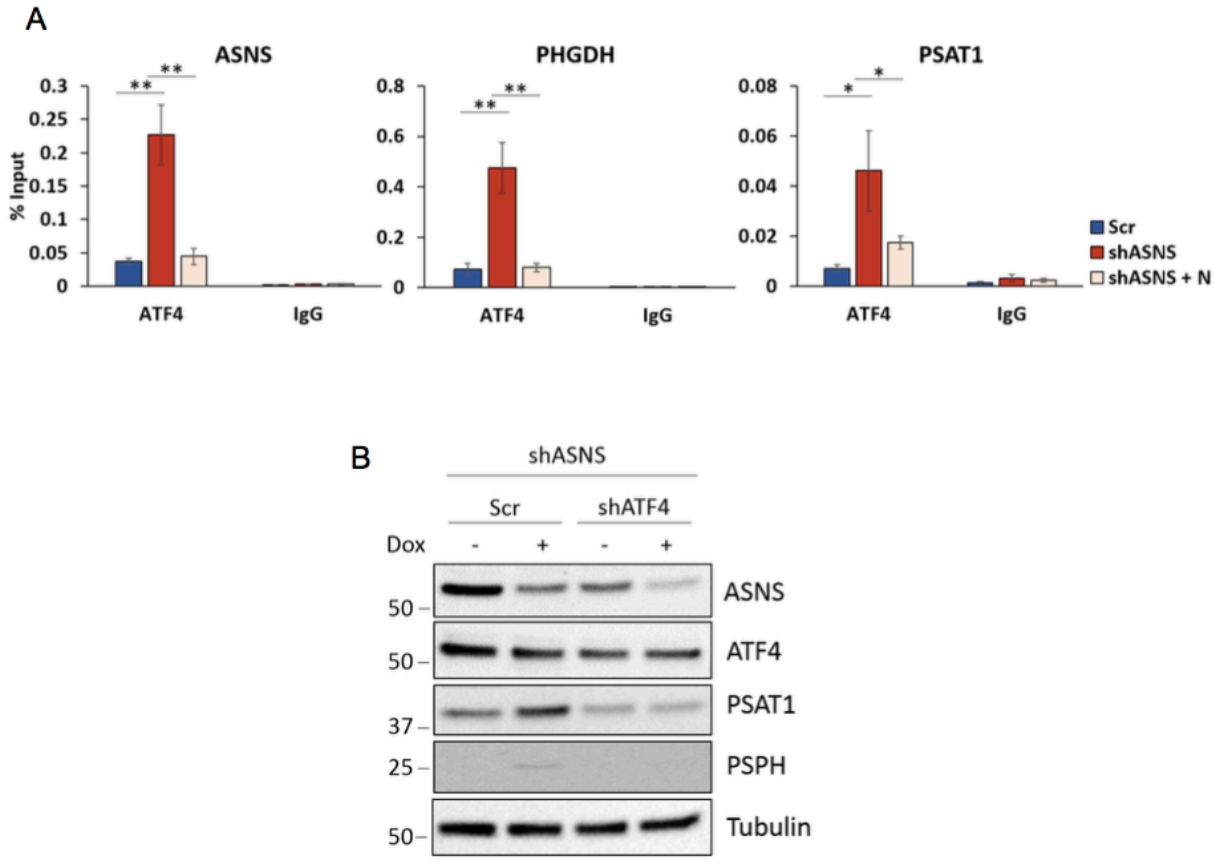

Figure 2-13. **Asparagine depletion results in ATF4-mediated transcriptional upregulation of the serine synthesis pathway. (A)** Levels of ATF4 binding to the indicated gene by ChIP-qPCR in HeLa cells 48 hours post-doxycycline induction of scrambled shRNA or ASNS shRNA expression in the presence or absence of 0.1 mM exogenous asparagine. Chromatin was immunoprecipitated using anti-ATF4 antibody or IgG as a negative control. Values indicate amount of immunoprecipitated DNA as a percentage of input chromatin. **(B)** Immunoblot showing ASNS, ATF4, PSAT1, and PSPH protein levels with or without a 48 hour doxycycline induction of ASNS shRNA in HeLa cells stably expressing scrambled or ATF4 shRNA. **(C)** Schematic illustrating ATF4 activation of serine synthesis pathway gene expression and serine synthesis pathway flux in response to low intracellular asparagine levels. Error bars denote standard deviation of the mean. *p < 0.05; **p < 0.01; ***p < 0.001.

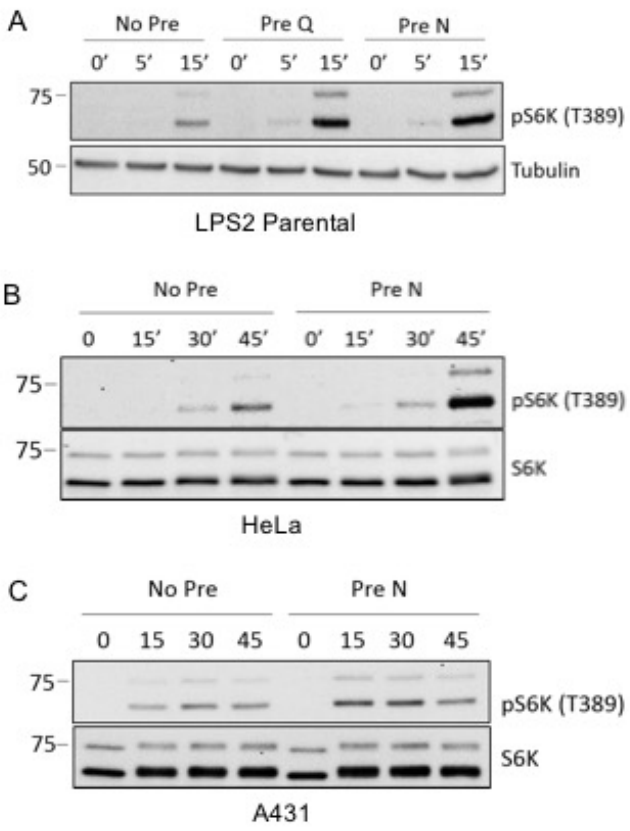

Figure 2-14. **Intracellular asparagine enhances mTORC1 activation upon amino acid stimulation of starved cells.** (A) Immunoblotting of lysates from serum- and amino acid-starved LPS2 parental cells pre-loaded with starve medium (No Pre), glutamine (Pre Q), or asparagine (Pre N), followed by amino acid stimulation for 0, 5, or 15 minutes. Lysates were probed with a phospho-specific antibody towards the mTOR target S6K at T389. (B-C) Immunoblotting of lysates from starved HeLa and A431 cells pre-loaded with starve medium (No Pre) or asparagine (Pre N) following amino acid stimulation for the indicated times. Lysates were probed for phosphorylation of S6K at T389 and total S6K.

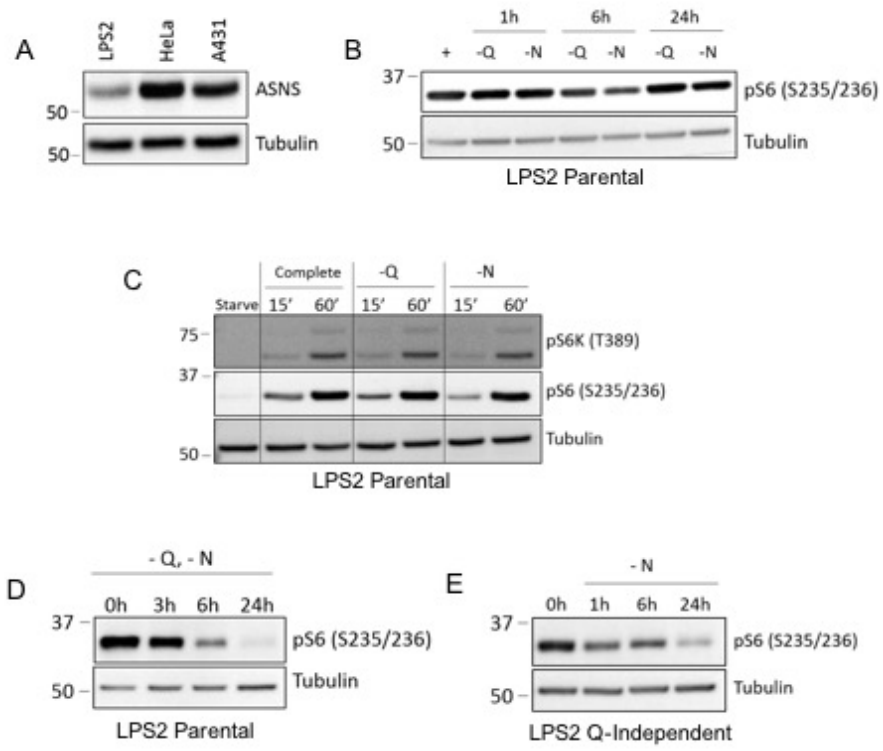

Figure 2-15. **mTORC1 activity in low ASNS-expressing cells is sensitive to asparagine withdrawal. (A)** Immunoblot comparing ASNS levels in lysates from LPS2, HeLa, and A431 cells under non-starved conditions. **(B)** Immunoblot showing phosphorylation of downstream mTOR effector S6 ribosomal protein (S235/236) following starvation of LPS2 parental cells of glutamine (-Q) or asparagine (-N) for the indicated times. + indicates no starvation. **(C)** Immunoblot showing phosphorylation of S6K (T389) and S6 ribosomal protein (S235/236) following stimulation of starved LPS2 parental cells with amino acids for the indicated times. Starved cells were stimulated with serum-free m-DMEM (Complete), serum-free m-DMEM lacking glutamine (-Q), serum-free m-DMEM lacking asparagine (-N), or left unstimulated (Starve). **(D)** Immunoblot showing S6 ribosomal protein phosphorylation (S235/236) following glutamine and asparagine starvation of LPS2 parental cells for the indicated times. **(E)** Immunoblot showing S6 ribosomal protein phosphorylation (S235/236) following asparagine starvation of LPS2 glutamine-independent cells for the indicated times.

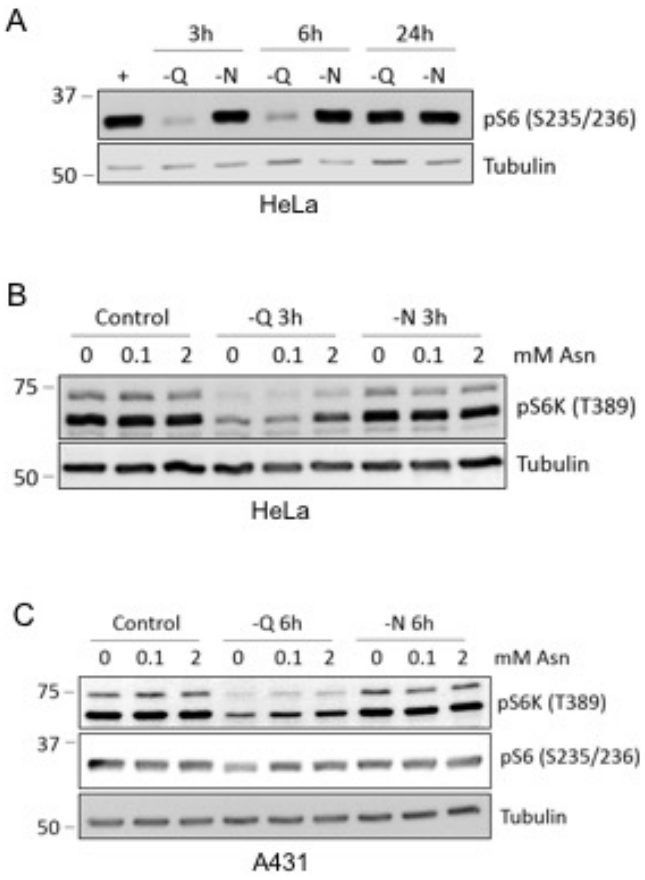

Figure 2-16. **Asparagine rescues mTORC1 activity upon glutamine withdrawal from high ASNS-expressing cells. (A)** Immunoblot showing S6 ribosomal protein phosphorylation (S235/236) following starvation of HeLa cells of glutamine (-Q) or asparagine (-N) for the indicated times. Prior to withdrawal, the medium contained 2 mM glutamine and 0.1 mM asparagine. **(B-C)** Immunoblots showing S6K phosphorylation (T389) following starvation of HeLa **(B)** or A431 **(C)** cells of glutamine (-Q) or asparagine (-N) for 3 hours. Prior to starvation, cells were cultured for 7 days in DMEM supplemented with the indicated asparagine concentration.

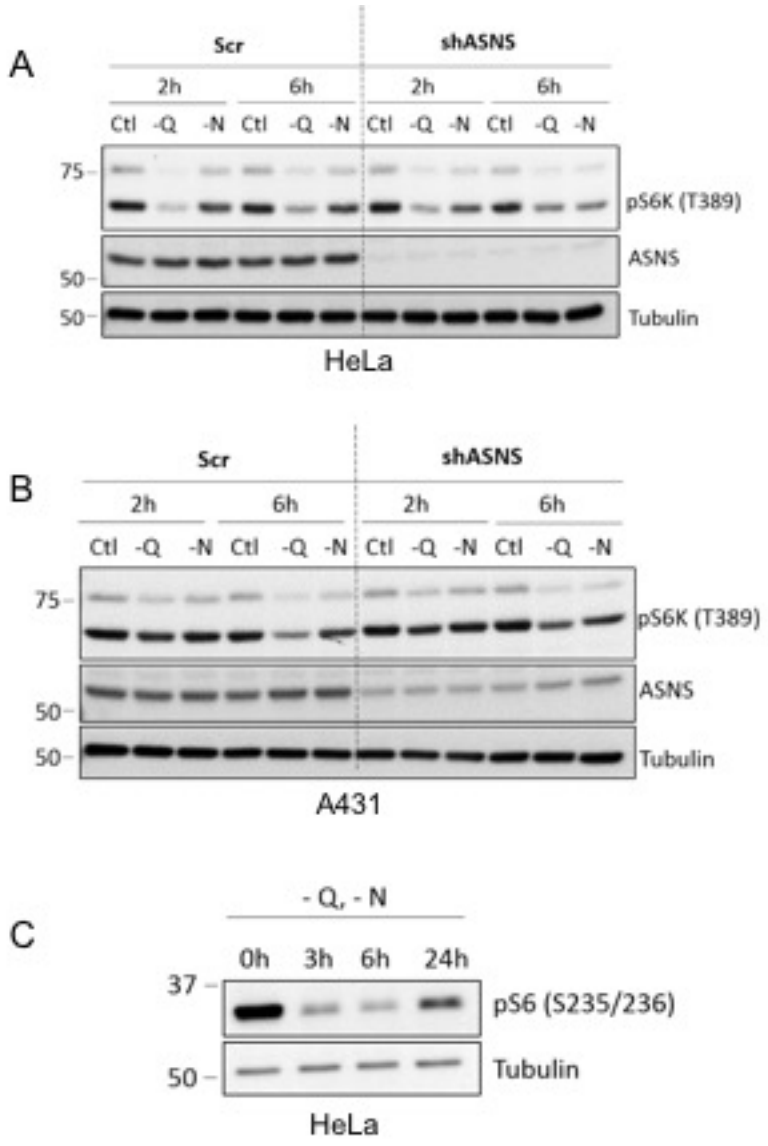

Figure 2-17. **ASNS knockdown in high ASNS-expressing HeLa and A431 cells generates mTORC1 sensitivity to exogenous asparagine and decreases sensitivity to exogenous glutamine. (A-B)** Immunoblot showing phosphorylation of S6K (T389) in HeLa **(A)** or A431 **(B)** cells stably expressing scrambled shRNA or ASNS shRNA with and without (Ctl) starvation of glutamine (-Q) or asparagine (-N) for the indicated times. **(C)** Immunoblot showing S6 ribosomal protein phosphorylation (S235/236) following glutamine and asparagine starvation of HeLa cells for the indicated times.

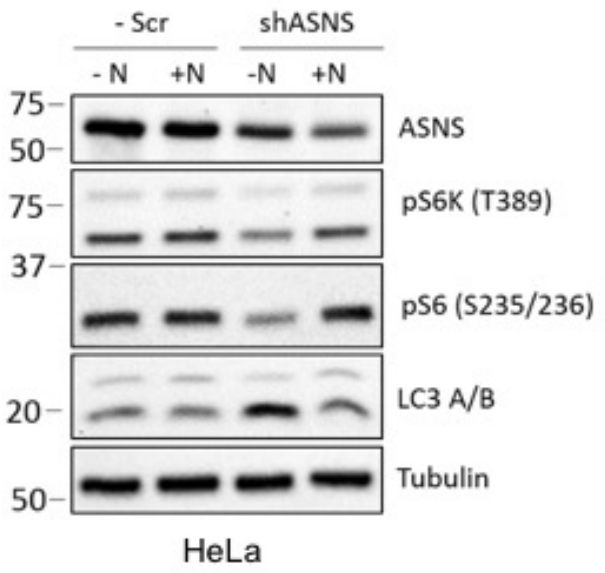

Figure 2-18. **Acute loss of ASNS expression results in reduced mTORC1 activity and increased autophagy.** Immunoblot of HeLa lysates 48 hours post doxycycline- induced expression of scrambled shRNA or ASNS shRNA in asparagine-free DMEM (-N) or DMEM supplemented with 0.1 mM asparagine (+N). Lysates were immunoblotted for autophagy marker LC3 II (bottom band), mTOR activity markers pS6K and pS6, and tubulin.

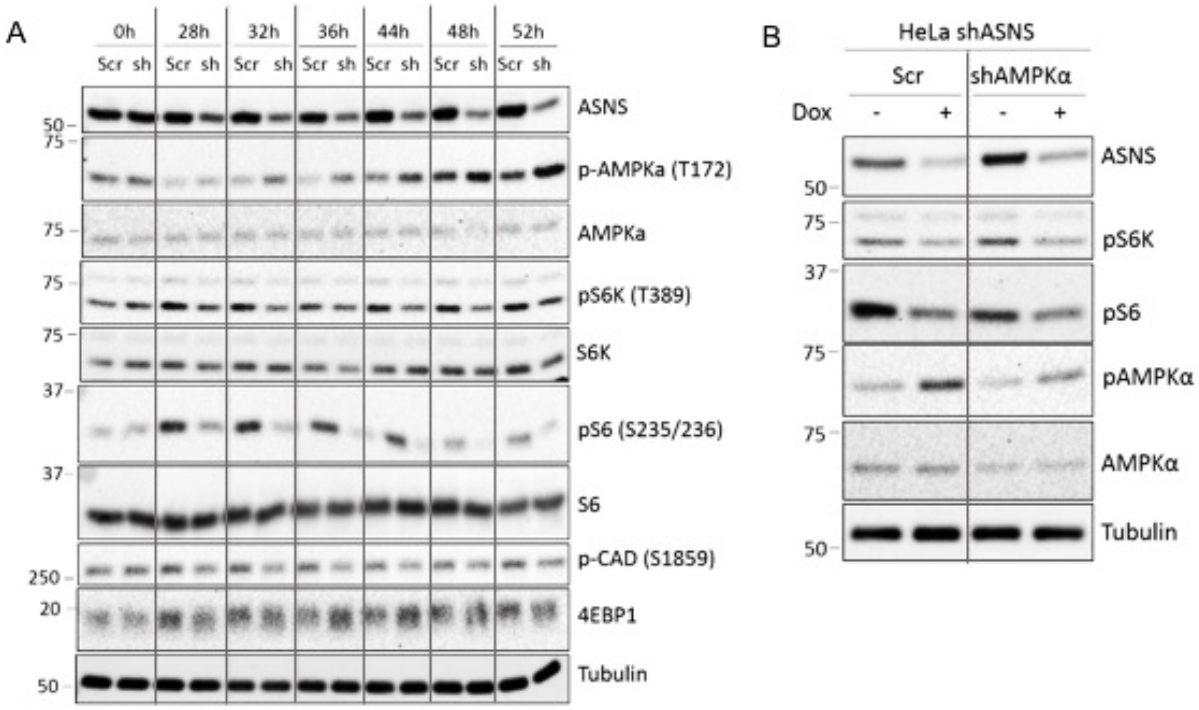

Figure 2-19. **AMPK activation is not responsible for altered mTORC1 activation with varying intracellular asparagine. (A)** Immunoblot showing ASNS, S6K phosphorylation (T389), S6 phosphorylation (S235/236), AMPKα phosphorylation (T172), and total S6K, S6, and AMPKα in HeLa cells at the indicated times post-doxycycline induction of scrambled shRNA (Scr) or ASNS shRNA expression. **(B)** Immunoblot showing ASNS, S6K phosphorylation (T389), S6 phosphorylation (S235/236), AMPKα phosphorylation (T172), and total AMPKα protein levels with or without a 48 hour doxycycline induction of ASNS shRNA in HeLa cells stably expressing scrambled or AMPKα shRNA.

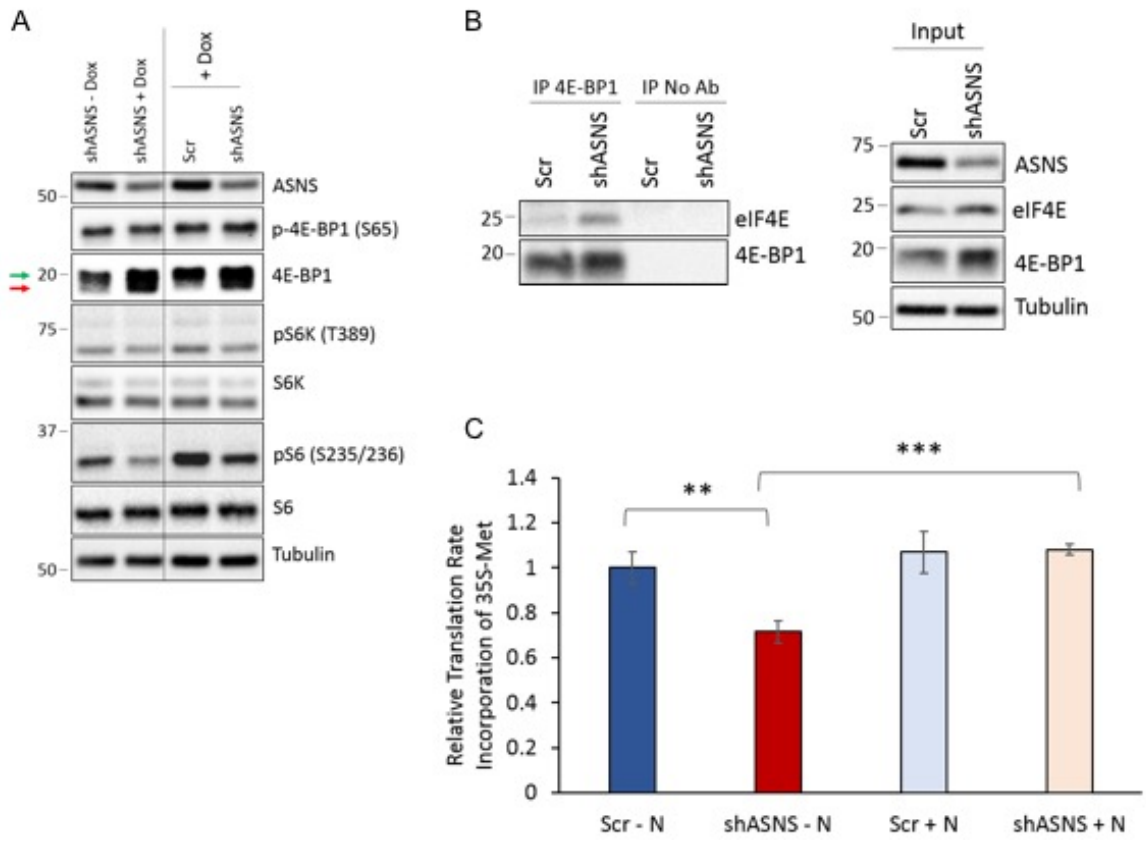

Figure 2-20. **Asparagine levels regulate mRNA translation.** (A) Immunoblot of HeLa lysates with (shASNS + Dox) and without (shASNS -Dox) a 48 hour induction of ASNS shRNA expression and HeLa lysates 48 hours after doxycycline induction of scrambled shRNA (Scr) or ASNS shRNA (shASNS). Lysates were immunoblotted for ASNS, phospho-4E-BP1 (S65), total 4E-BP1, phospho-S6K (T389), total S6K, phospho-S6 (S235/236), total S6, and tubulin. Arrow indicates phosphorylated form of 4E-BP1. **(B)** Immunoblot showing levels of eIF4E and 4E-BP1 immunoprecipitated with anti-4E-BP1 antibody (left panels) and in the input lysate (right panels) from HeLa cells 48 hours after doxycycline induction of scrambled shRNA (Scr) or ASNS shRNA (shASNS). **(C)** Relative rates of 35S-methionine incorporation into newly synthesized protein in HeLa cells 72 hours after doxycycline induction of scrambled shRNA (Scr) or ASNS shRNA (shASNS). . Error bars denote standard deviation of the mean. *$p < 0.05$; **$p < 0.01$; ***$p < 0.001$.

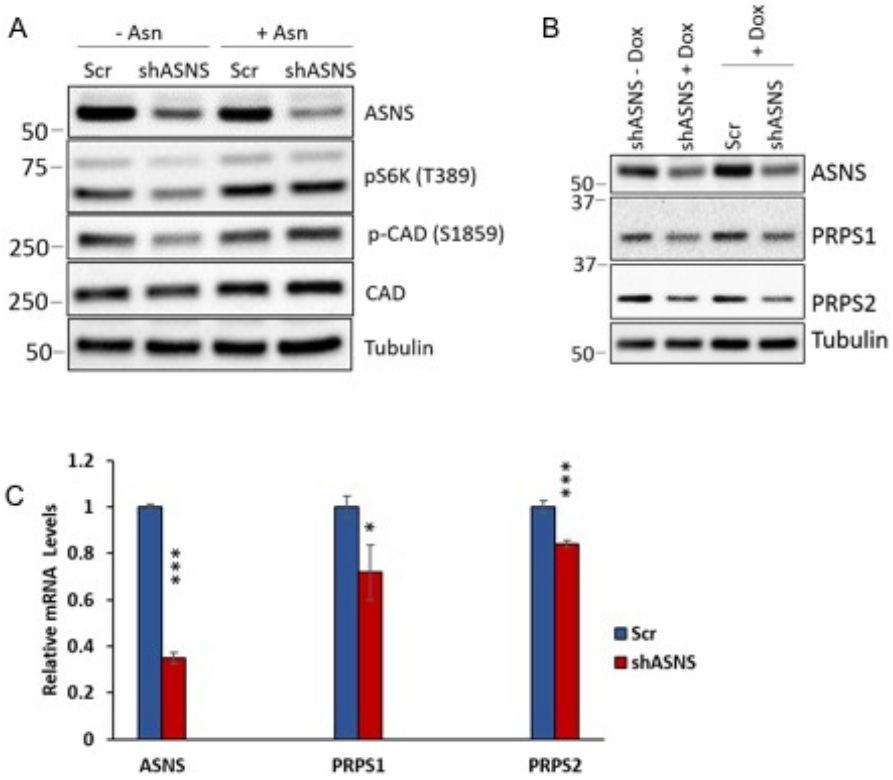

Figure 2-21. **Asparagine influences CAD phosphorylation and PRPS1/2 levels. (A)** Immunoblot of HeLa lysates 48 hours post doxycycline-induced expression of scrambled shRNA or ASNS shRNA in asparagine-free DMEM (-Asn) or DMEM supplemented with 0.1 mM asparagine (+Asn). Lysates were immunoblotted for mTOR activity marker pS6K, phospho-CAD (S1859), total CAD, and tubulin. **(B)** Immunoblot of HeLa lysates with (shASNS + Dox) and without (shASNS -Dox) a 48 hour induction of ASNS shRNA expression and HeLa lysates 48 hours after doxycycline induction of scrambled shRNA (Scr) or ASNS shRNA (shASNS). Lysates were immunoblotted for ASNS, PRPS1, PRPS2, and tubulin. **(C)** Relative PRPS1 and PRPS2 mRNA levels from HeLa cells 48 hours post-doxycycline induction of scrambled shRNA or ASNS shRNA. Quantitative real-time PCR was performed with primers specific to PRPS1 and PRPS2.

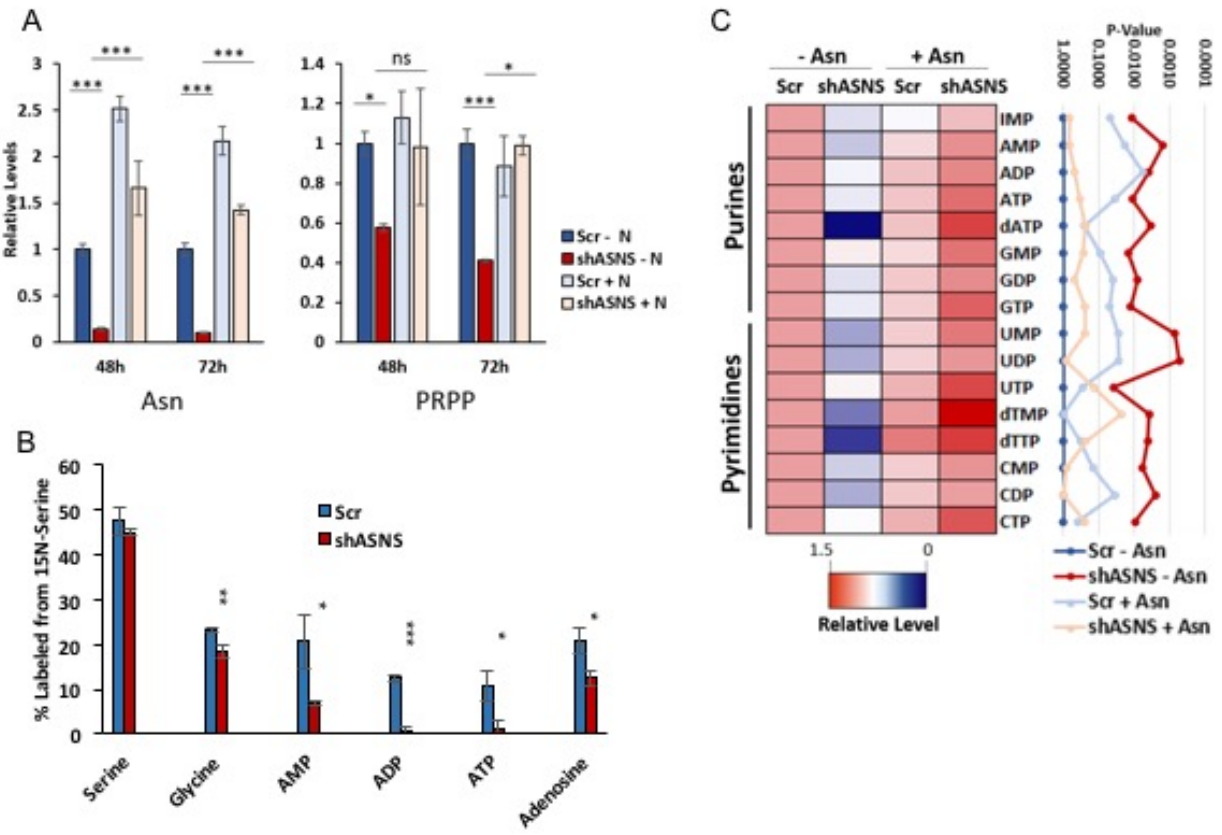

Figure 2-22. **(A)** Relative levels of asparagine and PRPP extracted from HeLa cells 48 and 72 hours after doxycycline induction of scrambled shRNA (Scr) or ASNS shRNA expression as measured by LC-MS. **(B)** Percentages of the indicated metabolites labeled with 15N extracted from HeLa cells labeled with exogenous 15N-serine (50:50 15N:14N) for 24 hours at 24 hours post-induction of scrambled shRNA (Scr) or ASNS shRNA expression. **(C)** Heatmap showing relative levels of the indicated intracellular metabolites extracted from HeLa cells 72 hours after doxycycline induction of scrambled shRNA (Scr) or ASNS shRNA expression as measured by LC-MS. Error bars denote standard deviation of the mean. *p < 0.05; **p < 0.01; ***p < 0.001.

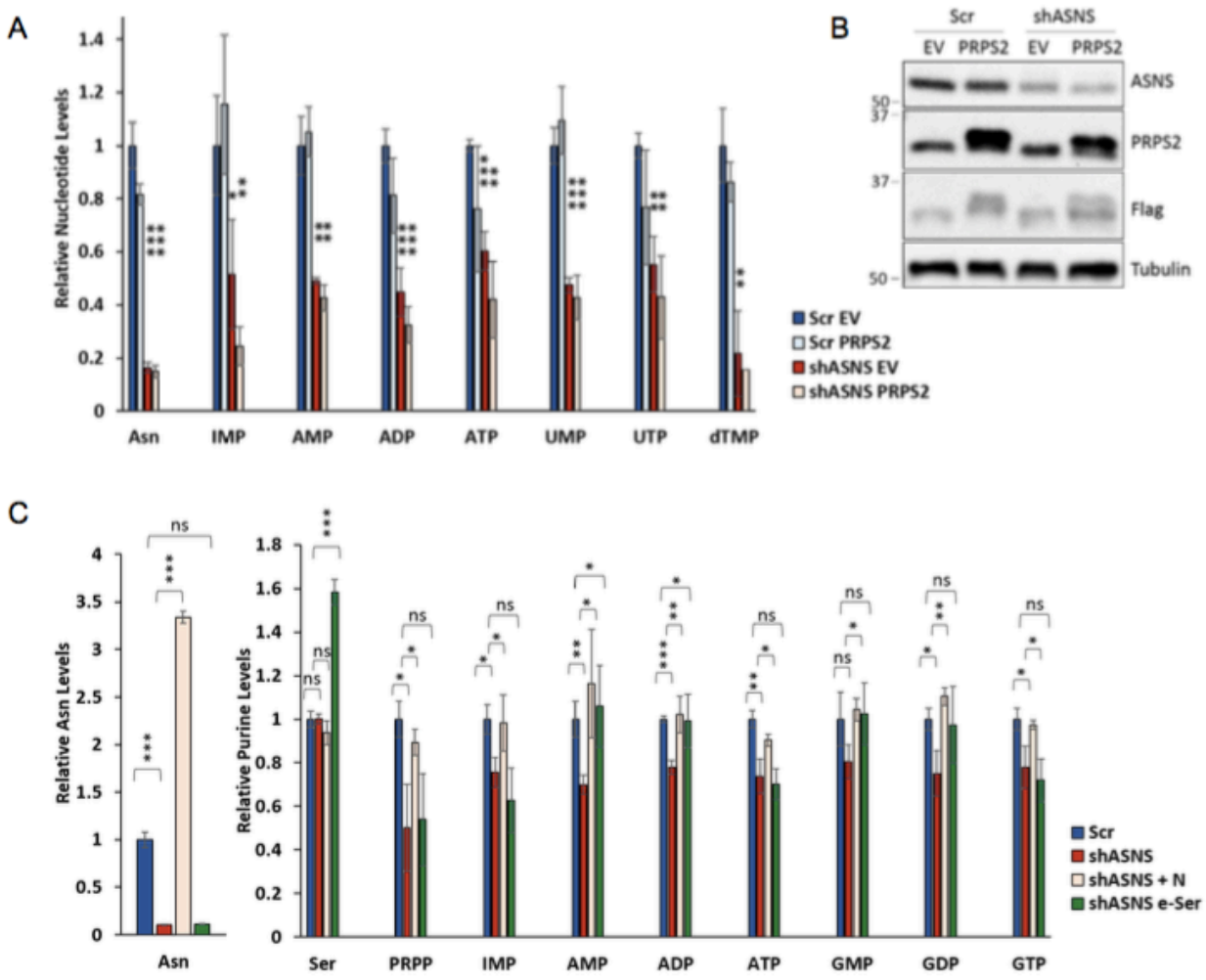

Figure 2-23. **(A)** Relative levels of the indicated intracellular metabolites extracted from HeLa cells stably expressing PRPS2 or possessing empty pLHCX vector (EV) 72 hours after doxycycline induction of scrambled shRNA (Scr) or ASNS shRNA expression as measured by LC-MS. **(B)** Immunoblot confirming PRPS2 expression in HeLa cells indicated in (A). **(C)** Relative levels of the indicated intracellular metabolites extracted from HeLa cells 48 hours after doxycycline induction of scrambled shRNA (Scr) or ASNS shRNA expression as measured by LC-MS. Error bars denote standard deviation of the mean. *p < 0.05; **p < 0.01; ***p < 0.001.

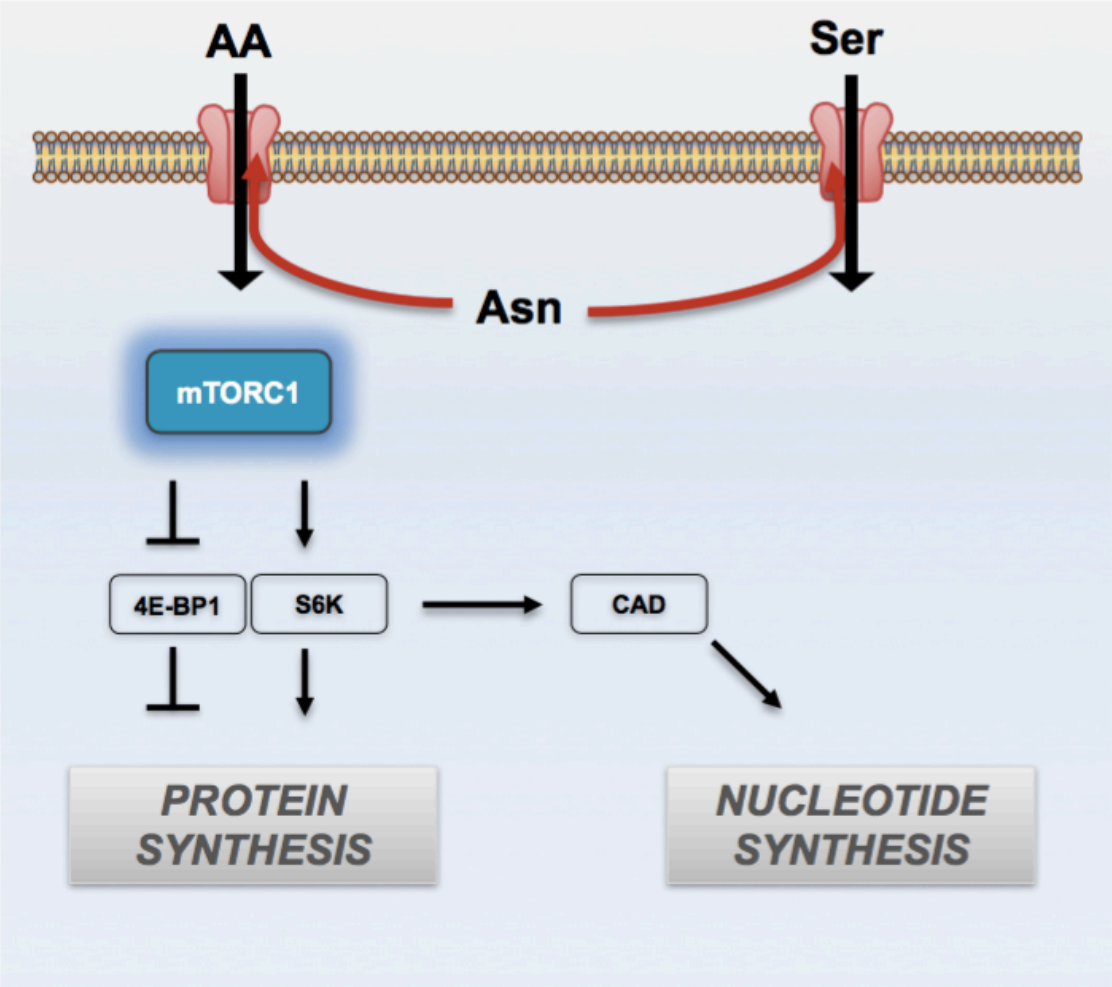

Figure 2-24. **Model illustrating asparagine contribution to protein synthesis and nucleotide synthesis.** Intracellular asparagine exchanges with amino acids (AA) and serine (Ser) to coordinate protein and nucleotide synthesis.

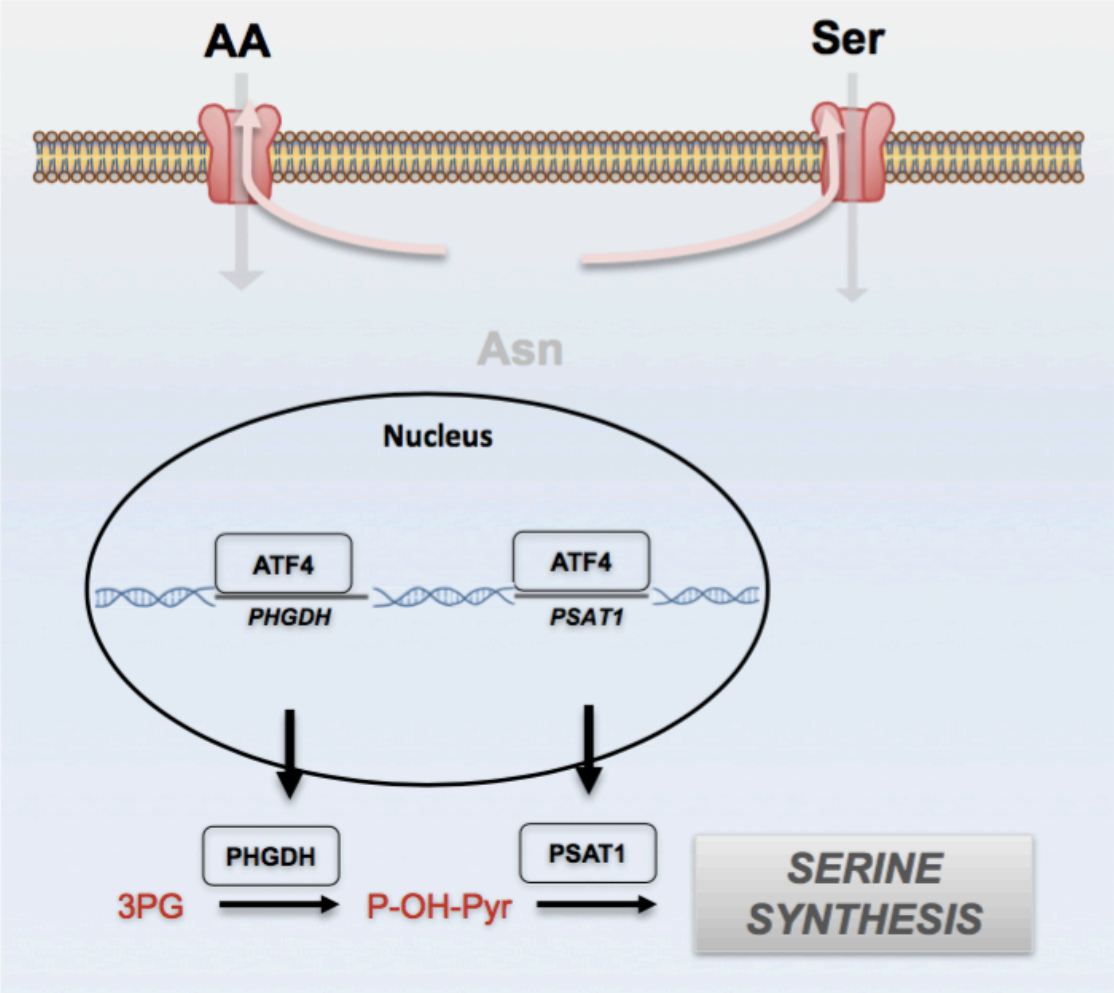

Figure 2-25. **Model illustrating ATF4 activation of serine synthesis pathway gene expression and serine synthesis pathway flux in response to low intracellular asparagine levels.**

REFERENCES

1. DeBerardinis RJ, Mancuso A, Daikhin E, Nissim I, Yudkoff M, Wehrli S, Thompson CB. Beyond aerobic glycolysis: transformed cells can engage in glutamine metabolism that exceeds the requirement for protein and nucleotide synthesis. Proc Natl Acad Sci U S A. 2007;104(49):19345-50. doi: 10.1073/pnas.0709747104. PubMed PMID: 18032601; PMCID: 2148292.

2. Chan WK, Lorenzi PL, Anishkin A, Purwaha P, Rogers DM, Sukharev S, Rempe SB, Weinstein JN. The glutaminase activity of L-asparaginase is not required for anticancer activity against ASNS-negative cells. Blood. 2014;123(23):3596-606. doi: 10.1182/blood-2013-10-535112. PubMed PMID: 24659632; PMCID: 4047499.

3. Lorenzi PL, Llamas J, Gunsior M, Ozbun L, Reinhold WC, Varma S, Ji H, Kim H, Hutchinson AA, Kohn EC, Goldsmith PK, Birrer MJ, Weinstein JN. Asparagine synthetase is a predictive biomarker of L-asparaginase activity in ovarian cancer cell lines. Mol Cancer Ther. 2008;7(10):3123-8. doi: 10.1158/1535-7163.MCT-08-0589. PubMed PMID: 18852115; PMCID: 4123961.

4. Holleman A, Cheok MH, den Boer ML, Yang W, Veerman AJ, Kazemier KM, Pei D, Cheng C, Pui CH, Relling MV, Janka-Schaub GE, Pieters R, Evans WE. Gene-expression patterns in drug-resistant acute lymphoblastic leukemia cells and response to treatment. N Engl J Med. 2004;351(6):533-42. doi: 10.1056/NEJMoa033513. PubMed PMID: 15295046.

5. Zhang J, Fan J, Venneti S, Cross JR, Takagi T, Bhinder B, Djaballah H, Kanai M, Cheng EH, Judkins AR, Pawel B, Baggs J, Cherry S, Rabinowitz JD, Thompson CB. Asparagine plays a critical role in regulating cellular adaptation to glutamine depletion. Mol Cell. 2014;56(2):205-18. doi: 10.1016/j.molcel.2014.08.018. PubMed PMID: 25242145; PMCID: 4224619.

6. Hettmer S, Schinzel AC, Tchessalova D, Schneider M, Parker CL, Bronson RT, Richards NG, Hahn WC, Wagers AJ. Functional genomic screening reveals asparagine dependence as a metabolic vulnerability in sarcoma. Elife. 2015;4. doi: 10.7554/eLife.09436. PubMed PMID: 26499495; PMCID: PMC4695385.

7. Gong SS, Guerrini L, Basilico C. Regulation of asparagine synthetase gene expression by amino acid starvation. Mol Cell Biol. 1991;11(12):6059-66. PubMed PMID: 1682798; PMCID: 361776.

8. Hutson RG, Kilberg MS. Cloning of rat asparagine synthetase and specificity of the amino acid-dependent control of its mRNA content. Biochem J. 1994;304 (Pt 3):745-50. PubMed PMID: 7818476; PMCID: 1137397.

9. Ye J, Kumanova M, Hart LS, Sloane K, Zhang H, De Panis DN, Bobrovnikova-Marjon E, Diehl JA, Ron D, Koumenis C. The GCN2-ATF4 pathway is critical for tumour cell survival and proliferation

in response to nutrient deprivation. EMBO J. 2010;29(12):2082-96. doi: 10.1038/emboj.2010.81. PubMed PMID: 20473272; PMCID: 2892366.

10. Gross MI, Demo SD, Dennison JB, Chen L, Chernov-Rogan T, Goyal B, Janes JR, Laidig GJ, Lewis ER, Li J, Mackinnon AL, Parlati F, Rodriguez ML, Shwonek PJ, Sjogren EB, Stanton TF, Wang T, Yang J, Zhao F, Bennett MK. Antitumor activity of the glutaminase inhibitor CB-839 in triple-negative breast cancer. Mol Cancer Ther. 2014;13(4):890-901. doi: 10.1158/1535-7163.MCT-13-0870. PubMed PMID: 24523301.

11. Robinson MM, McBryant SJ, Tsukamoto T, Rojas C, Ferraris DV, Hamilton SK, Hansen JC, Curthoys NP. Novel mechanism of inhibition of rat kidney-type glutaminase by bis-2-(5-phenylacetamido-1,2,4-thiadiazol-2-yl)ethyl sulfide (BPTES). Biochem J. 2007;406(3):407-14. doi: 10.1042/BJ20070039. PubMed PMID: 17581113; PMCID: 2049044.

12. Wang JB, Erickson JW, Fuji R, Ramachandran S, Gao P, Dinavahi R, Wilson KF, Ambrosio AL, Dias SM, Dang CV, Cerione RA. Targeting mitochondrial glutaminase activity inhibits oncogenic transformation. Cancer Cell. 2010;18(3):207-19. doi: 10.1016/j.ccr.2010.08.009. PubMed PMID: 20832749; PMCID: 3078749.

13. Tardito S, Oudin A, Ahmed SU, Fack F, Keunen O, Zheng L, Miletic H, Sakariassen PO, Weinstock A, Wagner A, Lindsay SL, Hock AK, Barnett SC, Ruppin E, Morkve SH, Lund-Johansen M, Chalmers AJ, Bjerkvig R, Niclou SP, Gottlieb E. Glutamine synthetase activity fuels nucleotide biosynthesis and supports growth of glutamine-restricted glioblastoma. Nat Cell Biol. 2015;17(12):1556-68. doi: 10.1038/ncb3272. PubMed PMID: 26595383; PMCID: PMC4663685.

14. Nicklin P, Bergman P, Zhang B, Triantafellow E, Wang H, Nyfeler B, Yang H, Hild M, Kung C, Wilson C, Myer VE, MacKeigan JP, Porter JA, Wang YK, Cantley LC, Finan PM, Murphy LO. Bidirectional transport of amino acids regulates mTOR and autophagy. Cell. 2009;136(3):521-34. doi: 10.1016/j.cell.2008.11.044. PubMed PMID: 19203585; PMCID: 3733119.

15. Duran RV, Oppliger W, Robitaille AM, Heiserich L, Skendaj R, Gottlieb E, Hall MN. Glutaminolysis activates Rag-mTORC1 signaling. Mol Cell. 2012;47(3):349-58. doi: 10.1016/j.molcel.2012.05.043. PubMed PMID: 22749528.

16. Jewell JL, Kim YC, Russell RC, Yu FX, Park HW, Plouffe SW, Tagliabracci VS, Guan KL. Metabolism. Differential regulation of mTORC1 by leucine and glutamine. Science. 2015;347(6218):194-8. doi: 10.1126/science.1259472. PubMed PMID: 25567907; PMCID: 4384888.

17. Bar-Peled L, Schweitzer LD, Zoncu R, Sabatini DM. Ragulator is a GEF for the rag GTPases that signal amino acid levels to mTORC1. Cell. 2012;150(6):1196-208. doi: 10.1016/j.cell.2012.07.032. PubMed PMID: 22980980; PMCID: 3517996.

18. Zoncu R, Efeyan A, Sabatini DM. mTOR: from growth signal integration to cancer, diabetes and ageing. Nat Rev Mol Cell Biol. 2011;12(1):21-35. doi: 10.1038/nrm3025. PubMed PMID: 21157483; PMCID: 3390257.

19. Wang S, Tsun ZY, Wolfson RL, Shen K, Wyant GA, Plovanich ME, Yuan ED, Jones TD, Chantranupong L, Comb W, Wang T, Bar-Peled L, Zoncu R, Straub C, Kim C, Park J, Sabatini BL, Sabatini DM. Metabolism. Lysosomal amino acid transporter SLC38A9 signals arginine sufficiency to mTORC1. Science. 2015;347(6218):188-94. doi: 10.1126/science.1257132. PubMed PMID: 25567906; PMCID: PMC4295826.

20. Dibble CC, Manning BD. Signal integration by mTORC1 coordinates nutrient input with biosynthetic output. Nat Cell Biol. 2013;15(6):555-64. doi: 10.1038/ncb2763. PubMed PMID: 23728461; PMCID: PMC3743096.

21. Ma XM, Blenis J. Molecular mechanisms of mTOR-mediated translational control. Nat Rev Mol Cell Biol. 2009;10(5):307-18. doi: 10.1038/nrm2672. PubMed PMID: 19339977.

22. Yamaguchi S, Ishihara H, Yamada T, Tamura A, Usui M, Tominaga R, Munakata Y, Satake C, Katagiri H, Tashiro F, Aburatani H, Tsukiyama-Kohara K, Miyazaki J, Sonenberg N, Oka Y. ATF4-mediated induction of 4E-BP1 contributes to pancreatic beta cell survival under endoplasmic reticulum stress. Cell Metab. 2008;7(3):269-76. doi: 10.1016/j.cmet.2008.01.008. PubMed PMID: 18316032.

23. Han J, Back SH, Hur J, Lin YH, Gildersleeve R, Shan J, Yuan CL, Krokowski D, Wang S, Hatzoglou M, Kilberg MS, Sartor MA, Kaufman RJ. ER-stress-induced transcriptional regulation increases protein synthesis leading to cell death. Nat Cell Biol. 2013;15(5):481-90. doi: 10.1038/ncb2738. PubMed PMID: 23624402; PMCID: PMC3692270.

24. Maddocks OD, Labuschagne CF, Adams PD, Vousden KH. Serine Metabolism Supports the Methionine Cycle and DNA/RNA Methylation through De Novo ATP Synthesis in Cancer Cells. Mol Cell. 2016;61(2):210-21. doi: 10.1016/j.molcel.2015.12.014. PubMed PMID: 26774282.

25. Ben-Sahra I, Howell JJ, Asara JM, Manning BD. Stimulation of de novo pyrimidine synthesis by growth signaling through mTOR and S6K1. Science. 2013;339(6125):1323-8. doi: 10.1126/science.1228792. PubMed PMID: 23429703; PMCID: 3753690.

26. Cunningham JT, Moreno MV, Lodi A, Ronen SM, Ruggero D. Protein and nucleotide biosynthesis are coupled by a single rate-limiting enzyme, PRPS2, to drive cancer. Cell. 2014;157(5):1088-103. doi: 10.1016/j.cell.2014.03.052. PubMed PMID: 24855946; PMCID: 4140650.

27. Stegink LD, Filer LJ, Jr., Brummel MC, Baker GL, Krause WL, Bell EF, Ziegler EE. Plasma amino acid concentrations and amino acid ratios in normal adults and adults heterozygous for

phenylketonuria ingesting a hamburger and milk shake meal. Am J Clin Nutr. 1991;53(3):670-5. PubMed PMID: 2000820.

28. Braas D, Ahler E, Tam B, Nathanson D, Riedinger M, Benz MR, Smith KB, Eilber FC, Witte ON, Tap WD, Wu H, Christofk HR. Metabolomics strategy reveals subpopulation of liposarcomas sensitive to gemcitabine treatment. Cancer Discov. 2012;2(12):1109-17. doi: 10.1158/2159-8290.CD-12-0197. PubMed PMID: 23230188; PMCID: PMC3531869.

29. Smith KB, Tran LM, Tam BM, Shurell EM, Li Y, Braas D, Tap WD, Christofk HR, Dry SM, Eilber FC, Wu H. Novel dedifferentiated liposarcoma xenograft models reveal PTEN down-regulation as a malignant signature and response to PI3K pathway inhibition. Am J Pathol. 2013;182(4):1400-11. doi: 10.1016/j.ajpath.2013.01.002. PubMed PMID: 23416162; PMCID: PMC3620414.

30. Abel EV, Basile KJ, Kugel CH, 3rd, Witkiewicz AK, Le K, Amaravadi RK, Karakousis GC, Xu X, Xu W, Schuchter LM, Lee JB, Ertel A, Fortina P, Aplin AE. Melanoma adapts to RAF/MEK inhibitors through FOXD3-mediated upregulation of ERBB3. J Clin Invest. 2013;123(5):2155-68. doi: 10.1172/JCI65780. PubMed PMID: 23543055; PMCID: 3635724.

31. Basile KJ, Abel EV, Dadpey N, Hartsough EJ, Fortina P, Aplin AE. In vivo MAPK reporting reveals the heterogeneity in tumoral selection of resistance to RAF inhibitors. Cancer Res. 2013;73(23):7101-10. doi: 10.1158/0008-5472.CAN-13-1628. PubMed PMID: 24121492; PMCID: 3851924.

Chapter 3

Asparagine is a Fundamental Product of Respiration

INTRODUCTION

We have shown that asparagine is critical for cancer cell proliferation through a role in amino acid import (Chapter 2). This asparagine function may explain the clinical efficacy of extracellular-acting asparaginase in the treatment of leukemia. Although asparaginase is effective as a therapeutic for cancers that obtain the majority of their asparagine from the environment, such as leukemia, cancers that are capable of synthesizing asparagine de novo via ASNS are less responsive to asparaginase therapy(1). Moreover, elevated ASNS expression, and presumably increased *de novo* asparagine synthesis, is associated with leukemic asparaginase resistance(2). Because cells can obtain asparagine from the environment or synthesize asparagine *de novo*, targeting both sources is critical for effectively exploiting tumor asparagine dependence. In support of this approach, genetic silencing of ASNS in sarcoma cells combined with depletion of plasma asparagine levels via asparaginase was recently shown to blunt tumor growth *in vivo*(3).

Cellular respiration couples nutrient oxidation to ATP production through oxidative phosphorylation. Nutrients are oxidized to CO_2 through the tricarboxylic acid (TCA) cycle. This process is dependent on NAD+ and FAD, which extract electrons from nutrients and transfer them to the electron transport chain (ETC) using oxygen as the final electron acceptor. The proton gradient across the inner mitochondrial membrane generated by the flow of electrons through the chain drives ATP synthesis. Complete oxidation of glucose to CO_2 through oxidative phosphorylation generates ~36 molecules of ATP from one molecule of glucose, whereas glycolytic metabolism of glucose to lactate yields only 2 molecules of ATP. Although most cancer cells convert the majority of consumed glucose to lactate, concurrent respiration is essential: suppressing respiration through ETC inhibition blocks proliferation(4-8).

Recent literature has shown that ATP synthesis via the ETC is dispensable for cancer cell proliferation. Rather, aspartate synthesis requirements explain the reliance of proliferating cells on respiration(4, 5). TCA cycle intermediates, in addition to yielding reducing power for ATP synthesis, are biosynthetic precursors for amino acids, fatty acids, and nucleotides, all of which are required for cell proliferation. Upon ETC inhibition, electron acceptors are limiting, resulting in compromised NAD+ recycling (Figure 3-1) and impaired flux through the TCA cycle. Aspartate, which is synthesized from TCA cycle-generated oxaloacetate (Figure 3-1B), is depleted upon ETC inhibition, as are aspartate-derived nucleotides. Notably, supplementing cell culture medium with supraphysiological levels of aspartate rescues the proliferation impairment caused by treatment with various ETC inhibitors without rescuing the redox state(4, 5). These studies indicate that aspartate is the limiting factor for proliferation with ETC inhibition and suggest proliferating cells require respiration primarily for aspartate synthesis and aspartate-dependent nucleotide synthesis.

However, in addition to contributing carbon and nitrogen to nucleotide synthesis, another cellular use of aspartate is as a substrate for ASNS, which converts aspartate and glutamine to asparagine and glutamate (Figure 2-5D). This raises the possibility that aspartate synthesis in proliferating cells may also have another benefit: maintenance of cellular asparagine levels. Here we show that in addition to reducing aspartate levels, ETC inhibition also reduces intracellular asparagine levels. Moreover, comparable to supraphysiologic aspartate supplementation, physiologic levels of exogenous asparagine rescue proliferation upon treatment with various ETC inhibitors in the absence of exogenous aspartate and without rescuing intracellular aspartate levels. Our data suggest that aspartate rescue of proliferation upon ETC inhibition may be due to conversion of aspartate to asparagine via ASNS. The data further suggest that, by limiting synthesis of ASNS substrate aspartate, ETC inhibition may be an effective means of impairing de novo asparagine synthesis therapeutically.

RESULTS

ETC inhibition depletes intracellular asparagine

Aspartate is a precursor for protein, nucleotide, and asparagine synthesis. It is unclear which of these biosynthetic contributions are limiting for proliferation upon cellular aspartate depletion with ETC inhibition. To ascertain cellular aspartate demand for *de novo* asparagine synthesis, we measured cell aspartate production rates in the presence or absence of exogenous asparagine and with or without ASNS knockdown. Providing exogenous asparagine, and thereby obviating the need for aspartate to serve as a substrate for ASNS, causes aspartate production to decrease by approximately 60 percent (Figure 3-2). Conversely, depletion of intracellular asparagine levels through ASNS knockdown in the absence of exogenous asparagine increases aspartate production by approximately 50 percent, indicating that cellular demand for asparagine biosynthesis influences aspartate production rates. Given that exogenous asparagine supplementation does not reduce proliferation (Figure 2-5C), these results suggest that aspartate levels sufficient for nucleotide synthesis may be insufficient to satisfy cellular asparagine requirements.

ETC inhibition has been shown to reduce intracellular aspartate and nucleotide levels(4, 5). Because asparagine is derived from aspartate, we examined the effect of ETC inhibition on asparagine. In addition to reducing aspartate levels, inhibition of the ETC with complex I inhibitor rotenone depletes intracellular asparagine in HeLa cells to levels that impair proliferation with ASNS shRNA expression (Figure 3-3A). Expression of ATF4 target genes is also elevated with rotenone treatment, consistent with asparagine depletion (Figure 3-3B). These data raise the possibility that proliferation impairment upon ETC inhibition may be a function of asparagine, rather than aspartate, limitation (Figure 3-1A).

Exogenous asparagine rescues cell proliferation upon ETC inhibition

To determine whether intracellular asparagine depletion contributes to the decreased proliferation observed with ETC inhibition, we inhibited the ETC in HeLa cells in the presence or absence of exogenous aspartate or asparagine. Comparable to supraphysiologic aspartate supplementation (20 mM), physiologic levels of exogenous asparagine (0.1 mM) rescue proliferation upon treatment with various ETC inhibitors, including rotenone, oligomycin, antimycin A, and metformin, in the absence of exogenous aspartate (Figures 3-4 and 3-5). Medium supplementation with either aspartate or asparagine rescues intracellular asparagine (Figure 3-6) and ATF4 activity (Figure 3-3B) upon rotenone treatment. Importantly, exogenous asparagine rescues ETC inhibition proliferation defects without rescuing aspartate levels (Figure 3-6). These data suggest that 1) asparagine, not aspartate, may be limiting for proliferation upon ETC inhibition; 2) aspartate rescue of proliferation upon ETC inhibition may be due to conversion of aspartate to asparagine via ASNS; and 3) asparagine synthesis may be a fundamental purpose of respiration in proliferating cells.

Exogenous asparagine and aspartate rescue mTORC1 activity and nucleotide levels upon ETC inhibition

Because intracellular asparagine exchanges with extracellular amino acids, reduced asparagine synthesis with ETC inhibition likely causes reduced amino acid uptake. We therefore examined mTORC1 activity with ETC inhibition. HeLa cell rotenone treatment decreases mTORC1 activation in a manner that is rescued by both exogenous asparagine and exogenous aspartate (Figure 3-7A), raising the possibility that mTORC1 inhibition due to asparagine depletion is responsible for the growth defects observed with ETC inhibition.

Although aspartate is a substrate for both purine and pyridine synthesis, asparagine also contributes to nucleotide synthesis through exchange with serine, a nucleotide precursor,

through regulation of CAD activity downstream of mTORC1 activation, and through regulation of PRPS1 and PRPS2 levels (Chapter 2). Confirming recent literature(4, 5), we observed rescue of nucleotide levels by exogenous aspartate with rotenone treatment (Figure 3-7B). However, exogenous asparagine, in the absence of exogenous aspartate and without rescuing intracellular aspartate levels, similarly rescues nucleotides with ETC inhibition (Figure 3-7B).

PRPS1/2 catalyze the conversion of ribose-5-phosphate to PRPP. Rotenone treatment results in ribose-5-phoshate accumulation and reduced PRPP (Figure 3-8), suggesting that PRPS activity may be rate limiting with ETC inhibition. Both asparagine and aspartate rescue this apparent PRPS block. Notably, PRPS activity precedes incorporation of aspartate atoms into nucleotides. This raises the possibility that aspartate is limiting for asparagine-induced PRPS activity rather than as a direct substrate for nucleotide biosynthesis. Collectively, our data suggest that the nucleotide deficiency observed with ETC inhibition may be, at least in large part, a consequence of asparagine depletion rather than aspartate depletion. Moreover, the data suggest that aspartate conversion to asparagine via ASNS contributes to aspartate rescue of nucleotide deficiency with ETC inhibition.

DISCUSSION

Here we provide evidence that asparagine synthesis is a fundamental purpose of respiration. We show that ETC inhibition results in intracellular asparagine depletion, and that exogenous asparagine supplementation rescues proliferation defects caused by various ETC inhibitors.

Aspartate is limiting for asparagine synthesis

We provide evidence that aspartate is limiting for the ASNS reaction upon ETC inhibition and that aspartate rescue of ETC inhibition is primarily due to aspartate-dependent asparagine synthesis. Without rescuing intracellular aspartate levels, exogenous asparagine rescues

nucleotide deficiency associated with ETC inhibition similarly to exogenous aspartate. Exogenous aspartate supplementation rescues intracellular asparagine levels, ATF4 activity, and mTORC1 similarly to exogenous asparagine supplementation. Our results suggest reduced mTORC1 activity and nucleotide synthesis downstream of asparagine deficiency may cause the proliferation impairment with ETC inhibition. Although the data are consistent with ASNS-dependent asparagine synthesis being a primary purpose of aspartate, future experiments will assess aspartate rescue of ETC inhibition-associated defects in ASNS knockout cells that cannot synthesize asparagine.

Targeting asparagine synthesis with ETC inhibitors

Targeting cancer cell asparagine dependence with asparaginase, which hydrolyzes extracellular asparagine, has had limited success. Tumors that express ASNS and are capable of *de novo* asparagine synthesis are insensitive to the therapy, and low-ASNS-expressing cancers often develop resistance to asparaginase through ASNS upregulation. Combination targeting of asparagine uptake and synthesis would be expected to have pan-tumor effectiveness and lacks foreseeable resistance mechanisms. Our results suggest that ETC inhibition is an effective means of inhibiting *de novo* asparagine synthesis. Metformin, which is currently used in the clinic to treat patients with type 2 diabetes, inhibits complex I of the ETC. We hypothesize that the inability of the cell to synthesize or consume asparagine due the combinatorial effects of metformin and asparaginase will prevent tumor growth. In addition, metformin may be effective in combination with a low-asparagine diet, which has recently been shown to lower blood asparagine levels(9). In support of this hypothesis, removal of asparagine from the cell culture medium sensitizes HeLa cells to metformin treatment *in vitro* (Figure 3-5).

Possible resistance mechanisms

Tumor xenograft experiments in mice are currently being performed to examine whether these combinations effectively deplete tumor asparagine to reduce tumor growth. Although our *in vitro* experiments showed that ETC inhibition decreases proliferation of cultured cancer cells in medium containing supraphysiologic levels of pyruvate, it is worth noting that tumors may become resistant to the combination of metformin and exogenous asparagine depletion by increasing pyruvate uptake. Supraphysiologic levels of pyruvate can restore redox homeostasis by acting as an electron acceptor to rescue proliferation upon ETC inhibition(4, 5, 10). Therefore, increased pyruvate uptake could potentially restore intracellular aspartate levels. Moreover, tumors characterized by loss-of-function mutations in TCA cycle enzymes succinate dehydrogenase (SDH) and fumarate hydratase (FH) increase reliance on pyruvate uptake and pyruvate carboxylase activity to generate aspartate(11). An additional potential resistance mechanism is consumption of extracellular aspartate generated from asparaginase hydrolysis of asparagine. However, particularly high concentrations of exogenous aspartate (10-20 mM) are required to rescue intracellular aspartate and growth upon ETC inhibition(4, 5). Because blood asparagine levels range from 0.05-0.1 mM, it is unlikely that asparaginase treatment will rescue intracellular aspartate levels upon metformin treatment.

EXPERIMENTAL PROCEDURES

Cell lines and culture conditions. HeLa cells (ATCC) were cultured in DMEM containing 1 mM pyruvate and supplemented with 10% fetal bovine serum and 1% penicillin-streptomycin, unless otherwise stated.

Proliferation assays. Cells were seeded in triplicate in 6-well plates at 5 x 10^4 cells/well. 24 hours after seeding, the culture medium was replaced with 3 mL of DMEM containing the indicated concentrations of rotenone, oligomycin, antimycin A, metformin, or DMSO (vehicle control), with or without 20 mM aspartate or 0.1 mM asparagine. Cells were counted at 0 hours and 72 hours post-medium change (for rotenone, oligomycin, and antimycin A) or every 24 hours for 96 hours (metformin) using a Beckman Coulter particle counter.

Intracellular metabolite extraction and analysis. Cells were seeded in 6-well plates, and metabolites were extracted at 70-80% confluence. When heavy isotope labeling was performed, medium was replaced 24 hours prior to extraction with medium containing the labeled metabolite. Cells were washed with ice-cold 150 mM ammonium acetate, and scraped off the plate in 800 µl ice-cold 50% methanol. 10 nmol norvaline was added as an internal standard, followed by 400 µl chloroform. After vigorous vortexing, the samples were centrifuged at maximum speed, the aqueous layer was transferred to a glass vial, and the metabolites were dried under vacuum. Metabolites were resuspended in 50 µL 70% acetonitrile (ACN) and 5 µL of this solution used for the mass spectrometer-based analysis. The analysis was performed on a Q Exactive (Thermo Scientific) in polarity-switching mode with positive voltage 4.0 kV and negative voltage 4.0 kV. The mass spectrometer was coupled to an UltiMate 3000RSLC (Thermo Scientific) UHPLC system. Mobile phase A was 5 mM NH4AcO, pH 9.9, B) was ACN, and the separation achieved on a Luna 3mm NH2 100A (150 x 2.0 mm) (Phenomenex) column. The flow was 200 µL / min, and the gradient ran from 15% A to 95% A in 18 min, followed by an isocratic step for 9 min and re-equilibration for 7 min. Metabolites were detected and quantified as area under the curve (AUC) based on retention time and accurate mass (≤ 3 ppm) using the TraceFinder 3.1 (Thermo Scientific) software.

Aspartate production measurements. For aspartate export measurements, 5 µL medium was mixed with 800 µl ice-cold 50% methanol. 10 nmol norvaline was added as an internal standard, followed by 400 µl chloroform. After vigorous vortexing, the samples were centrifiuged at maximum speed, the aqueous layer was transferred to a glass vial, and the metabolites were dried under vacuum. Metabolites were resuspended in 100 µL 70% acetonitrile (ACN) and 5 µL of this solution used for the mass spectrometer-based analysis, as described above for intracellular metabolites. The experiment was initiated by the addition of fresh medium to the cells, and blank medium from a cell-free plate was included in the analysis.

Cell lysis and immunoblotting. Cells were lysed in buffer containing 50 mM Tris pH 7.4, 1% Nonidet P-40, 0.25% sodium deoxycholate, 1 mM EDTA, 150 mM NaCl, 1 mM dithiothreitol, 1 mM sodium orthovanadate, 20 mM sodium fluoride, 10 mM sodium pyrophosphate, 10 mM beta-glycerophosphate, 2 µg/ml aprotinin, 2µg/ml leupeptin and 0.7 µg/ml pepstatin. Western blot analysis was performed using standard protocols, and the following commercial antibodies were used as probes: ASNS (Proteintech 14681-1-AP, 1:1000), phospho-T389 S6 kinase (Cell Signaling 9234, 1:500), phospho-S235/235 S6 ribosomal protein (Cell Signaling 4858, 1:3000), PHGDH (Cell Signaling 13428, 1:1000), PSAT1 (Abnova H00029968-A01, 1:500), and α-tubulin (Sigma T6074, 1:10000).

Inducible shRNA-mediated ASNS knockdown. shRNA oligonucleotides (shASNS 5'-CACCGCTGTATGTTCAGAAGCTAAATTCAAGAGATTTAGCTTCTGAACATACAGC-3' and 5'-AAAAGCTGTATGTTCAGAAGCTAAATCTCTTGAATTTAGCTTCTGAACATACAGC-3';
and shScramble 5'-CACCGTAGCGACTAAACACATCAATTCAAGAGATTGATGTGTTTAGTCGCTA-3' and 5'-AAAATAGCGACTAAACACATCAATCTCTTGAATTGATGTGTTTAGTCGCTAC-3') were annealed and ligated into pENTR™/H1/TO vector (Invitrogen #K4920-00) following the BLOCK-

iT™ Inducible H1 RNAi Entry Vector Kit manual. Resulting shRNA constructs were recombined into pLentipuro/BLOCK-iT-DEST using Gateway® LR Clonase II® (Invitrogen #11791-020). pLentipuro/BLOCK-iT-DEST is a modification of pLenti4/BLOCK-iT-DEST (Invitrogen #K4925-00) wherein the SV40 promoter/zeocin resistance cassette was replaced with the human PGK promoter/puromycin resistance gene and the cPPT/WPRE elements were added, and was kindly provided by Dr. Andrew Aplin (Thomas Jefferson University, Kimmel Cancer Center)(12, 13). Recombinant lentiviruses were packaged in 293T cells by co-transfecting 4 µg each of lentivirus plasmid with expression vectors containing the *gag*/*pol*, *rev* and *vsvg* genes. Lentivirus was harvested 48 hours after transfection and added to subconfluent HeLa cells with 4 ug/ml polybrene for 16 hours. Cells were selected in 2 ug/ml puromycin for 1 week. Doxycycline induction of knockdown is control by the Tet repressor (TetR) protein expressed from the pLenti0.3/EF/GW/IVS-Kozak-TetR-P2A-Bsd vector, which was constructed by Dr. Ethan Abel and was kindly provided by Dr. Diane M. Simeone (University of Michigan, Translational Oncology Program). Knockdown was induced with 25 ng/ml doxycycline.

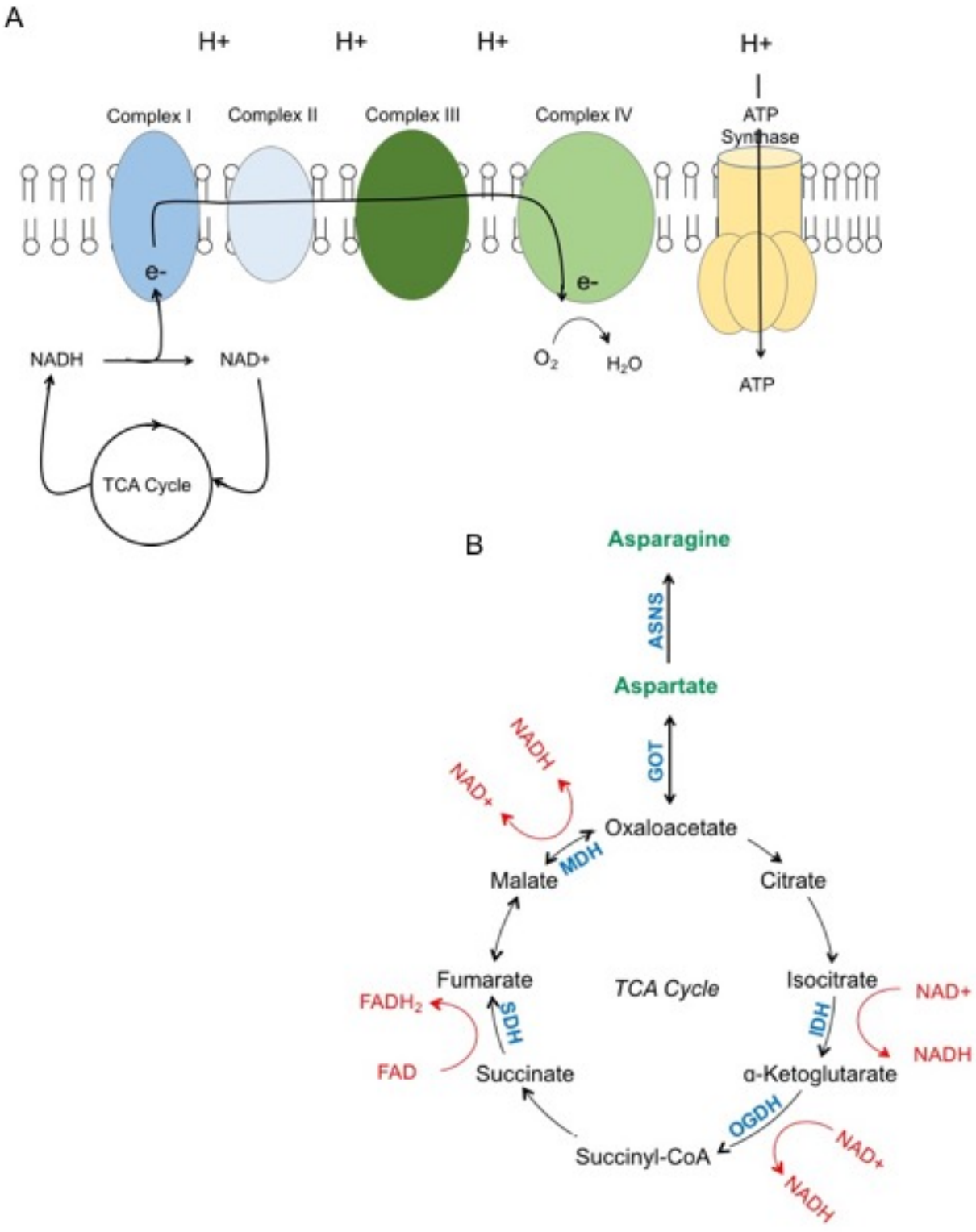
A
H+
H+
H+
H+
Complex I
Complex II
Complex III
Complex IV
ATP Synthase
e-
e-
NADH
NAD+
O_2
H_2O
ATP
TCA Cycle
B
Asparagine
ASNS
Aspartate
GOT
NADH
NAD+
Oxaloacetate
MDH
Malate
Citrate
Fumarate
TCA Cycle
Isocitrate
NAD+
NADH
IDH
$FADH_2$
FAD
SDH
Succinate
α-Ketoglutarate
OGDH
NAD+
NADH
Succinyl-CoA

Figure 3-1. **Reduced recycling of NAD+ with electron transport chain inhibition impairs TCA cycle flux and aspartate synthesis**. **(A)** Diagram of the electron transport chain (ETC). Electrons are transferred to the chain via NADH and $FADH_2$, with oxygen as the final electron acceptor. Electron transfer recycles NAD+ and FAD (not shown), which are required for reactions of the TCA cycle. **(B)** Diagram of the TCA cycle. NAD^+- and FAD-dependent reactions are indicated in red. Synthesis of aspartate has been shown to be a fundamental purpose of cellular respiration. Aspartate and asparagine (shown in green) each rescue proliferation with ETC inhibition, suggesting that reduced aspartate conversion to asparagine via ASNS may be responsible for ETC inhibition-mediated proliferation impairment.

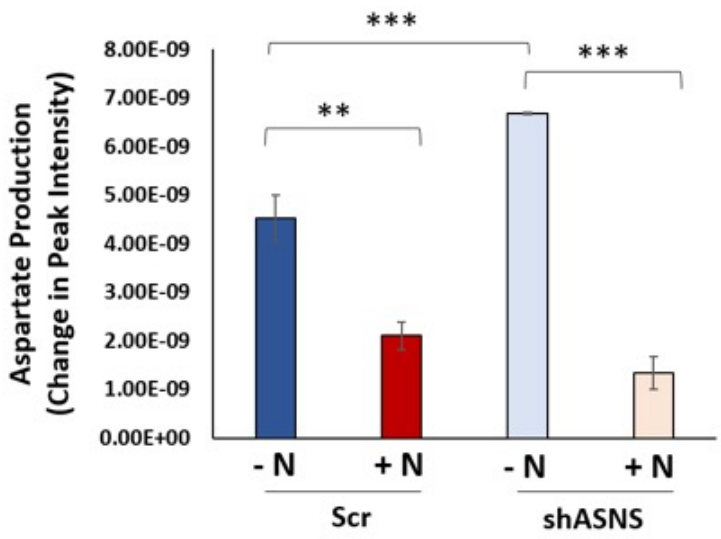

Figure 3-2. **Cellular asparagine requirements dictate aspartate production rates.** Changes in extracellular aspartate levels during a 24 hour incubation with HeLa cells. The 24 hour incubation began 24 hours post-doxycycline-induced expression of a scrambled shRNA (Scr) or ASNS shRNA in the presence or absence of 0.1 mM exogenous asparagine (N). Error bars denote standard deviation of the mean. *$p < 0.05$; **$p < 0.01$; ***$p < 0.001$.

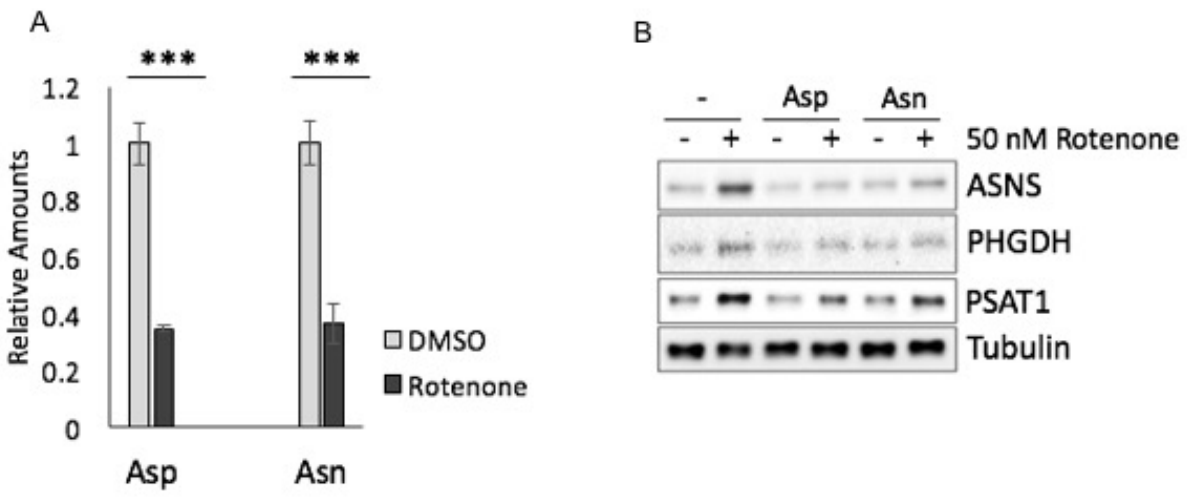

Figure 3-3. **ETC inhibition with rotenone causes intracellular depletion of aspartate and asparagine and increases expression of ATF4 target genes. (A)** Intracellular asparagine and aspartate levels after treatment with 50 nM rotenone for 72 hours. **(B)** Immunoblot showing expression of ATF4 target genes ASNS, PHGDH, and PSAT1 after treatment with 50 nM rotenone for 24 hours.

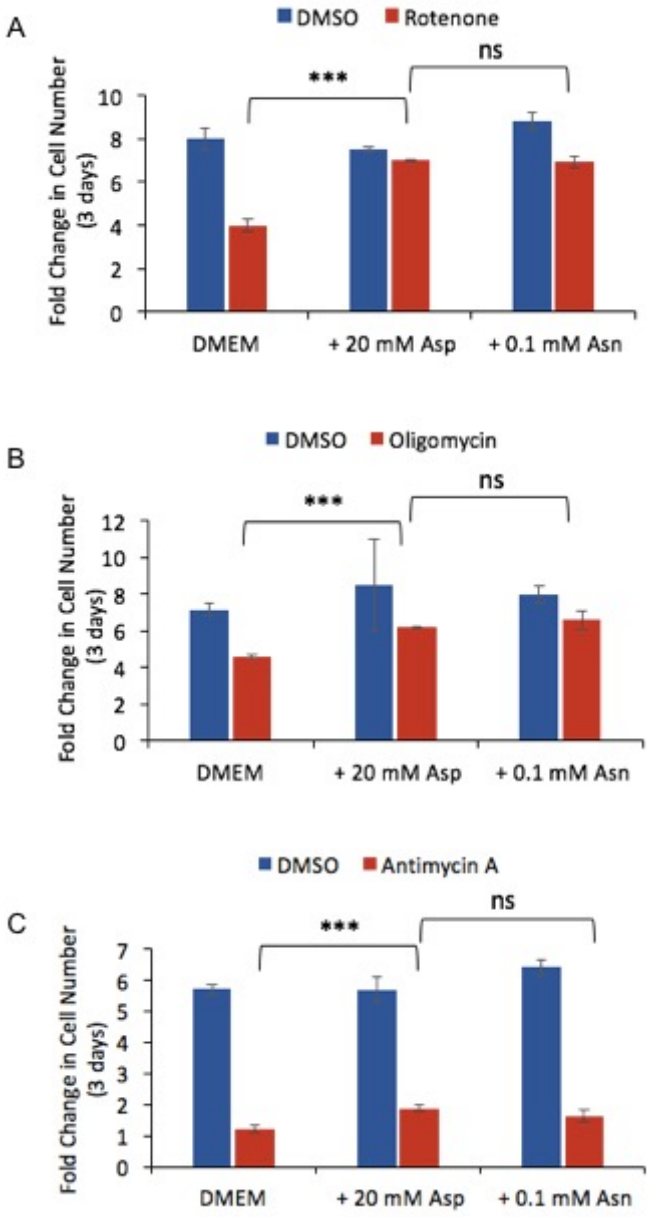

Figure 3-4. **Aspartate and asparagine each rescue proliferation with ETC inhibition.** Fold change in HeLa cell number over 72 hours in the presence or absence of 20 mM aspartate (Asp) or 0.1 mM asparagine (Asn) upon treatment with DMSO or (A) rotenone, (B) oligomycin, and (C) antimycin A. Error bars denote standard deviation of the mean. *p < 0.05; **p < 0.01; ***p < 0.001; ns, not significant.

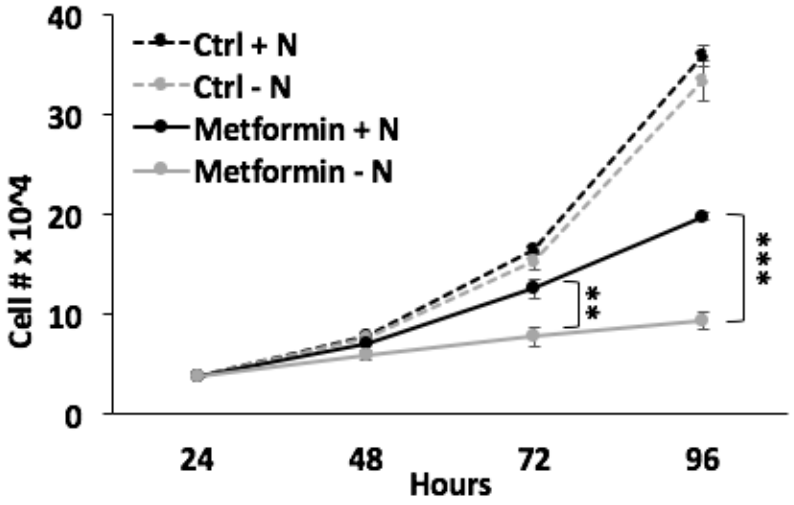

Figure 3-5. **Asparagine withdrawal sensitizes cancer cells to metformin treatment.** Proliferation curves of HeLa cells grown in the presence or absence of 5 mM metformin and 0.1 mM asparagine (N). Error bars denote standard deviation of the mean. *p < 0.05; **p < 0.01; ***p < 0.001; ns, not significant.

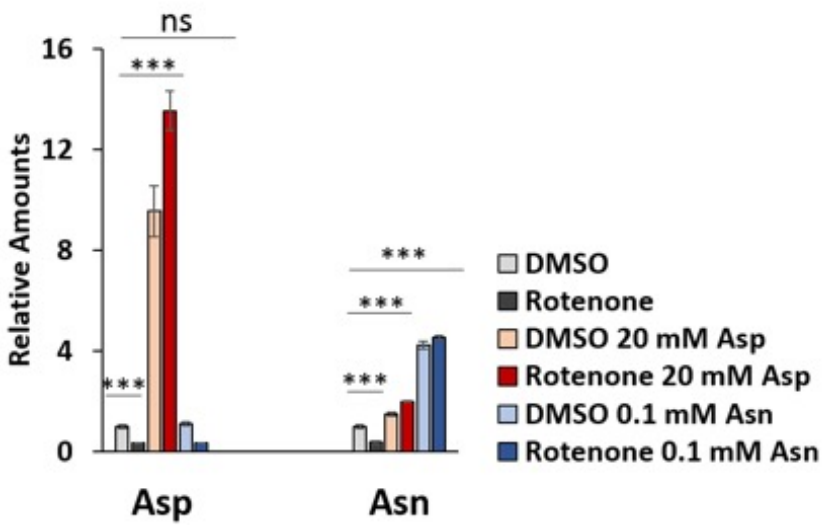

Figure 3-6. **Exogenous aspartate rescues intracellular asparagine levels, but exogenous asparagine does not rescue intracellular aspartate levels, upon ETC inhibition.** Intracellular aspartate and asparagine levels after treatment with 50 nM rotenone for 72 hours in the presence or absence of 20 mM aspartate (Asp) or 0.1 mM asparagine (Asn). *p < 0.05; **p < 0.01; ***p < 0.001; ns, not significant.

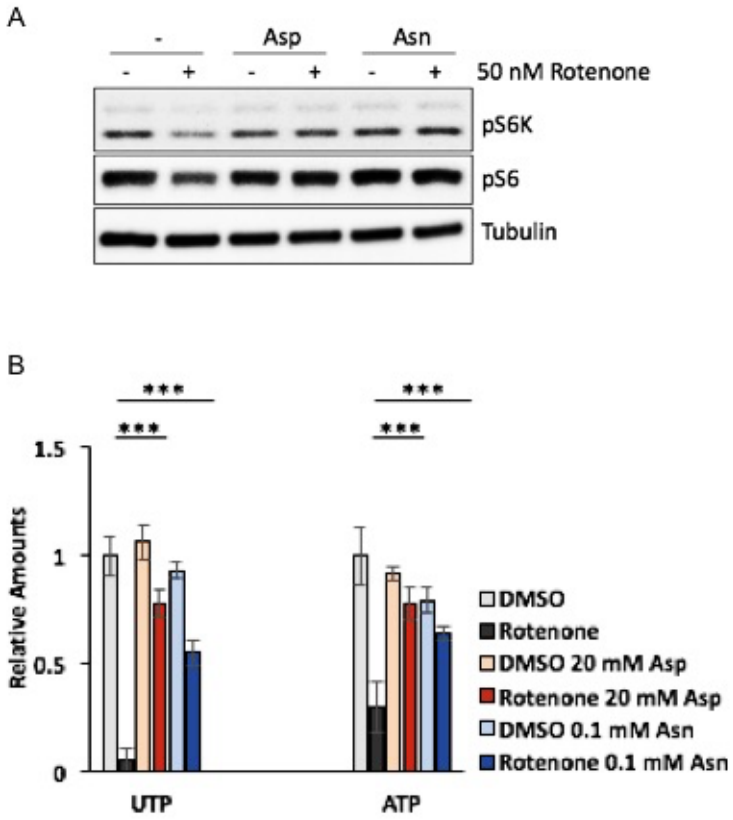

Figure 3-7. **Aspartate and asparagine each rescue mTORC1 activity and nucleotide levels with ETC inhibition. (A)** Immunoblot showing phosphorylation of mTORC1 substrate S6K (T389) after treatment with 50 nM rotenone for 6 hours in the presence or absence of 20 mM aspartate (Asp) or 0.1 mM asparagine (Asn). **(B)** Intracellular nucleotide levels after treatment with 50 nM rotenone for 72 hours in the presence or absence of 20 mM aspartate (Asp) or 0.1 mM asparagine (Asn).

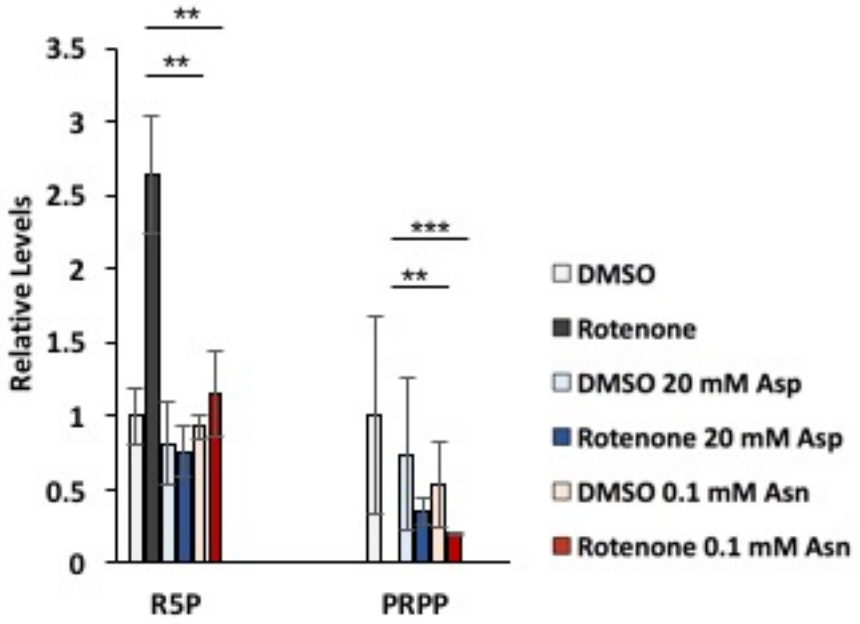

Figure 3-8. Intracellular ribose-5-phosphate (R5P) and phosphoribosyl pyrophosphate (PRPP) levels after treatment with 50 nM rotenone for 72 hours in the presence or absence of 20 mM aspartate (Asp) or 0.1 mM asparagine (Asn).

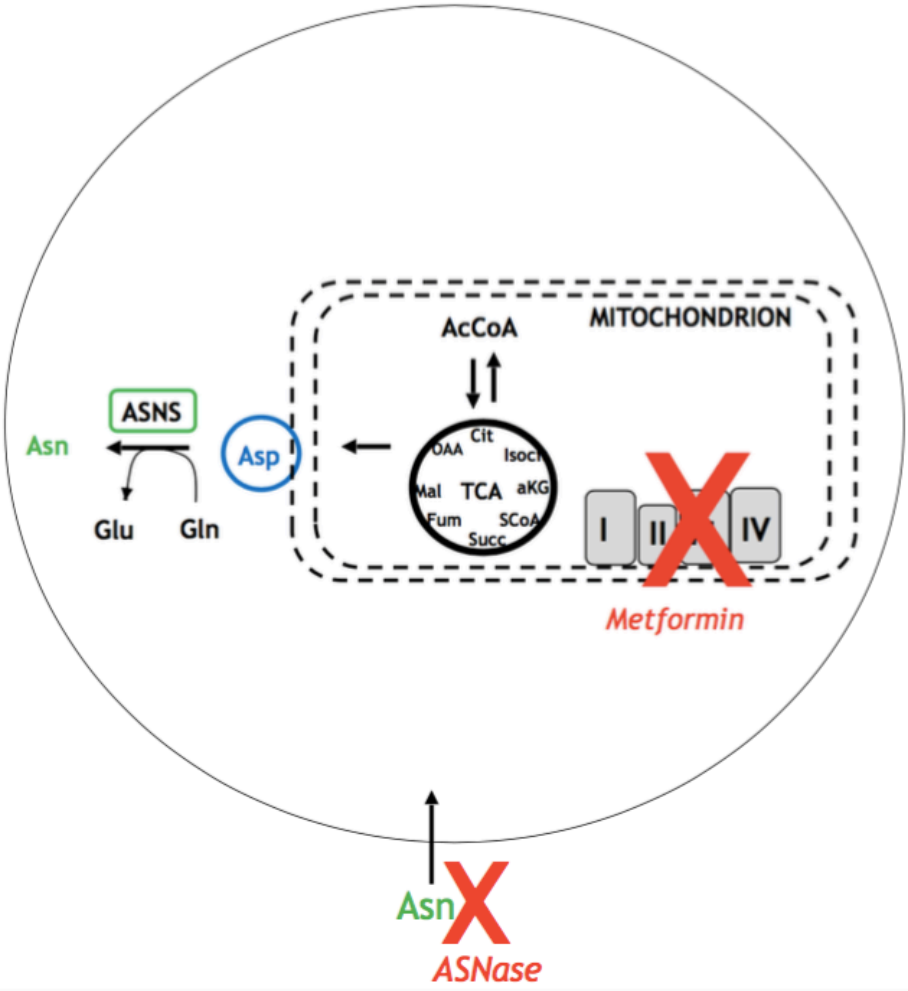

Figure 3-9. **Model depicting strategy for targeting cancer cell asparagine dependence.** Hypothesis: Targeting extracellular asparagine with asparaginase (ASNase) and *de novo* asparagine synthesis with metformin will deplete intracellular asparagine and inhibit tumor growth.

REFERENCES

1. Lorenzi PL, Llamas J, Gunsior M, Ozbun L, Reinhold WC, Varma S, Ji H, Kim H, Hutchinson AA, Kohn EC, Goldsmith PK, Birrer MJ, Weinstein JN. Asparagine synthetase is a predictive biomarker of L-asparaginase activity in ovarian cancer cell lines. Mol Cancer Ther. 2008;7(10):3123-8. doi: 10.1158/1535-7163.MCT-08-0589. PubMed PMID: 18852115; PMCID: 4123961.

2. Holleman A, Cheok MH, den Boer ML, Yang W, Veerman AJ, Kazemier KM, Pei D, Cheng C, Pui CH, Relling MV, Janka-Schaub GE, Pieters R, Evans WE. Gene-expression patterns in drug-resistant acute lymphoblastic leukemia cells and response to treatment. N Engl J Med. 2004;351(6):533-42. doi: 10.1056/NEJMoa033513. PubMed PMID: 15295046.

3. Hettmer S, Schinzel AC, Tchessalova D, Schneider M, Parker CL, Bronson RT, Richards NG, Hahn WC, Wagers AJ. Functional genomic screening reveals asparagine dependence as a metabolic vulnerability in sarcoma. Elife. 2015;4. doi: 10.7554/eLife.09436. PubMed PMID: 26499495; PMCID: PMC4695385.

4. Birsoy K, Wang T, Chen WW, Freinkman E, Abu-Remaileh M, Sabatini DM. An Essential Role of the Mitochondrial Electron Transport Chain in Cell Proliferation Is to Enable Aspartate Synthesis. Cell. 2015;162(3):540-51. doi: 10.1016/j.cell.2015.07.016. PubMed PMID: 26232224; PMCID: PMC4522279.

5. Sullivan LB, Gui DY, Hosios AM, Bush LN, Freinkman E, Vander Heiden MG. Supporting Aspartate Biosynthesis Is an Essential Function of Respiration in Proliferating Cells. Cell. 2015;162(3):552-63. doi: 10.1016/j.cell.2015.07.017. PubMed PMID: 26232225; PMCID: PMC4522278.

6. Harris M. Pyruvate blocks expression of sensitivity to antimycin A and chloramphenicol. Somatic Cell Genet. 1980;6(6):699-708. PubMed PMID: 7444717.

7. Wheaton WW, Weinberg SE, Hamanaka RB, Soberanes S, Sullivan LB, Anso E, Glasauer A, Dufour E, Mutlu GM, Budigner GS, Chandel NS. Metformin inhibits mitochondrial complex I of cancer cells to reduce tumorigenesis. Elife. 2014;3:e02242. doi: 10.7554/eLife.02242. PubMed PMID: 24843020; PMCID: PMC4017650.

8. Zhang X, Fryknas M, Hernlund E, Fayad W, De Milito A, Olofsson MH, Gogvadze V, Dang L, Pahlman S, Schughart LA, Rickardson L, D'Arcy P, Gullbo J, Nygren P, Larsson R, Linder S. Induction of mitochondrial dysfunction as a strategy for targeting tumour cells in metabolically compromised microenvironments. Nat Commun. 2014;5:3295. doi: 10.1038/ncomms4295. PubMed PMID: 24548894; PMCID: PMC3929804.

9. Knott SRV, Wagenblast E, Khan S, Kim SY, Soto M, Wagner M, Turgeon MO, Fish L, Erard N, Gable AL, Maceli AR, Dickopf S, Papachristou EK, D'Santos CS, Carey LA, Wilkinson JE, Harrell JC,

Perou CM, Goodarzi H, Poulogiannis G, Hannon GJ. Asparagine bioavailability governs metastasis in a model of breast cancer. Nature. 2018;554(7692):378-81. doi: 10.1038/nature25465. PubMed PMID: 29414946.

10. King MP, Attardi G. Human cells lacking mtDNA: repopulation with exogenous mitochondria by complementation. Science. 1989;246(4929):500-3. PubMed PMID: 2814477.

11. Cardaci S, Zheng L, MacKay G, van den Broek NJ, MacKenzie ED, Nixon C, Stevenson D, Tumanov S, Bulusu V, Kamphorst JJ, Vazquez A, Fleming S, Schiavi F, Kalna G, Blyth K, Strathdee D, Gottlieb E. Pyruvate carboxylation enables growth of SDH-deficient cells by supporting aspartate biosynthesis. Nat Cell Biol. 2015. doi: 10.1038/ncb3233. PubMed PMID: 26302408.

12. Abel EV, Basile KJ, Kugel CH, 3rd, Witkiewicz AK, Le K, Amaravadi RK, Karakousis GC, Xu X, Xu W, Schuchter LM, Lee JB, Ertel A, Fortina P, Aplin AE. Melanoma adapts to RAF/MEK inhibitors through FOXD3-mediated upregulation of ERBB3. J Clin Invest. 2013;123(5):2155-68. doi: 10.1172/JCI65780. PubMed PMID: 23543055; PMCID: 3635724.

13. Basile KJ, Abel EV, Dadpey N, Hartsough EJ, Fortina P, Aplin AE. In vivo MAPK reporting reveals the heterogeneity in tumoral selection of resistance to RAF inhibitors. Cancer Res. 2013;73(23):7101-10. doi: 10.1158/0008-5472.CAN-13-1628. PubMed PMID: 24121492; PMCID: 3851924.

Chapter 4

Lactate is a Homeostatic Signal that Regulates ATF4 Activity

INTRODUCTION

Cells in multicellular organisms are generally exposed to a constant supply of nutrients through the bloodstream. Multicellular organisms, therefore, must have systems in place to prevent unrestricted anabolism and proliferation of individual cells. The regulation of nutrient uptake by growth factor signaling is one mechanism to prevent unrestricted proliferation, such that cellular nutrient consumption is restricted in the absence of growth cues. Metabolite sensing may be an alternative, and underexplored, method. Metabolites are indicators of both nutrient abundance and anabolic pathway activity. They would therefore be fitting negative feedback signals to restrict growth when the basal anabolic requirements of the cell have been met.

Lactate is generated from pyruvate through the lactate dehydrogenase (LDH) reaction and is the end product of glycolysis. However, this metabolite does not have a known function and has long been thought to be a cellular waste product. It has been suggested that lactate generation benefits proliferating cells. For instance, lactate can be imported into the cell and catabolized to fuel the TCA cycle by being converted to pyruvate via LDH in the reverse direction(1-4). In addition, the conversion of pyruvate to lactate is thought to promote cell growth by recycling the NAD+ consumed during glycolysis and allowing for additional flux through the pathway. However, the purpose of lactate generation remains unclear for several reasons. First, given that pyruvate can also be transported into and out of cells, shuttling of pyruvate from cell to cell as a nutrient would be more efficient since pyruvate is one step closer to mitochondrial oxidation than is lactate. Second, lactate conversion to pyruvate consumes NAD+ that would benefit TCA cycle flux and anabolism. Third, pyruvate can be converted to alanine as an alternative to lactate to yield a useful substrate for protein synthesis(5, 6). Moreover, like lactate, alanine is reduced relative to pyruvate and its conversion can also regenerate NAD+. Although the transaminase reaction that converts pyruvate to alanine is not

explicitly a redox reaction, α-ketoglutarate is also generated by the reaction, sparing NAD+ consumption by glutamate dehydrogenase-mediated α-ketoglutarate synthesis(7).

Many cancer cells increase glucose consumption and lactate secretion. This cancer hallmark is known as the Warburg effect and is thought to promote the anabolism required for cell growth and division. It is clear how increased glucose uptake supports elevated anabolic metabolism – by providing substrates for biosynthetic pathways.(8) However, cancer cell lactate secretion suggests that lactate may negatively impact anabolic metabolism. Despite the fact that lactate can be catabolized, impaired lactate export through monocarboxylate transporter (MCT) inhibition blocks tumor growth and T cell activation(9-11).

ATF4 is a transcription factor that is activated to restore cellular homeostasis after exposure to stress, including amino acid starvation. Unicellular and multicellular organisms have nearly identical homeostatic responses to amino acid deprivation (Figure 4-1). For instance, in both yeast and animals, the kinase GCN2 is activated by uncharged tRNA molecules upon amino acid starvation, leading to the phosphorylation and inhibition of its substrate eiF2α, a translation initiation factor. This results in a global halt in translation but specifically increases translation of a transcription factor that promotes *de novo* amino acid synthesis(12, 13). However, the transcription factor that carries out this response differs in unicellular and multicellular organisms: yeast utilize GCN4, whereas multicellular organisms utilize ATF4 (or ATF4 homologs). Although functional orthologs with respect to the amino acid deprivation response, GCN4 and ATF4 have minimal sequence homology. The evolutionary replacement of GCN4 with ATF4 upon multicellularity raises the possibility that ATF4 may have additional functions that specifically benefit multicellular organisms.

We propose that lactate is a homeostatic signal that mediates its normalizing effects through direct binding to ATF4. We show that ATF4 is activated in response to elevated intracellular lactate and provide evidence that lactate directly binds to ATF4 to promote its stability. We propose that asparagine depletion is sensed through accumulation of intracellular lactate which promotes ATF4-mediated ASNS expression to restore intracellular asparagine. We further find that lactate inhibits mTORC1 activity in an ATF4-dependent manner. We hypothesize that lactate, as the end product of a pathway that supports the use of glucose carbons in anabolic processes, serves as a negative feedback signal to limit anabolic metabolism in conditions when growth is not beneficial.

RESULTS

Asparagine depletion activates ATF4 through non-canonical pathway

Intracellular asparagine depletion results in increased ATF4 localization to the promoters of canonical ATF4 target genes, including ASNS and genes involved in *de novo* serine synthesis (Figure 2-13A). Canonical ATF4 activation downstream of amino acid deprivation occurs through increased translation of ATF4 mRNA through the GCN2- eiF2α axis(12, 13). To address whether asparagine depletion activates ATF4 through the canonical activation pathway, we examined eiF2α phosphorylation and ATF4 protein levels upon ASNS knockdown. ATF4 protein levels are elevated with ASNS knockdown, and supplementing the cell culture medium with 0.1 mM asparagine completely rescues this increase (Figure 4-2). eiF2α phosphorylation, however, is not similarly responsive to intracellular asparagine levels: phosphorylation of eiF2α is not elevated by ASNS knockdown, and exogenous asparagine supplementation, which rescues ATF4 protein levels, does not reduce eiF2α phosphorylation in the context of ASNS knockdown (Figure 4-2). These results suggest that the canonical activation mechanism is not be responsible for increased ATF4 activity upon asparagine depletion.

Instead, our data suggest that the ATF4 activation observed upon asparagine depletion may result from changes in intracellular lactate levels. ASNS knockdown reduces plasma membrane localization of the lactate transporters MCT1 and MCT4 (Figure 4-3A). Moreover, asparagine depletion decreases lactate export rate (Figure 4-3B), without affecting glucose uptake rate (Figure 4-3C). The reduction in lactate export does not appear to be due to decreased glucose to lactate flux in favor of pyruvate entry into the TCA cycle for asparagine synthesis: kinetics of lactate labeling with glucose-derived carbons are unchanged (Figure 4-3D), and glucose labeling of TCA cycle intermediates is, in fact, slower with ASNS knockdown (Figure 4-4). Collectively, these data raise the possibility that intracellular lactate accumulation is involved in the cellular response to asparagine depletion.

Lactate increases ATF4 protein levels and activity

Because reduced lactate export is associated with asparagine depletion, we investigated whether changes in lactate levels influence ATF4 activation. HeLa cell treatment with exogenous lactate results in increased expression of ASNS and other canonical ATF4 target genes, with 10 mM lactate being sufficient to induce expression (Figure 4-5A,B). ATF4 target genes are also elevated in mouse epidermis topically treated with 20 mM lactate (Figure 4-5C). Conversely, reducing intracellular lactate through LDHA knockdown reduces expression of ATF4 target genes (Figure 4-5D). Together, these results indicate that elevated intracellular lactate activates ATF4.

To determine how lactate induces ATF4 activity, we assessed ATF4 protein and mRNA levels at various time points post-treatment. Lactate treatment of HeLa cells increases ATF4 protein levels, with changes apparent by one hour post-treatment (Figure 4-6A). Elevated ATF4 protein with lactate does not appear to be due to changes in ATF4 mRNA levels (Figure 4-6B) or to changes in ATF4 translation, as lactate treatment does not alter eiF2α phosphorylation (Figure

4-6C). The data imply that lactate regulates ATF4 levels at the post-translational level. Consistently, inhibition of proteasomal degradation with MG-132 prevents lactate induction of ATF4 protein levels (Figure 4-6D), suggesting that lactate promotes ATF4 protein stability.

Evidence that lactate binds ATF4 to inhibit its proteasomal degradation

Because lactate increases ATF4 protein levels without affecting mRNA levels or eiF2α phosphorylation, we considered that lactate may promote intracellular ATF4 stability through direct binding. To address this possibility, we used the biochemical approach DARTS(14, 15), which identifies metabolite-protein interactions by exploiting the protection of proteins from protease degradation by bound metabolites. DARTS is particularly useful for detecting low affinity or transient interactions because, as opposed to alternative binding assays, the technique does not require washing steps which might dissociate the interaction. We found that lactate protects ATF4 in cell lysate from protease digestion (Figure 4-7A), suggesting a potential interaction between ATF4 and lactate. Furthermore, 10 mM lactate protects *in vitro* translated (IVT) ATF4 from protease digestion (Figure 4-7B), while chemically similar compounds D-lactate and pyruvate have no effect (Figure 4-7C). These results indicate a specific and direct interaction between L-lactate and ATF4. We measured intracellular lactate levels in asynchronous, rapidly dividing HeLa cells to be in the 4-8 mM range (Figure 4-8). Therefore, our finding that 10 mM lactate interacts with ATF4 (Figure 4-7B) suggests ATF4 binds to lactate within the physiologic range.

To locate the binding site for lactate on ATF4, we performed DARTS on truncated IVT versions of ATF4 that include or exclude known degradation domains (Figure 4-9A). Lactate protects a truncation containing ATF4 residues 1-300 but does not protect a truncation containing residues 1-200, narrowing down the putative lactate binding site to within resides 200-300 (Figure 4-9B). This region of ATF4 contains a recognition motif for ubiquitin ligase subunit βTrCP (Figure 4-

9C). Phosphorylation of serine 219 on ATF4 leads to βTrCP recruitment and proteasomal degradation(16). To determine if the βTrCP recognition motif on ATF4 is required for lactate binding, we performed DARTS on IVT ATF4 containing mutations within the motif. Mutation of serine 219 to alanine (S219A) prevents lactate protection of ATF4 with protease treatment (Figure 4-9D), whereas lactate protection is maintained with a serine 224 mutant (S224A) (Figure 4-9E). The data are consistent with lactate binding ATF4 at serine 219 and suggest that lactate binding may inhibit ATF4 proteasomal degradation either by preventing phosphorylation of serine 219 or by interfering with βTrCP binding.

Lactate inhibits mTORC1 activity in an ATF4-dependent manner

In addition to increasing ATF4 activity, we find that lactate inhibits mTORC1 activity. The presence of lactate inhibits mTORC1 *in vitro kinase* activity in cell lysate, as assessed by S6 kinase (S6K) S239 phosphorylation after the addition of ATP for 5 minutes (Figure 4-10A), and 10 mM extracellular lactate treatment reduces mTORC1 activity in HeLa cells (Figure 4-10B). Conversely, LDHA knockdown in HeLa cells increases mTORC1 activity (Figure 4-10C).

In addition, similar to its protection of ATF4, lactate protects mTOR in cell lysate from protease digestion (Figure 4-7A). The protection of both ATF4 and mTOR from protease digestion in cell lysate suggests either that lactate individually binds to both ATF4 and mTOR or that lactate binds specifically to ATF4 and protects an ATF4-mTOR complex. To distinguish between these possibilities, we examined potential binding between ATF4 and mTOR. ATF4 immunoprecipitated from HeLa cells co-purifies mTOR and mTOR binding partners, Raptor and Rictor (Figure 4-11A). In addition, endogenous ATF4 from HeLa cell lysate binds to immobilized IVT mTOR; vice versa, endogenous mTOR and Rictor bind to immobilized IVT ATF4 (Figure 4-11B). These results are consistent with the existence of an ATF4-mTOR complex. We next assessed the effect of lactate on mTORC1 activity in the context of ATF4 knockdown.

Knockdown of ATF4 eliminates lactate inhibition of mTORC1 (Figure 4-12). Moreover, ATF4 knockdown results in notably elevated baseline mTORC1 activation. These results indicate: 1) ATF4 inhibits mTORC1 activity; and 2) lactate inhibition of mTORC1 activity is mediated by ATF4.

Evidence that lactate influences mTOR complex formation

We next wanted to determine how mTORC1 inhibition is achieved downstream of ATF4 induction by lactate. Cellular mTORC1 activation requires activation of two sets of lysosomal membrane-tethered GTPases: Rheb and Rag proteins. Rheb directly interacts with and activates mTORC1 downstream of growth factor signaling; Rag proteins bind mTORC1 complex member Raptor upon amino acid stimulation, recruiting mTORC1 to the lysosome where it can be activated by Rheb(17). We find that lactate influences mTORC1 lysosomal localization. Consistent with lactate inhibition of mTORC1, exogenous lactate reduces colocalization between mTOR and lysosomal marker LAMP2, whereas LDHA knockdown increases colocalization (Figure 4-13).

Although lactate appears to inhibit mTORC1 lysosomal localization, we also observe lactate inhibition of mTORC1 activity in cell extract (Figure 4-10A), which lacks intact lysosomes and lysosome-mediated signaling. This suggests that lactate inhibition of mTORC1 is independent of Rag GTPases. Raptor is a multifaceted mTORC1 adaptor protein: it mediates the recruitment of mTORC1 to the lysosomal surface by Rag proteins as well as mTORC1 recruitment of its substrates(18). Altered mTOR-Raptor complex formation could therefore explain both altered lysosomal localization in HeLa cells and altered *in vitro* kinase activity in cell extract. Consistent with altered mTOR complex formation, mTORC2 activity is elevated upon HeLa cell lactate treatment, as assessed by phosphorylation of mTORC2 target AKT (Figure 4-14A). Moreover, mTOR-Raptor binding is increased upon LDHA knockdown (Figure 4-14B) and

decreased by exogenous lactate, as indicated by co-immunoprecipitation in the presence of crosslinking agent DSP (Figure 4-14C). Taken together, our data are consistent with lactate inhibiting mTORC1 by interfering with mTOR-Raptor binding. This interference is likely mediated by increased mTOR-ATF4 binding upon lactate-induced ATF4 stability.

Evidence that lactate binds additional βTrCP substrates

The βTrCP recognition motif found in ATF4 is common to numerous proteins (Figure 4-15), including β-catenin, IkBα, and PFKFB3. We therefore considered that lactate may have additional protein binding partners. Exogenous lactate results in increased IkBα and PFKFB3 protein levels in HeLa cells (Figure 4-16A,B). In addition, topical treatment of mouse epidermis with 20 mM lactate increases epidermal levels of these proteins (Figure 4-16C). Lactate treatment also increased increases β-catenin levels in MCF10A, a non-transformed breast epithelial cell line (Figure 4-16D). Although total levels of β-catenin protein appear unaltered in HeLa cells, lactate results in increased expression of well-characterized β-catenin target genes as early as one hour post-treatment (Figure 4-17), suggesting that lactate may increase the active β-catenin pool.

To examine the possibility of β-catenin-lactate binding, we performed DARTS on IVT β-catenin. 25 mM lactate protect β-catenin from protease digestion (Figure 4-18A), consistent with β-catenin-lactate binding. To determine if the βTrCP recognition motif in β-catenin is responsible for its protection by lactate, DARTS was performed on β-catenin mutated at both serines within the motif. As opposed to wildtype β-catenin, a S33A,S37A double mutant version of β-catenin is not protected by lactate upon protease treatment (Figure 4-18B) - evidence that, similar to lactate- ATF4 binding, lactate binds within the βTrCP recognition motif of β-catenin.

How lactate binding at serines within the motif prevents their recognition by βTrCP remains unclear. One possibility is that lactate binding obstructs an interaction with βTrCP. A second possibility is that lactate prevents the phosphorylation events required for βTrCP recognition. To investigate the latter, we performed an *in vitro* kinase assay in the presence or absence of lactate. Endogenous β-catenin in cell lysate is phosphorylated at S33/37 upon the addition of ATP for 5 minutes. Lactate, however, prevents this phosphorylation (Figure 4-18C). These preliminary results suggest lactate may promote the stability of βTrCP substrates by inhibiting phosphorylation of serines required for βTrCP recognition and proteasomal degradation.

DISCUSSION

Here we provide evidence that lactate is a signaling molecule that directly binds to ATF4 to promote its stability. We show that ATF4 levels affect mTORC1 activity, suggesting that ATF4 broadly influences anabolic metabolism. We propose that 1) lactate is an indicator of the cellular metabolic status, and 2) ATF4 is a nutrient sensor that communicates metabolite information to anabolic pathways. Lactate-ATF4 networking enables cellular metabolism and behavior to be modified according to the existing metabolic state. Based on our findings, we hypothesize the following:

Lactate is a signal of amino acid availability

Our data suggest that lactate-ATF4 binding causes inhibition of mTORC1, a master regulator of anabolic metabolism, activity of which is particularly sensitive to intracellular amino acid levels. We found that asparagine is critical for cellular amino acid uptake: intracellular asparagine is exported in exchange for import of extracellular amino acids (Chapter 2). Intracellular asparagine depletion, in addition to reducing amino acid uptake, reduces lactate export (Figure 4-3). Lactate signaling, therefore, may be a novel mechanism to communicate intracellular

amino acid levels to mTORC1 (Figure 4-19) as a means of coordinating anabolic metabolism with nutrient availability.

Lactate is a signal of anabolic saturation

Lactate is the end product of glycolysis, a pathway that supports and coordinates anabolic metabolism by providing substrates for numerous biosynthetic pathways. Our data suggest that lactate inhibits mTORC1 downstream of lactate-ATF4 binding. mTORC1 is a master-anabolic regulator. It promotes glycolytic flux by translationally upregulating c-Myc and HIF-1(19, 20). In addition, mTORC1 activity promotes the use of glucose carbons in anabolic pathways through direct activation of enzymes involved in nucleotide, lipid, and protein synthesis(21). mTORC1 is therefore a fitting target of a negative feedback signal. Based on our results, we propose that lactate, as the end product of an anabolism-coordinating pathway, serves as a negative feedback signal to limit anabolism when the biosynthetic needs of the cell have been met or when growth is not beneficial (Figure 4-20).

Just as mTORC1 is a fitting target of a negative feedback signal, lactate is a fitting signal. Pyruvate derived from glycolysis has three possible fates: 1) entry into mitochondria for oxidation; 2) transamination to produce alanine; or 3) reduction to produce lactate. Mitochondrial oxidation and alanine synthesis are growth promoting options, as they generate substrates for nucleotide, lipid, and protein synthesis. However, lactate cannot be further metabolized or incorporated into biomass. Pyruvate entry into mitochondria is a highly-regulated process(22, 23) which could generate a bottleneck for pyruvate oxidation. Although yet to be thoroughly examined, the possibility exists that lactate represents the overflow pyruvate that cannot be metabolized when the oxidation and transamination pathways are saturated. Lactate, as an unusable form of pyruvate, would be an appropriate signal of this saturation to down-regulate further anabolism through mTORC1 inhibition.

Lactate-ATF4 binding mediates cellular homeostasis

Because asparagine promotes lactate export (Figure 4-3) and lactate binds the transcription factor responsible for asparagine synthesis, intracellular asparagine and lactate levels are tightly linked in a homeostatic loop. Our results suggest that asparagine depletion is sensed through accumulation of intracellular lactate which promotes ATF4-mediated ASNS expression and restoration of intracellular asparagine. Newly synthesized asparagine, in turn, leads to increased lactate export to turn down ATF4 activity and asparagine synthesis (Figure 4-21).

The fact that ATF4, a transcription factor, mediates lactate inhibition of mTORC1 raises the possibility that the lactate-ATF4-mTORC1 axis mediates metabolic and cellular homeostasis. The coupling of mTORC1 inhibition to ATF4 transcriptional activity suggests that anabolic inhibition via lactate is tied to asparagine synthesis. In the context of amino acid availability, this signaling axis ensures that mTORC1-mediated anabolic inhibition upon nutrient deprivation coincides with nutrient restoration via ATF4/asparagine-mediated amino acid uptake. In the context of cell quiescence, we hypothesize that lactate promotes cellular homeostasis by downregulating anabolism through ATF4-mediated mTORC1 inhibition while simultaneously preventing its own accumulation through ATF4-mediated asparagine synthesis and downstream asparagine-mediated lactate transporter trafficking (Figure 4-22A). This homeostatic network would, in theory, stabilize intracellular lactate levels as well as metabolic rates, preventing cell growth beyond what is needed to maintain basic cellular functions.

Our preliminary results suggest that lactate may also bind to a nearly identical sequence in β-catenin, which is also a βTrCP substrate, to increase its activity. β-Catenin activation by lactate may be an additional contributor to homeostatic lactate export. β-Catenin is known to upregulate MCT1 through several mechanisms. For instance, MCT1 is a direct transcriptional target of both Wnt/β-catenin(24) and Myc, which is a β-catenin target gene(9). In addition, β-

catenin activation can increase MCT1 plasma membrane localization by reducing its endocytosis and degradation(25). Therefore, similar to activation of ATF4-mediated asparagine synthesis, lactate activation of β-catenin may support lactate expulsion to prevent lactate accumulation.

Multicellular organisms must have cellular homeostatic systems to restrict the growth and proliferation of individual cells that are exposed to a constant supply of nutrients in the bloodstream. We propose that the lactate-ATF4-mTORC1 network is one such system. Notably, the βTrCP recognition motif in ATF4 is conserved in multicellular organisms, such as *C. elegans* ATF4 homolog ATFS-1, but is not present in yeast GCN4 (Figure 4-23), consistent with the idea that lactate sensing by ATF4 provides a function that is specifically beneficial for multicellularity.

Despite the fact that lactate can be catabolized, malignant transformation is generally accompanied by a dramatic increase in lactate export, which is thought to be mediated by Myc- and HIF1α-driven MCT1 and MCT4 upregulation. Cancer cell MCT1 and MCT4 upregulation may be a means to break the homeostatic loop established by the lactate-ATF4-mTORC1 axis. We hypothesize that by increasing lactate export, cancer cells relieve mTORC1 inhibition to allow for unrestricted anabolism and growth (Figure 4-22B).

Lactate is a paracrine signal

A question ensuing from our data is why cancer cells would increase lactate synthesis by upregulating lactate dehydrogenase(26). Exporting excess pyruvate or alanine would make sense from a biosynthetic standpoint because minimizing lactate would maximize mTORC1 activity. One reason for tumor lactate dehydrogenase upregulation is presumably to recycle

NAD+ for biosynthetic purposes. However, NAD+ can be generated through alternative means that do not yield an anti-growth signaling molecule as a byproduct.

The use of lactate as a paracrine signaling molecule may be a primary purpose for cancer cell lactate synthesis. For instance, cancer cells may use lactate export as a weapon against infiltrating immune cells, which have biosynthetic requirements comparable to those of cancer cells. Lactate has been shown to inhibit T cell proliferation and cytokine production(27), and myeloid-specific deletion of LDHA was recently shown to promote macrophage accumulation and suppress lung tumor growth(28). Moreover, blocking lactate export through MCT1 inhibition causes immunosuppression(10, 11). Rapamycin, an inhibitor of mTORC1, is a well-established immunosuppressant. It will be interesting to see whether lactate exerts its immunosuppressive effects through mTORC1 inhibition.

Lactate export into the tumor microenvironment may also promote tumor growth by stimulating non-cell autonomous autophagy in stromal cells. We observe increased autophagy with exogenous lactate treatment (Figure 4-10B). Lactate-induced autophagy may be downstream of mTORC1 inhibition or ATF4 activation(29, 30). There is accumulating evidence that tumors exploit stromal cells to obtain nutrients, especially in poorly vascularized regions(31, 32). For instance, it was demonstrated that pancreatic cancer cells stimulate autophagy in surrounding stromal cells leading to tumor consumption of alanine secreted by stromal cells(31). These findings raise the possibility that tumor-secreted lactate is a signal to stimulate stromal cell autophagy and the release of amino acids for tumor consumption.

Finally, lactate export into the tumor microenvironment may benefit the tumor by promoting angiogenesis. As a tumor expands, it grows beyond the limits of the local blood supply, creating regions of nutrient deprivation and hypoxia. Tumor expansion, therefore, depends on the

formation of new blood vessels. Vascular endothelial growth factor (VEGF) is a known transcriptional target of HIF(33), ATF4(34, 35) and β-catenin(36). Hypoxia-mediated HIF stability results in cell-autonomous VEGF expression. Tumor lactate export into the microenvironment may stimulate non-cell-autonomous ATF4- and β-catenin-mediated VEGF expression to augment the angiogenic program.

Altered cellular metabolism is now accepted as a hallmark of cancer(37). Cancer cells increase glucose uptake to support biosynthetic processes. This increased glucose uptake inevitably results in increased synthesis of pyruvate, of which cancer cells commonly convert a large fraction to lactate. However, cancer cells, unlike most differentiated cells in the body, have developed the ability to dispose of the synthesized lactate through increased expression of lactate transporters. Our data provide possible explanations as to why cancer cells export large quantities of lactate. Lactate export by cancer cells may be a means to evade lactate-mediated downregulation of anabolism to support unrestricted tumor proliferation. It may also enable tumor exploitation of the cellular environment and evasion the immune system.

EXPERIMENTAL PROCEDURES

Cell lines and culture conditions. HeLa cells (ATCC) were cultured in DMEM containing 1 mM pyruvate and supplemented with 10% fetal bovine serum and 1% penicillin-streptomycin, unless otherwise stated.

Lactate treatments. Medium was replaced for the indicated times with pyruvate-free DMEM containing 10% dialyzed FBS and 1% penicillin-streptomycin, with or without the indicated amounts of sodium L-lactate. Media were adjusted to pH 7.4 immediately prior to treatment.

Cell lysis and immunoblotting. Cells were lysed in buffer containing 50 mM Tris pH 7.4, 1% Nonidet P-40, 0.25% sodium deoxycholate, 1 mM EDTA, 150 mM NaCl, 1 mM dithiothreitol, 1 mM sodium orthovanadate, 20 mM sodium fluoride, 10 mM sodium pyrophosphate, 10 mM beta-glycerophosphate, 2 µg/ml aprotinin, 2 µg/ml leupeptin and 0.7 µg/ml pepstatin. Western blot analysis was performed using standard protocols, and the following commercial antibodies were used as probes: ASNS (Proteintech 14681-1-AP, 1:1000), phospho-T389 S6 kinase (Cell Signaling 9234, 1:500), S6 kinase (Cell Signaling 2708, 1:1000), phospho-S235/235 S6 ribosomal protein (Cell Signaling 4858, 1:3000), S6 ribosomal protein (Cell Signaling 2217, 1:1000), LC3A/B (Cell Signaling 4108, 1:1000), PHGDH (Cell Signaling 13428, 1:1000), PSAT1 (Abnova H00029968-A01, 1:500), PSPH (Sigma HPA020376, 1:500), SHMT2 (Cell Signaling 12762, 1:1000), phospho-S52 eIF2α (Cell Signaling 3398, 1:500), eIF2α (Cell Signaling 5324, 1:1000), ATF4 (Cell Signaling 11815, 1:500), MCT1 (Abcam), MCT4 (Proteintech 22787-1-AP, 1:1000), Na/K ATPase (Cell Signaling 3010, 1:1000), mTOR (Cell Signaling 2972, 1:1000), Flag (Abcam ab49763), Raptor (Millipore 09-217, 1:1000), Rictor (Cell Signaling 2114, 1:1000), β-catenin (Cell Signaling 8480, 1:1000), PFKFB3 (Cell Signaling 13123, 1:1000), IkBα (Cell Signaling 4814, 1:2000), actin (Abcam ab3280 1:1000), and α-tubulin (Sigma T6074, 1:10000).

Drug Affinity Responsive Target Stability (DARTS). DARTS experiments were performed as previously described(14, 15). DARTS performed in cell lysate: Briefly, HeLa cells were lysed in m-PER buffer (Thermo Scientific 78501) supplemented with 1 mM sodium orthovanadate, 20 mM sodium fluoride, 2 µg/ml aprotinin, 2 µg/ml leupeptin and 0.7 µg/ml pepstatin. Lysate was incubated with vehicle control (H2O) or the specified concentration of asparagine for 90 minutes at room temperature. Lysate was digested with pronase (Roche 10165921001) for 30 minutes at room temperature, and the reaction was terminated by the addition of SDS loading buffer and immediate boiling of the samples for 10 minutes. DARTS performed on *in vitro* translated (IVT) protein: *In vitro* translation was performed according to the manufacturer's instructions (nT® T7

Quick Coupled Transcription/Translation System. For each sample, 5 uL of IVT reaction was incubated at 30°C (10 minutes for ATF4-pcDNA3; 60 minutes for β-catenin-pcDNA3), followed by incubation on ice for 30 minutes in TNC buffer (50 mM Tris pH 7.5, 50 mM NaCl, 10 mM $CaCl_2$) with or without the indicated concentrations of sodium L-lactate, sodium D-lactate, or sodium pyruvate. Samples were digested for pronase for 30 minutes at room temperature, and the reaction was terminated by the addition of SDS loading buffer and immediate boiling of the samples for 10 minutes.

Relative and Absolute quantification of intracellular lactate. Cells were seeded in 6-well plates, and metabolites were extracted at 70-80% confluence. Cells were washed with ice-cold 150 mM ammonium acetate, and scraped off the plate in 800 µl ice-cold 50% methanol. Serial dilutions of 1-^{13}C-L-lactate at known concentrations were added to sample triplicates, followed by 10 nmol norvaline and 400 µl chloroform. After vigorous vortexing, the samples were centrifuged at maximum speed, the aqueous layer was transferred to a glass vial, and the metabolites were dried under vacuum. Metabolites were resuspended in 50 µL 70% acetonitrile (ACN) and 5 µL of this solution used for the mass spectrometer-based analysis. The analysis was performed on a Q Exactive (Thermo Scientific) in polarity-switching mode with positive voltage 4.0 kV and negative voltage 4.0 kV. The mass spectrometer was coupled to an UltiMate 3000RSLC (Thermo Scientific) UHPLC system. Mobile phase A was 5 mM NH4AcO, pH 9.9, B) was ACN, and the separation achieved on a Luna 3mm NH2 100A (150 x 2.0 mm) (Phenomenex) column. The flow was 200 µL / min, and the gradient ran from 15% A to 95% A in 18 min, followed by an isocratic step for 9 min and re-equilibration for 7 min. Metabolites were detected and quantified as area under the curve (AUC) based on retention time and accurate mass (≤ 3 ppm) using the TraceFinder 3.1 (Thermo Scientific) software. Sample lactate amounts were calculated according to standard curves generated from the ^{13}C standards. To calculate molar concentrations, cell volume was approximated based on cell diameter.

Kinase assays. Cells were lysed in m-PER buffer supplemented wih 1 mM sodium orthovanadate, 20 mM sodium fluoride, 2 µg/ml aprotinin, 2 µg/ml leupeptin and 0.7 µg/ml pepstatin. 20 mM lactate or pyruvate, prepared as a 20X stock in TBS, was added to 100 ug of cell lysate. The reaction was initiated by the addition of 5X ATP/$MgCl_2$ (1 mM ATP/50 mM $MgCl_2$ in TBS) and terminated after 5 minutes by the addition of SDS loading buffer followed by immediate boiling for 10 minutes.

Quantitative Real-Time PCR. RNA was purified with Qiagen RNeasy Kit. 1 µg of total RNA was used to synthesize cDNA using the iScript cDNA Synthesis Kit (Bio-Rad) as per manufacturer's instructions. Quantitative PCR (qPCR) was conducted on the Roche LightCycler 480 using SYBR Green I Master Mix (Roche) and 0.5 µM primers. Relative expression values are normalized to control gene (60S acidic ribosomal protein P0). qPCR was performed with the following primers:

ATF4 Fwd: GTCCCTCCAACAACAGCAAG
ATF4 Rev: CTATACCCAACAGGGCATCC
ASNS Fwd: CAGAAGATGGATTTTTGGCTG
ASNS Rev: TGTCCAGGAAGAAAAGGCTC
PSAT1 Rev: GCAATTCCCGCACAAGATTCT
PSPH Fwd: GAGGACGCGGTGTCAGAAAT
β-catenin-1 Fwd: TTTTAAGCCTCTCGGTCTGTG
β-catenin-1 Rev: CACGCTGGATTTTCAAAACA
β-catenin-2 Fwd: AGGTCTGAGGAGCAGCTTCA
β-catenin-2 Rev: CCATCAAATCAGCTTGAGTAGC
c-Myc-1 Fwd: CTTACAACACCCGAGCAAGG
c-Myc-1 Rev: CACCGAGTCGTAGTCGAGGT
c-Myc-2 Fwd: TCCACGAAACTTTGCCCATA
c-Myc-2 Rev: AGCTAACGTTGAGGGGCATC
Axin2-1 Fwd: TAAGGTCCTGGCAACTCAGTAAC
Axin2-1 Rev: CTTCCAGTTCCTCTCAGCAATC
Axin2-2 Fwd: GAGAGCCGGGAAATAAAAATAACC
Axin2-2 Rev: GGGAGGCAAGTCACCAACATA
Cyclin D1-1 Fwd: AAACAGATCATCCGCAAACAC
Cyclin D1-1 Rev: CCGGGTCACACTTGATCACT
Cyclin D1-2 Fwd: GCTGCGAAGTGGAAACCATC
Cyclin D1-2 Rev: CCTCCTTCTGCACACATTTGAA

Inducible shRNA-mediated ASNS knockdown. shRNA oligonucleotides (shASNS 5'-CACCGCTGTATGTTCAGAAGCTAAATTCAAGAGATTTAGCTTCTGAACATACAGC-3' and 5'-AAAAGCTGTATGTTCAGAAGCTAAATCTCTTGAATTTAGCTTCTGAACATACAGC-3'; and shScramble 5'-CACCGTAGCGACTAAACACATCAATTCAAGAGATTGATGTGTTTAGTCGCTA-3' and 5'-AAAATAGCGACTAAACACATCAATCTCTTGAATTGATGTGTTTAGTCGCTAC-3') were annealed and ligated into pENTR™/H1/TO vector (Invitrogen #K4920-00) following the BLOCK-iT™ Inducible H1 RNAi Entry Vector Kit manual. Resulting shRNA constructs were recombined into pLentipuro/BLOCK-iT-DEST using Gateway® LR Clonase II® (Invitrogen #11791-020). pLentipuro/BLOCK-iT-DEST is a modification of pLenti4/BLOCK-iT-DEST (Invitrogen #K4925-00) wherein the SV40 promoter/zeocin resistance cassette was replaced with the human PGK promoter/puromycin resistance gene and the cPPT/WPRE elements were added, and was kindly provided by Dr. Andrew Aplin (Thomas Jefferson University, Kimmel Cancer Center)(38, 39) . Recombinant lentiviruses were packaged in 293T cells by co-transfecting 4 µg each of lentivirus plasmid with expression vectors containing the *gag*/*pol*, *rev* and *vsvg* genes. Lentivirus was harvested 48 hours after transfection and added to subconfluent HeLa cells with 4 ug/ml polybrene for 16 hours. Cells were selected in 2 ug/ml puromycin for 1 week. Doxycycline induction of knockdown is control by the Tet repressor (TetR) protein expressed from the pLenti0.3/EF/GW/IVS-Kozak-TetR-P2A-Bsd vector, which was constructed by Dr. Ethan Abel and was kindly provided by Dr. Diane M. Simeone (University of Michigan, Translational Oncology Program). Knockdown was induced with 25 ng/ml doxycycline.

Immunofluorescence. Cells were fixed for 20 minutes in 4% paraformaldehyde, permeabilized for 5 minutes in 0.1% tritonX-100 in PBS, and blocked for 30 minutes in 10% donkey serum in PBS. Coverslips were incubated overnight at 4°C in primary antibody diluted in blocking

solution (mTOR: 1:300 Cell Signaling 2983, LAMP2: 1:300 Santa Cruz sc-18822), and in secondary antibody (1:300 in blocking solution) for 1 hour at room temperature.

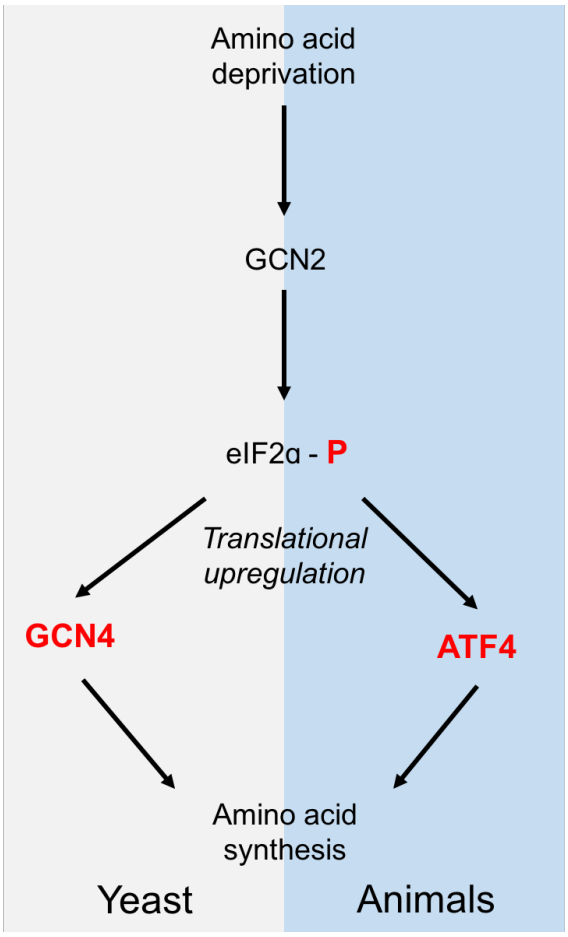

Figure 4-1. **Comparison of amino acid deprivation response in unicellular and multicellular organisms.** In both yeast (unicellular) and animals (multicellular), uncharged tRNA molecules are sensed by the kinase GCN2, leading to phosphorylation of eIF2α. This phosphorylation event globally inhibits translation, but specifically increases translation of GCN4 in yeast and ATF4 in animals due to the presence of upstream open reading frames on the mRNA of these genes that outcompete the coding open reading frames for translation initiation when eIF2α is active. GCN4 and ATF4 both promote transcription of genes involved in *de novo* amino acid synthesis and amino acid transport as a response to low intracellular amino acid levels.

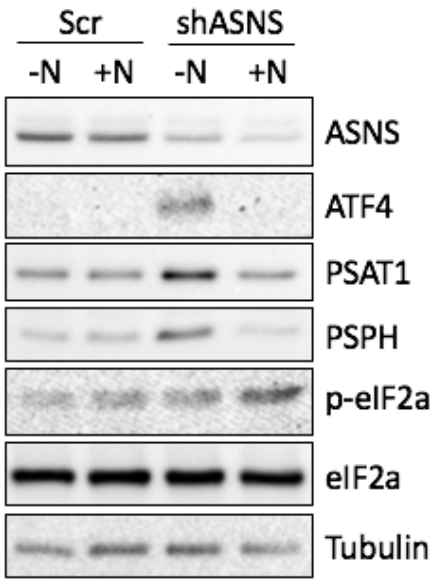

Figure 4-2. **Asparagine depletion may activate ATF4 through a non-canonical mechanism**. Immunoblot showing levels of phosphorylated eIF2α (S52), total eIF2α, ATF4, and ATF4 target genes PSAT1 and PSPH 48 hours post-doxycycline induction of scrambled shRNA or ASNS shRNA expression in the presence or absence of 0.1 mM exogenous asparagine.

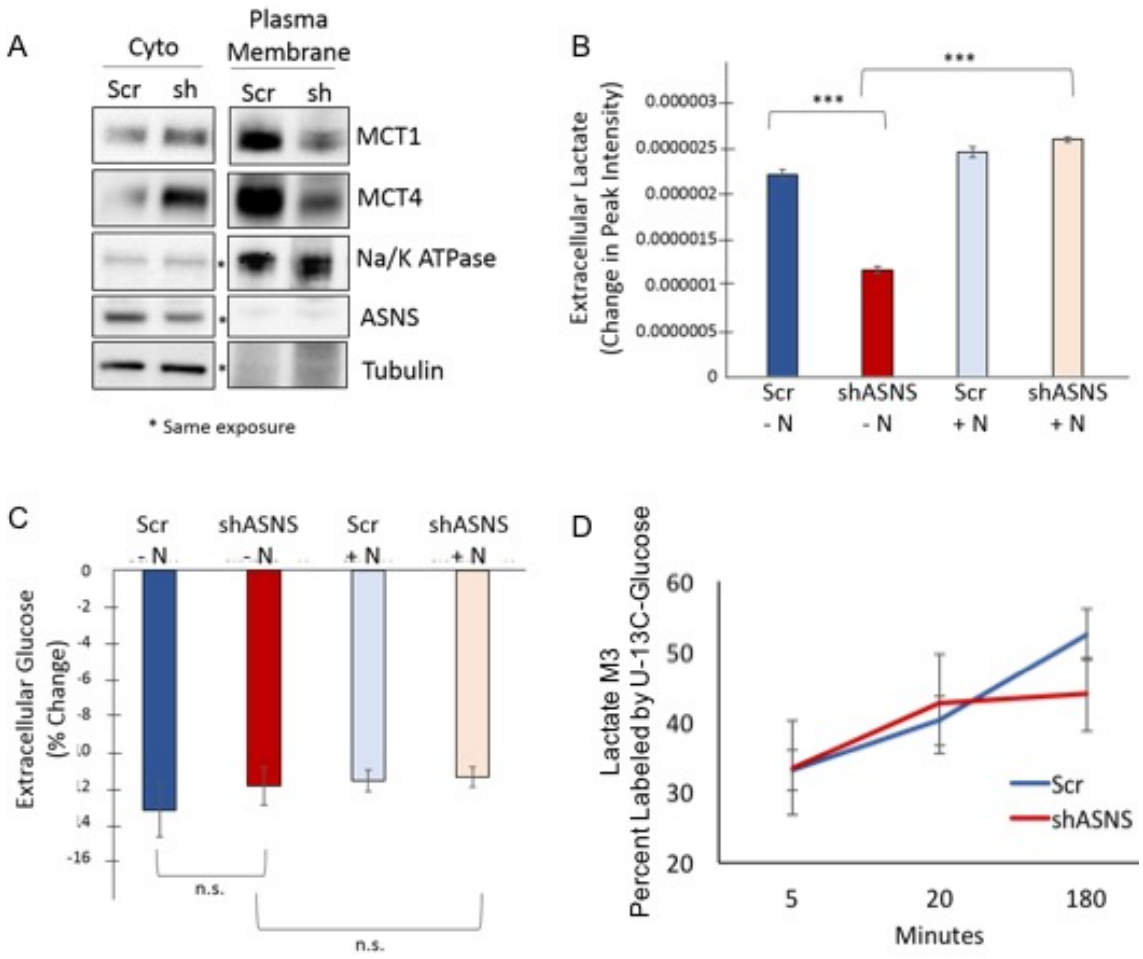

Figure 4-3. **Asparagine depletion leads to reduced lactate export**. **(A)** Immunoblot showing cytoplasmic (Cyto) and plasma membrane levels of MCT1 and MCT4 24 hours post-doxycycline induction of scrambled shRNA or ASNS shRNA expression. Tubulin and Na/K ATPase are markers of cytoplasm and plasma membrane, respectively. Changes in extracellular lactate (B) and glucose (C) levels during a 24 hour incubation with HeLa cells. The incubation began 24 hours post-doxycycline-induced expression of a scrambled shRNA (Scr) or ASNS shRNA in the presence or absence of 0.1 mM exogenous asparagine (N). **(D)** Percentage of lactate labeled with carbons derived from U-^{13}C-glucose at timepoints preceding steady state labeling of lactate. Experiment was performed 48 hours post-doxycycline shRNA induction. Relative lactate levels were unchanged. Error bars denote standard deviation of the mean. *p < 0.05; **p < 0.01; ***p < 0.001; ns, not significant

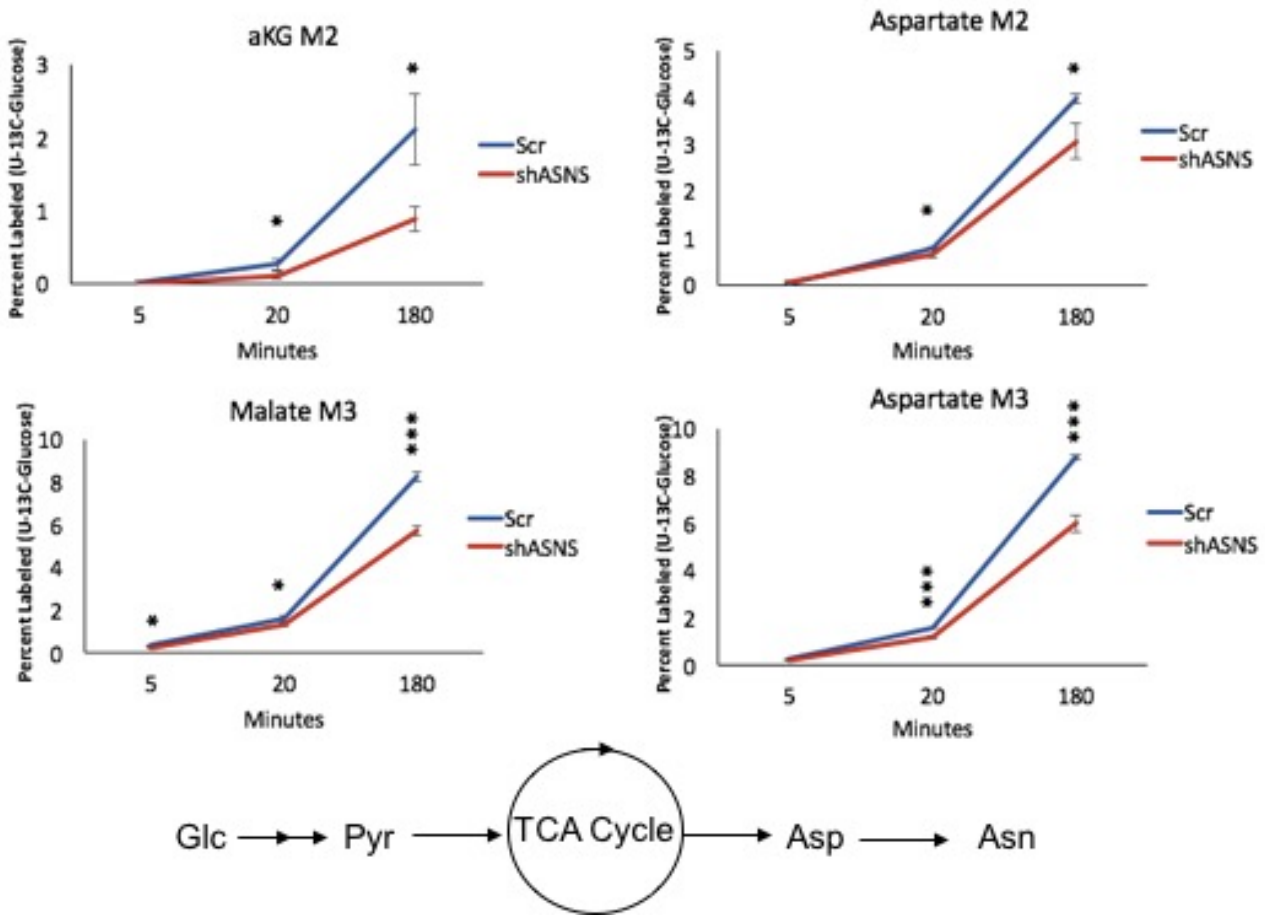

Figure 4-4. **ASNS knockdown reduces the rate of glucose entry into the TCA cycle**. The percentage of each metabolite labeled by U-^{13}C-glucose at 5, 20 and 180 minutes post-glucose addition (pre-steady state). The experiment was initiated 24 hours post-doxycycline induction of scrambled shRNA or ASNS shRNA expression. Pyruvate dehydrogenase-mediated entry of glucose into the TCA is indicated by labeling with two glucose-derived carbons (M2), whereas pyruvate carboxylase-mediated anaplerosis is indicated by labeling with three glucose-derived carbons (M3). Relative levels of the indicated metabolites were unchanged (data not shown). Error bars denote standard deviation of the mean. *$p < 0.05$; **$p < 0.01$; ***$p < 0.001$.

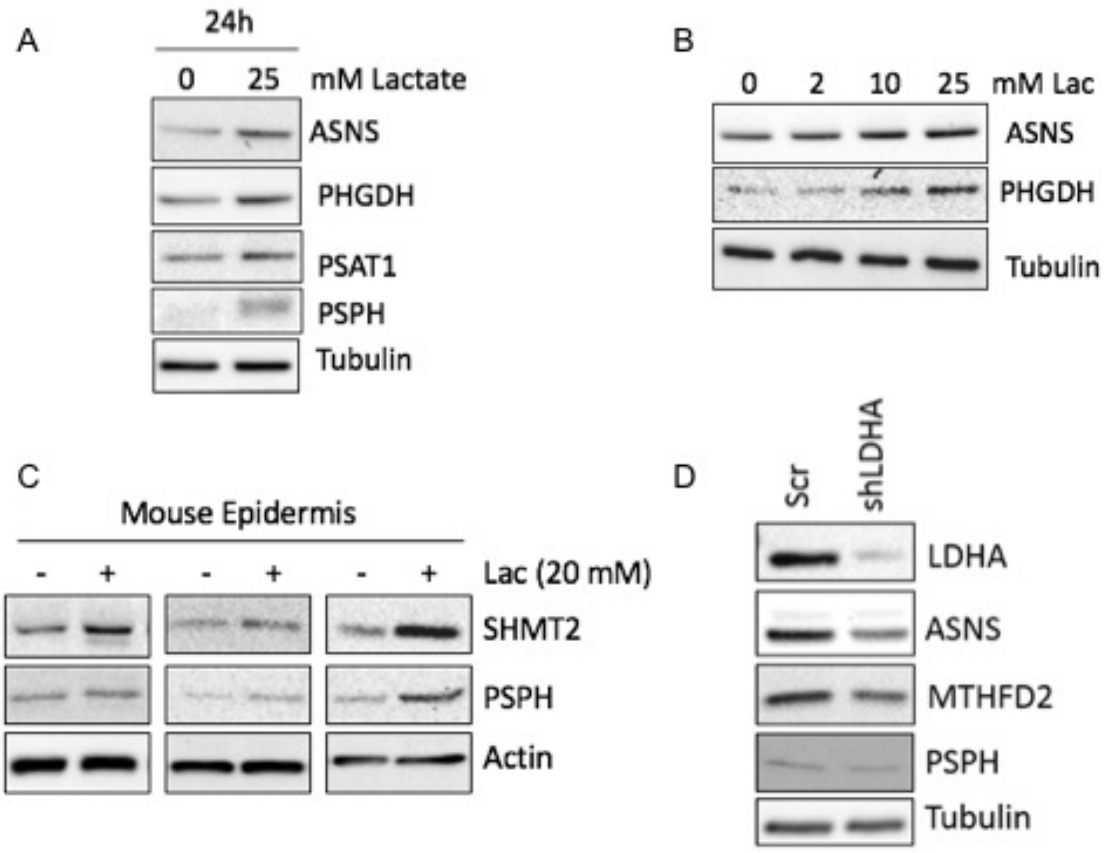

Figure 4-5. **Exogenous lactate treatment increases expression of ATF4 target genes**. **(A)** Immunoblot showing expression of ATF4 target genes ASNS, PHGDH, PSAT1, and PSPH 24 hours after treatment with 25 mM lactate. **(B)** Immunoblot showing expression of ATF4 target genes ASNS and PHGDH with increasing amounts of lactate. **(C)** Immunoblot showing expression of ATF4 target genes SHMT2 and PSPH in total mouse epidermis after topical treatment of mouse epidermis with 20 mM lactate. **(D)** Immunoblot showing expression of ATF4 target genes ASNS, MTHFD2, and PSPH after expression of scrambled (Scr) or LDHA shRNA in HeLa cells.

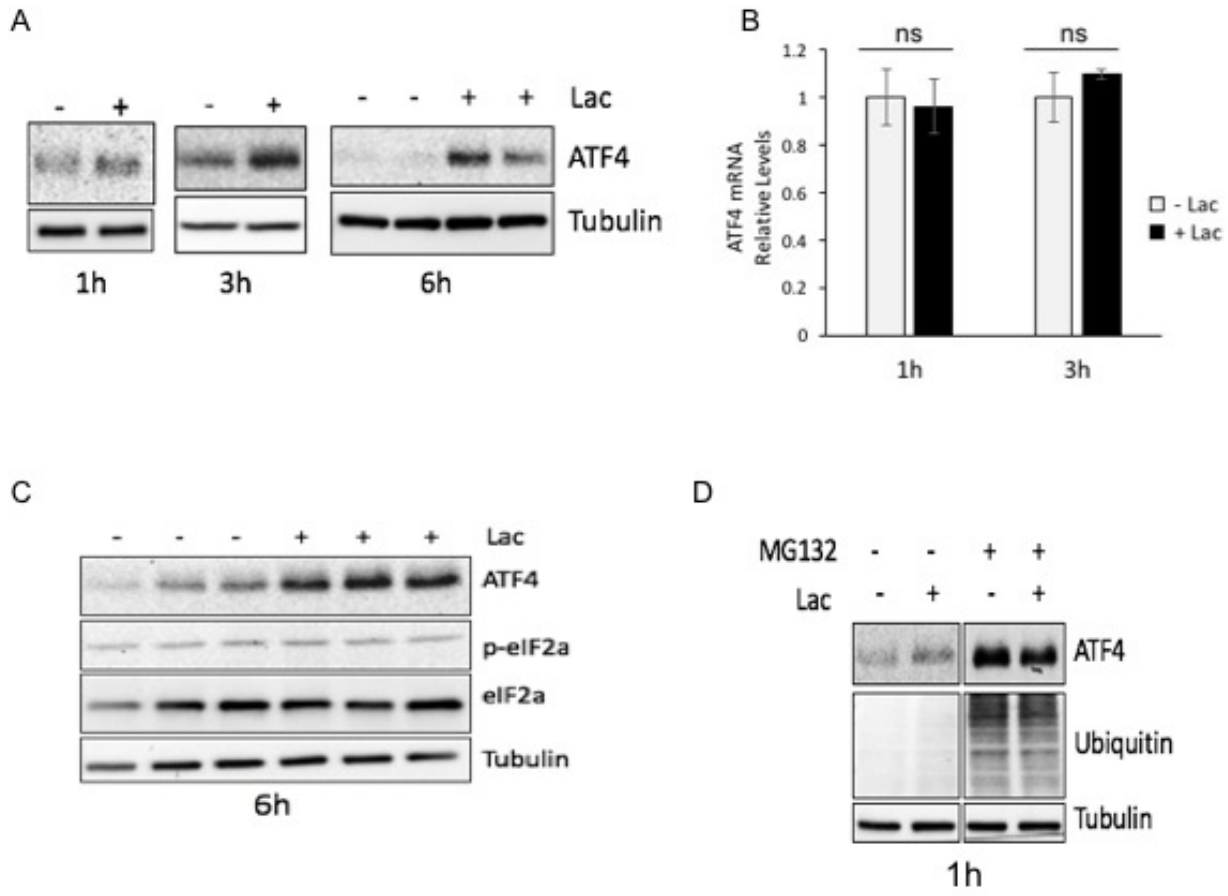

Figure 4-6. **Lactate post-translationally regulates ATF4**. **(A)** Immunoblot showing ATF4 protein levels at 1, 3, and 6 hours post-treatment of HeLa cells with 25 mM lactate. **(B)** ATF4 mRNA levels in HeLa cells 1 hour and 3 hours post-treatment with 25 mM lactate. **(C)** Immunoblot showing levels of phosphorylated eIF2α (S52) and total eIF2α in HeLa cells 6 hours post-treatment with 25 mM lactate. **(D)** Immunoblot showing ATF4 protein levels after one hour HeLa cell treatment with 25 mM lactate in the presence or absence of proteasome inhibitor MG132. Error bars denote standard deviation of the mean; ns, not significant.

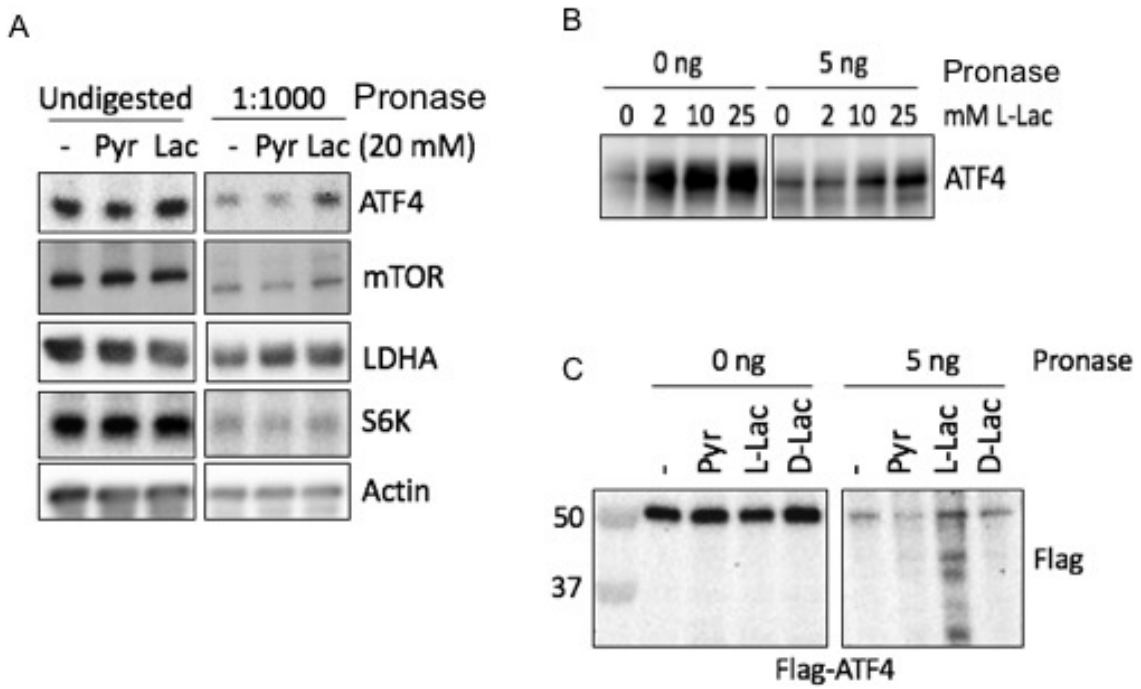

Figure 4-7. **Evidence of L-lactate-ATF4 binding: L-Lactate protects ATF4 from protease digestion. (A)** DARTS: Immunoblot showing levels of ATF4 and mTOR from HeLa cell lysate treated with or without pronase (1:1000 ug pronase:cell extract), and in the presence or absence of 20 mM pyruvate or 20 mM L-lactate. LDHA, which binds both pyruvate and lactate, and S6K, which is not known to bind either pyruvate or lactate, are shown as positive and negative controls, respectively. **(B)** DARTS: Immunoblot showing ATF4 levels after pronase treatment of *in vitro* translated (IVT) Flag-ATF4 in the presence of increasing concentrations of L-lactate. **(C)** DARTS: Immunoblot showing ATF4 levels after pronase treatment of IVT Flag-ATF4 in the presence or absence of pyruvate, L-lactate, or D-lactate. Lower ATF4 bands are ATF4 fragments generated by pronase digestion.

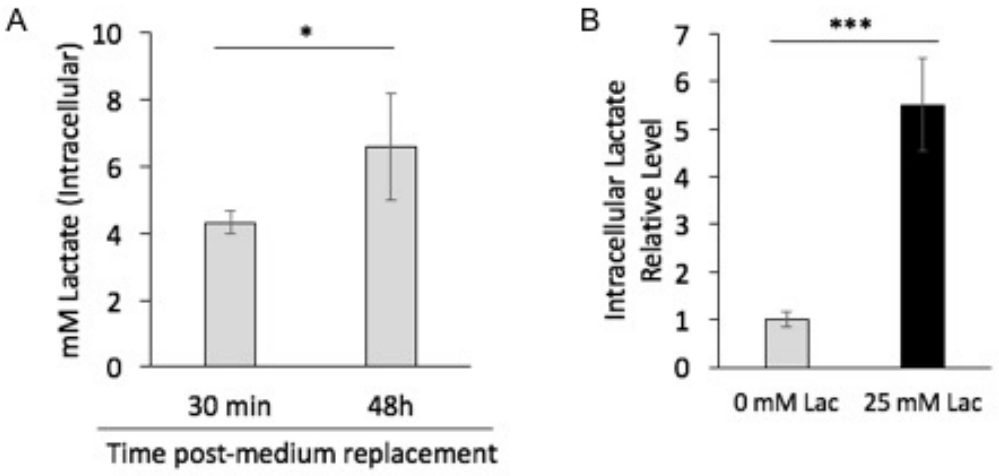

Figure 4-8. **Intracellular lactate concentrations. (A)** Absolute intracellular lactate concentrations in HeLa cells after medium replacement for the indicated time. **(B)** Relative intracellular lactate levels 30 minutes after HeLa cell replacement with control medium or medium containing 25 mM lactate. The absolute lactate concentration of approximately 4 mM in untreated cells (A) and the five-fold increase in relative lactate levels with a 30-minute treatment (B) indicates treatment with 25 mM lactate for 30 minutes increases intracellular lactate levels to 20-25 mM in HeLa cells. Error bars denote standard deviation of the mean. *$p < 0.05$; **$p < 0.01$; ***$p < 0.001$.

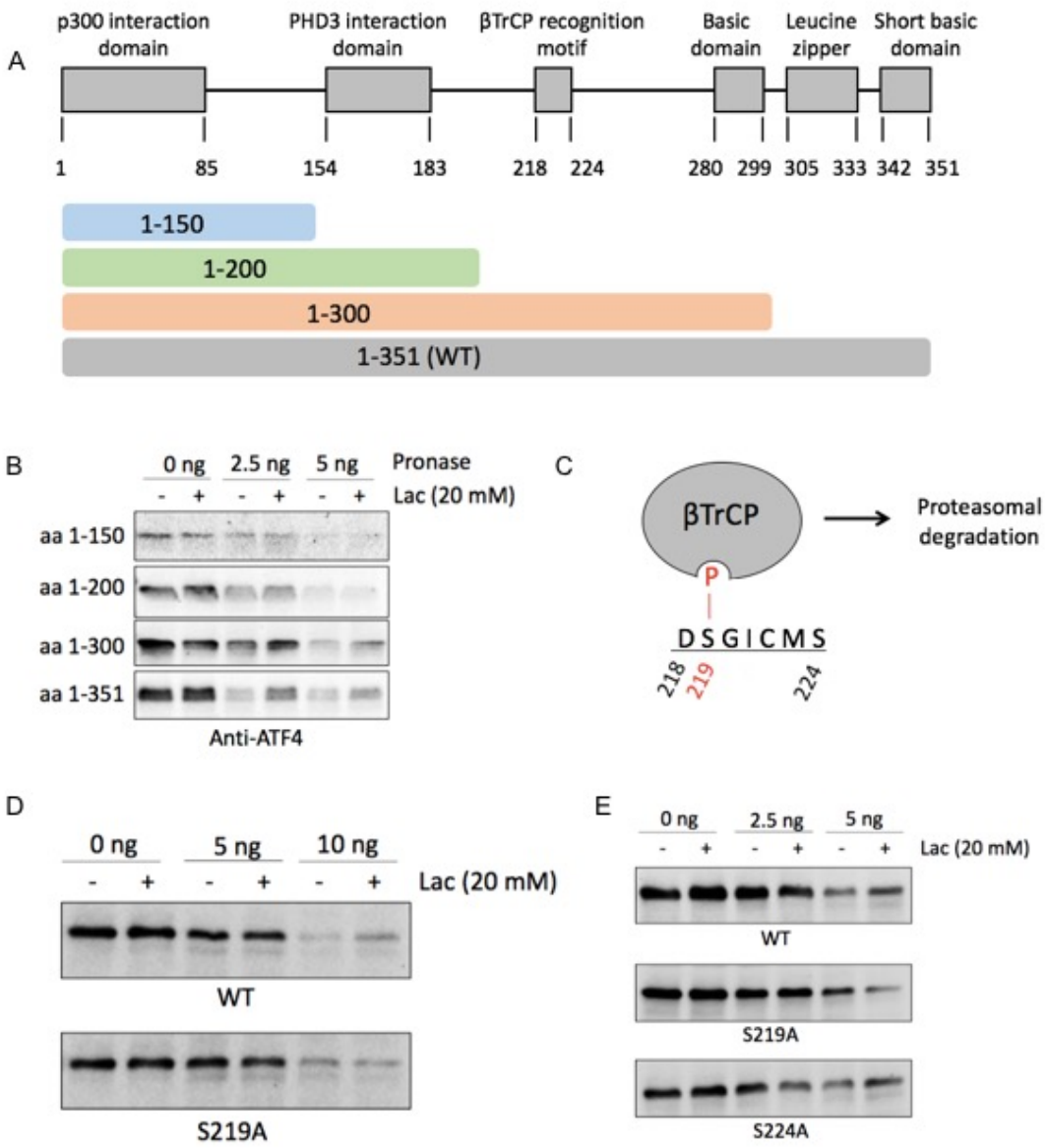

Figure 4-9. **Lactate binds ATF4 at βTrCP recognition motif. (A)** ATF4 domain structure used for truncation design. Colored bars indicate amino acid residues retained in truncated forms of ATF4 used in (B). **(B)** DARTS: Immunoblot showing IVT ATF4 levels after pronase treatment of full-length (1-351) and truncated forms of ATF4 in the presence or absence of 20 mM lactate. **(C)** βTrCP recognition motif within ATF4. Serine 219 phosphorylation promotes βTrCP/ubiquitin ligase recruitment and proteasomal degradation. **(D-E)** DARTS: Immunoblot showing IVT ATF4 levels after pronase treatment of wildtype (WT) and ATF4 containing a mutation at serine 219 (S219A) in the presence or absence of 20 mM lactate.

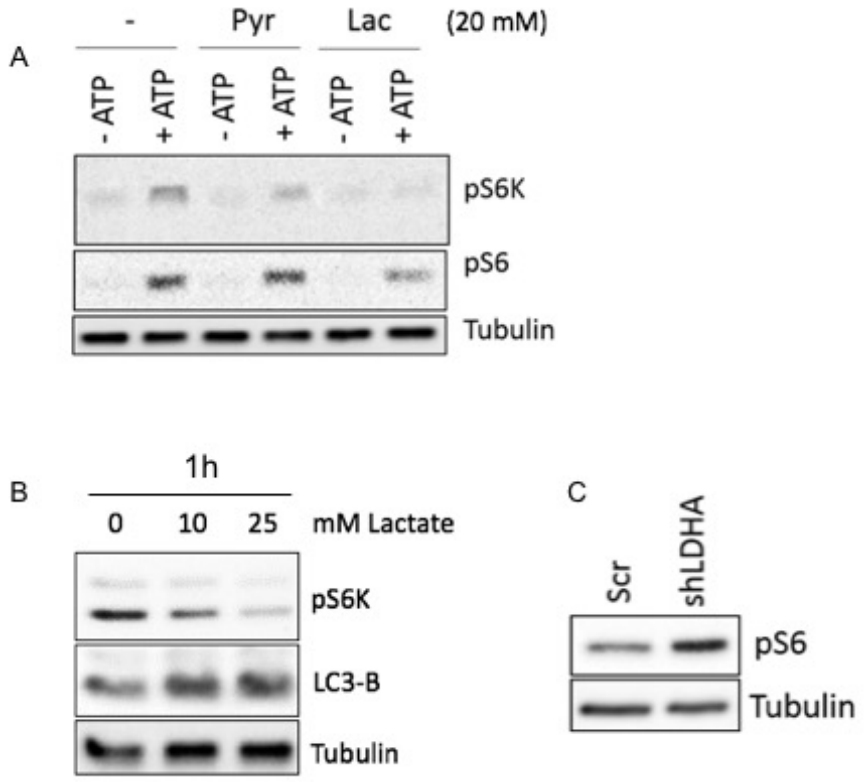

Figure 4-10. **Lactate inhibits mTORC1 activity. (A)** *In vitro* kinase assay: Immunoblot showing phosphorylated levels of mTORC1 substrate S6K (T389) and S6K substrate S6 (S235/236) 5 minutes after the addition of 500 uM ATP to HeLa cell lysate in the presence or absence of 20 mM pyruvate or lactate. **(B)** Immunoblot showing S6K phosphorylation (T389) and cleaved LC3, a marker of autophagy, with increasing amounts of exogenous lactate. **(C)** Immunoblot showing levels of phosphorylated S6 (S235/236) after expression of scrambled (Scr) or LDHA shRNA in HeLa cells.

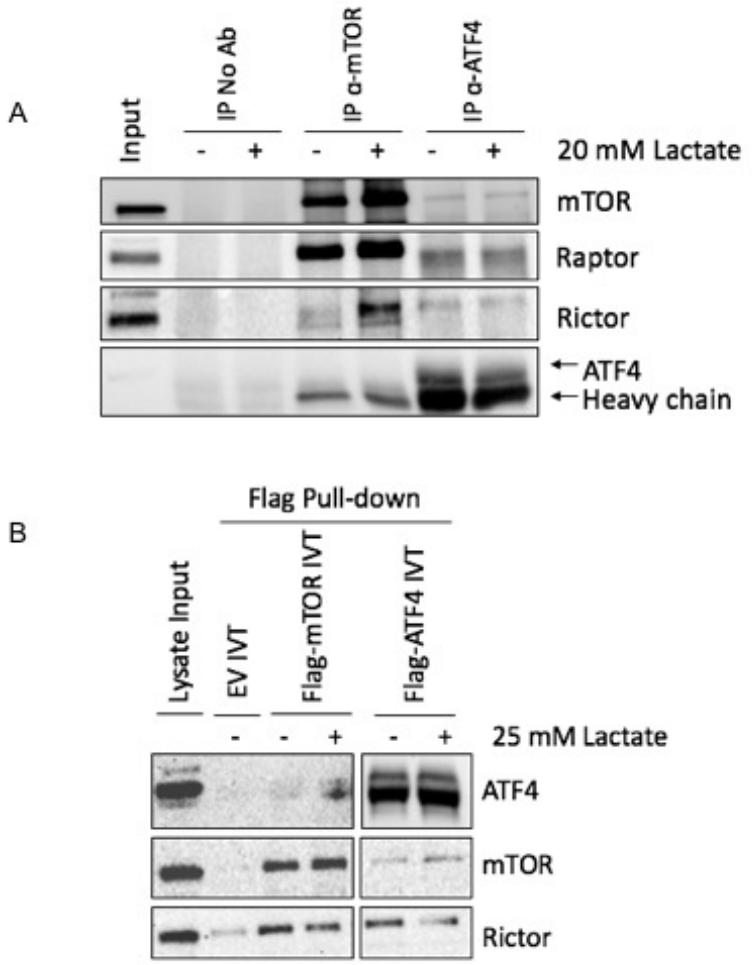

Figure 4-11. **Evidence of an ATF4-mTOR complex. (A)** Immunoblot showing co-immunoprecipitation of mTOR and mTOR binding partners, Raptor and Rictor with ATF4 in HeLa cells. **(B)** Immunoblot showing ATF4 from HeLa cell lysate binding to *in vitro* translated Flag-mTOR; mTOR and Rictor from cell lysate binding to *in vitro* translated Flag-ATF4.

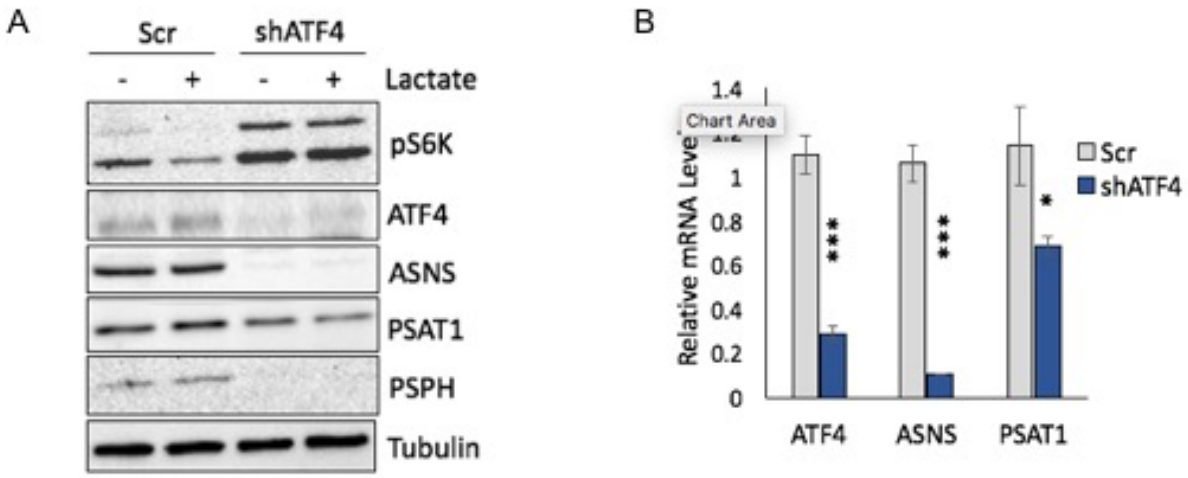

Figure 4-12. **ATF4 mediates Lactate inhibition of mTORC1. (A)** Immunoblot showing phosphorylated levels of mTORC1 substrate S6K (T389) after treatment with 25 mM lactate for one hour in HeLa cells expressing scrambled (Scr) or ATF4 shRNA **(B)** mRNA levels of ATF4 and ATF4 target genes as verification of ATF4 knockdown. Error bars denote standard deviation of the mean. *p < 0.05; **p < 0.01; ***p < 0.001.

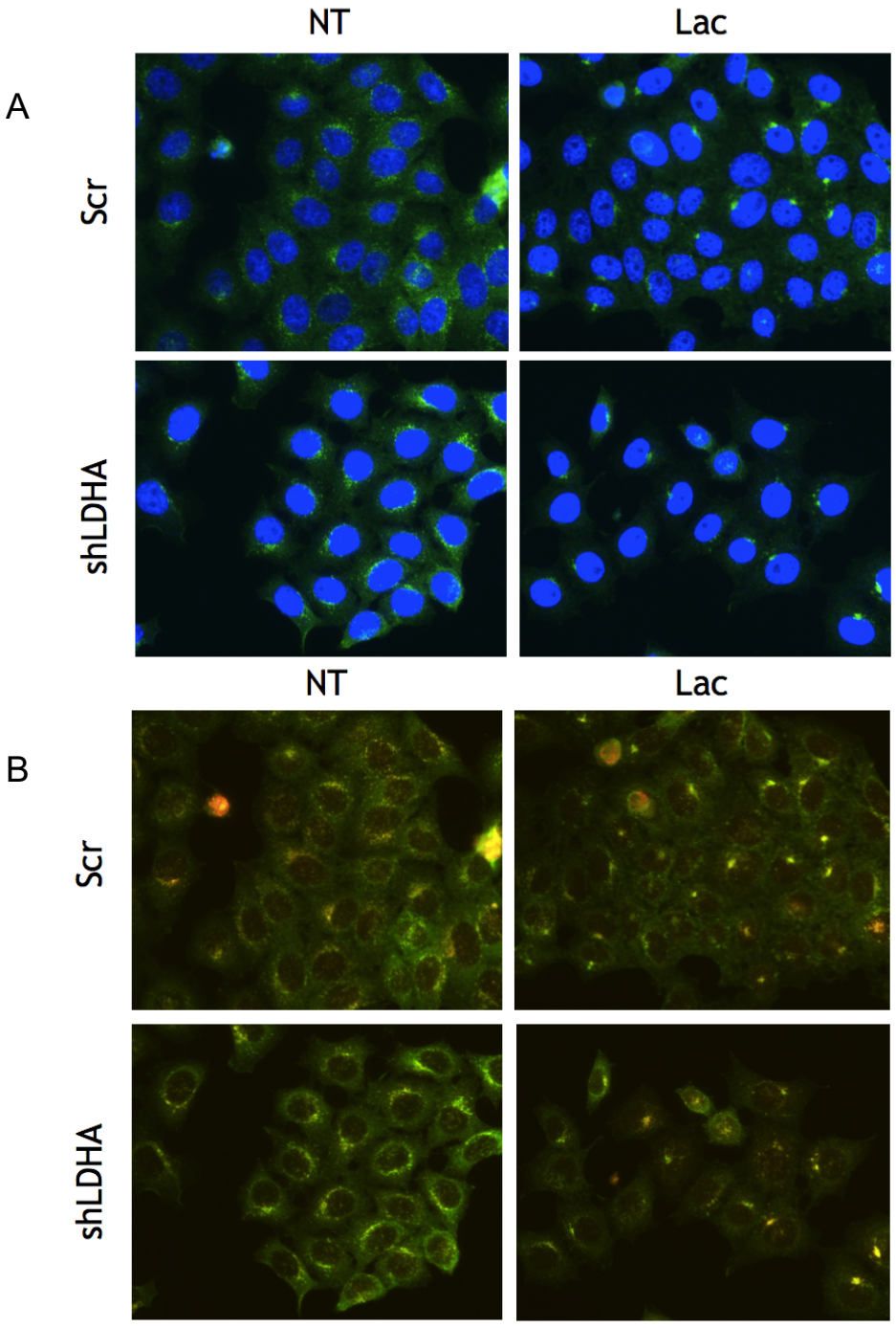

Figure 4-13. **Lactate decreases mTOR lysosomal localization.** mTOR (green) and LAMP2 (red) immunofluorescence in HeLa cells after expression of LDHA shRNA or treatment with 100 mM lactate for one hour. **(A)** mTOR staining merged with DAPI (nuclear stain); **(B)** mTOR staining merged with LAMP2 (lysosome marker) staining.

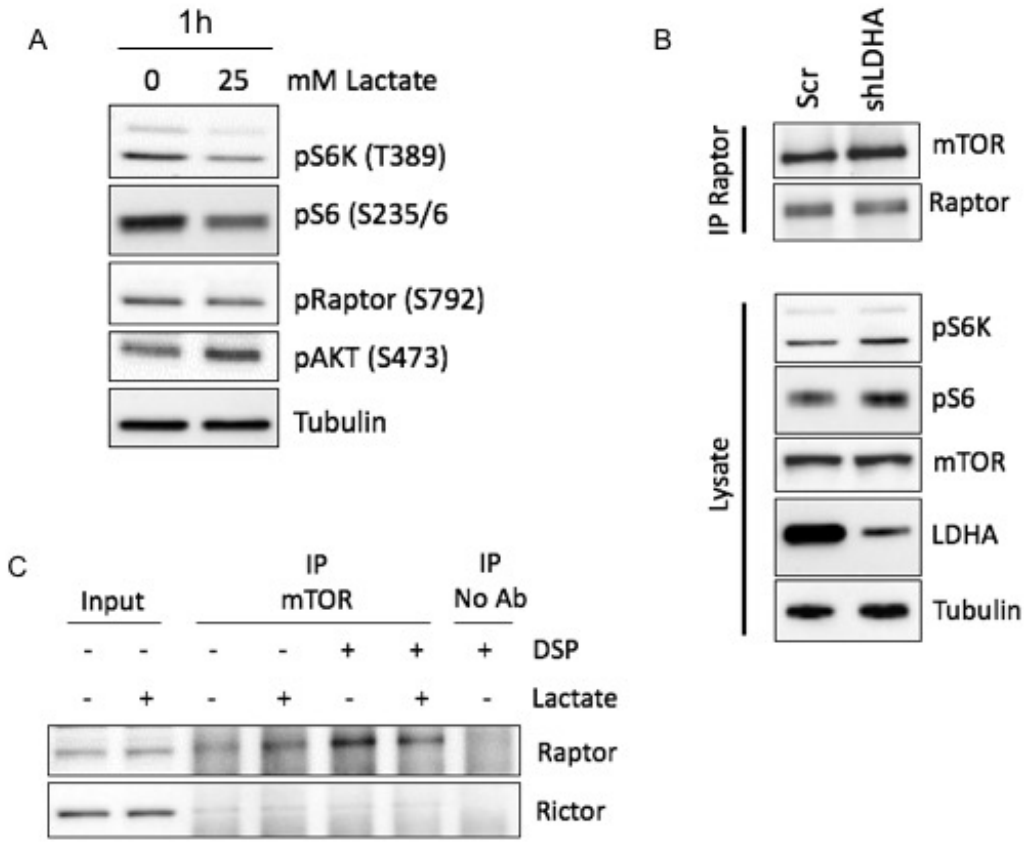

Figure 4-14. **Lactate decreases mTOR-Raptor binding. (A)** Immunoblot showing phosphorylation of mTORC1 substrate S6K (T389), S6K substrate S6 (S235/236), AMPK substrate Raptor (S792), and mTORC2 substrate AKT (S473) in HeLa cells after treatment with 25 mM lactate for one hour. **(B)** Immunoblot showing mTOR co-immunoprecipitation with Raptor in HeLa cells expressing scrambled (Scr) or LDHA shRNA (top). Input levels of pS6K (T389), pS6 (S 235/236), mTOR and LDHA are shown below (lysate). **(C)** Immunoblot showing Raptor co-immunoprecipitation with mTOR from HeLa cells treated with 25 mM lactate for one hour. Co-immunoprecipitation was performed in the presence or absence of crosslinking agent Dithiobissuccinimidyl propionate (DSP).

Protein	Sequence
ATF4	$_{218}$DSGICMS$_{224}$
PFKFB3	$_{268}$DSGLSSR$_{274}$
B-Catenin	$_{32}$DSGIHSG$_{38}$
IkBα	$_{31}$DSGLDSM$_{37}$
NRF2	$_{343}$DSGISLN$_{349}$

Figure 4-15. **Proteins that contain the consensus βTrCP recognition motif.** Several proteins involved in cell signaling and metabolism are known βTrCP substrates and possess a βTrCP recognition motif.

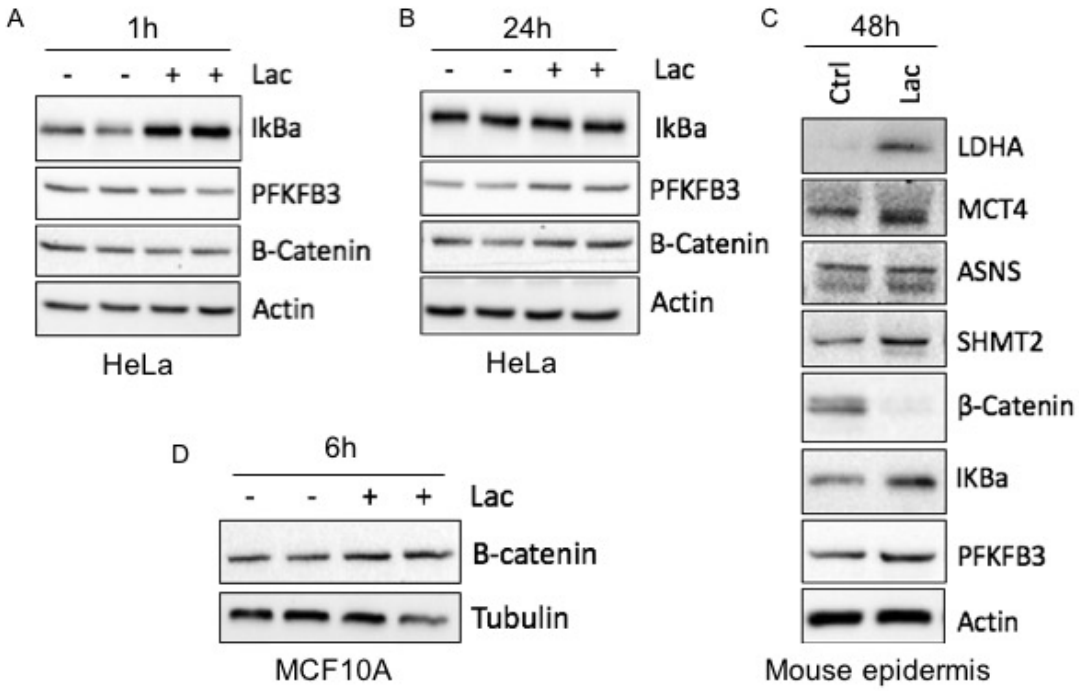

Figure 4-16. **Lactate increases levels of additional βTrCP substrates.** Immunoblots showing IkBa, PFKFB3, and β-catenin levels in HeLa cells after 25 mM lactate treatment for one hour **(A)** or 24 hours **(B)**. **(C)** Immunoblot showing levels of βTrCP substrates in mouse epidermis after topical treatment with 20 mM lactate. **(D)** Immunoblot showing β-catenin levels in MCF10A cells after treatment with 25 mM lactate for 6 hours.

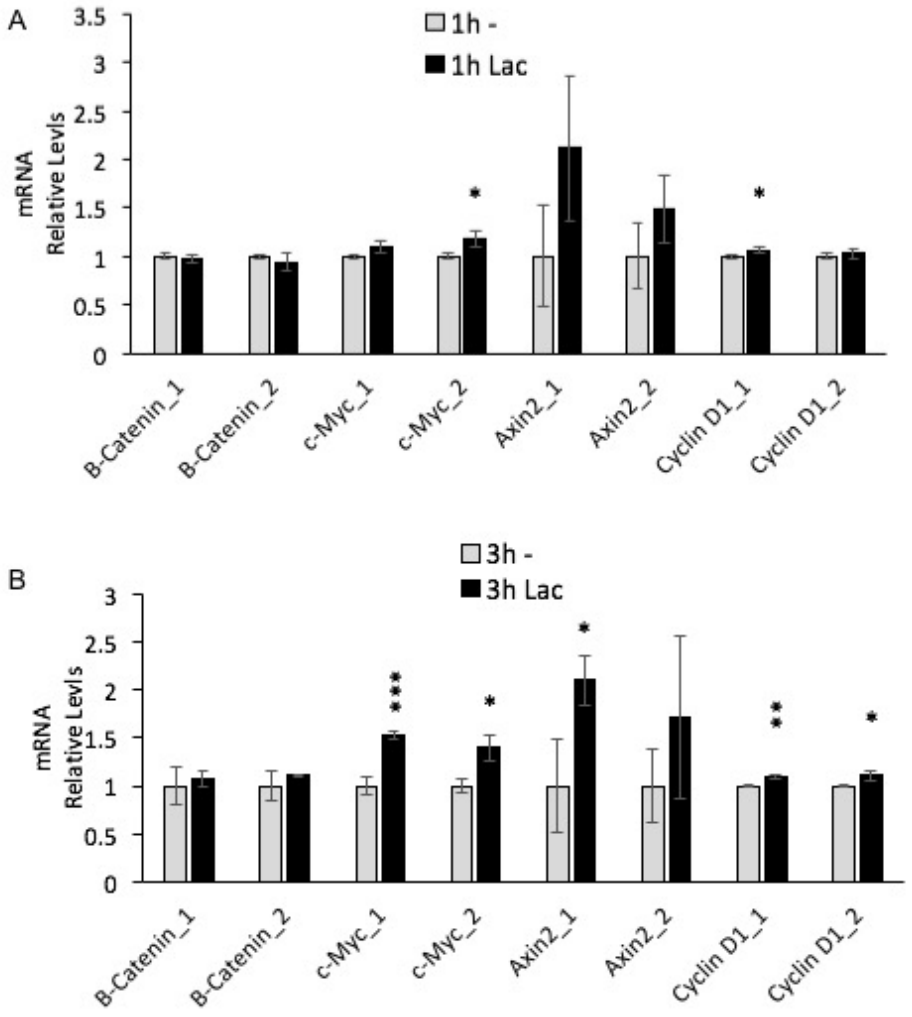

Figure 4-17. **Lactate increases expression of β-catenin target genes.** mRNA levels of known β-catenin target genes in HeLa cells after 25 mM lactate treatment for **(A)** 1 hour **(B)** 3 hours. Numbers following gene labels represent unique primer pairs. Error bars denote standard deviation of the mean. *p < 0.05; **p < 0.01; ***p < 0.001.

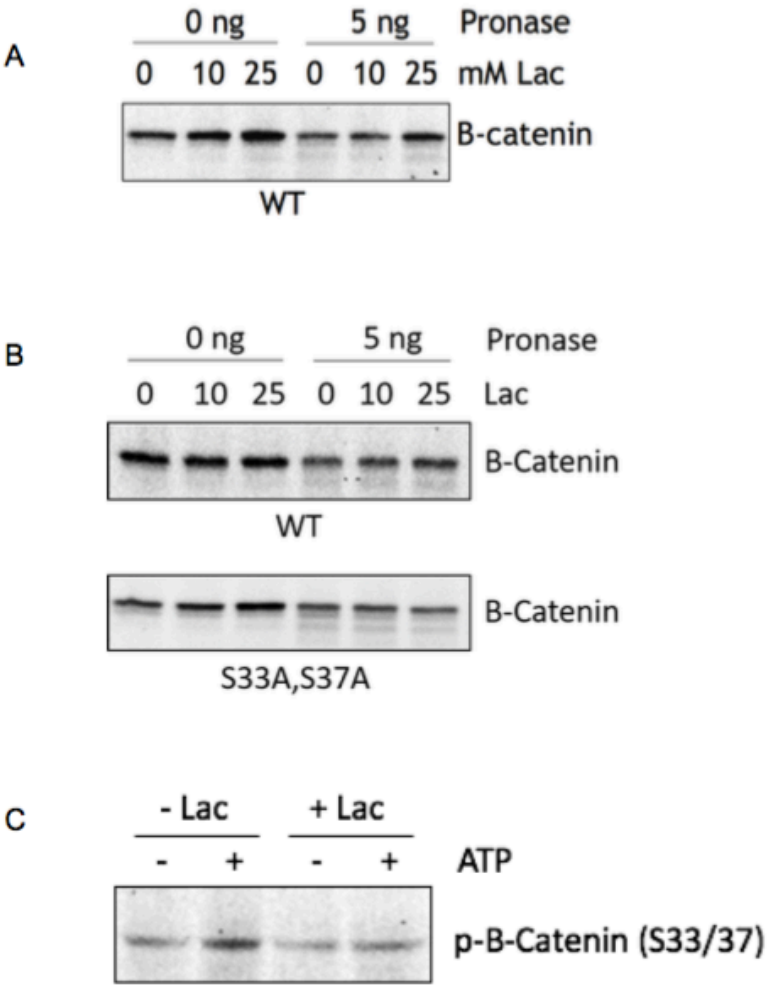

Figure 4-18. **Evidence of lactate-β-catenin binding. (A)** DARTS: Immunoblot showing *in vitro* translated (IVT) β-catenin after pronase digestion in the presence of increasing concentrations of lactate. **(B)** DARTS: Immunoblot showing levels of IVT β-catenin (WT or S33A,S37A) after pronase digestion in the presence of increasing concentrations of lactate. **(C)** *In* vitro kinase assay: Immunoblot showing levels of phosphorylated β-catenin (S33/37) in HEK293T cell lysate after the addition of 500 uM ATP for 5 minutes in the presence or absence of 20 mM lactate.

A

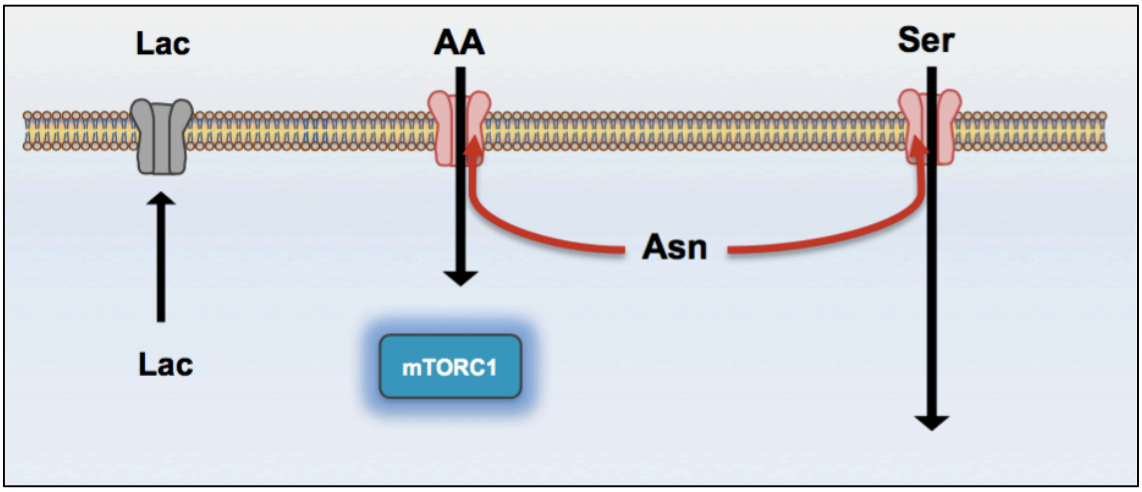

B

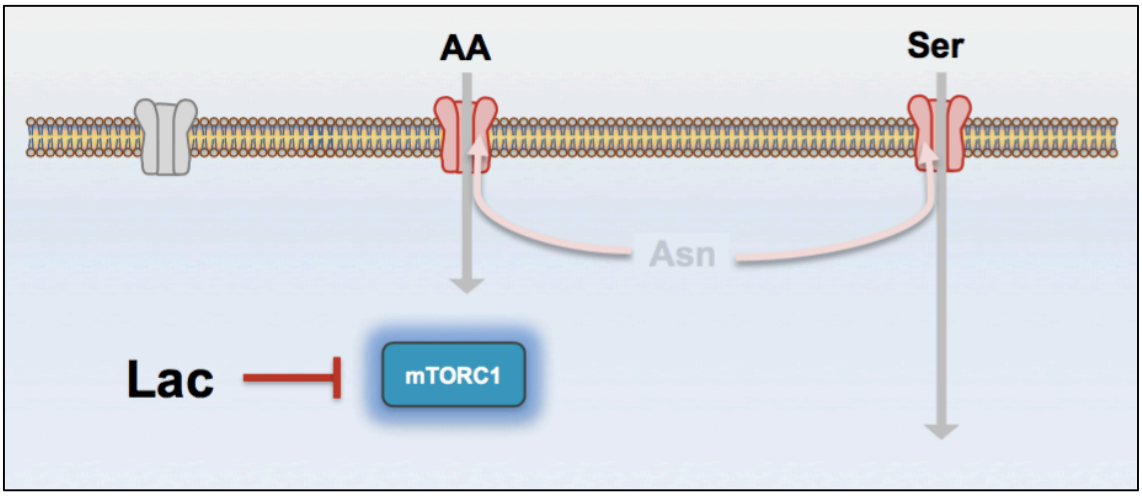

Figure 4-19. **Lactate signals amino acid levels to mTORC1.** Schematic indicating lactate regulation of mTORC1 in the context of asparagine abundance **(A)** or depletion **(B)**.

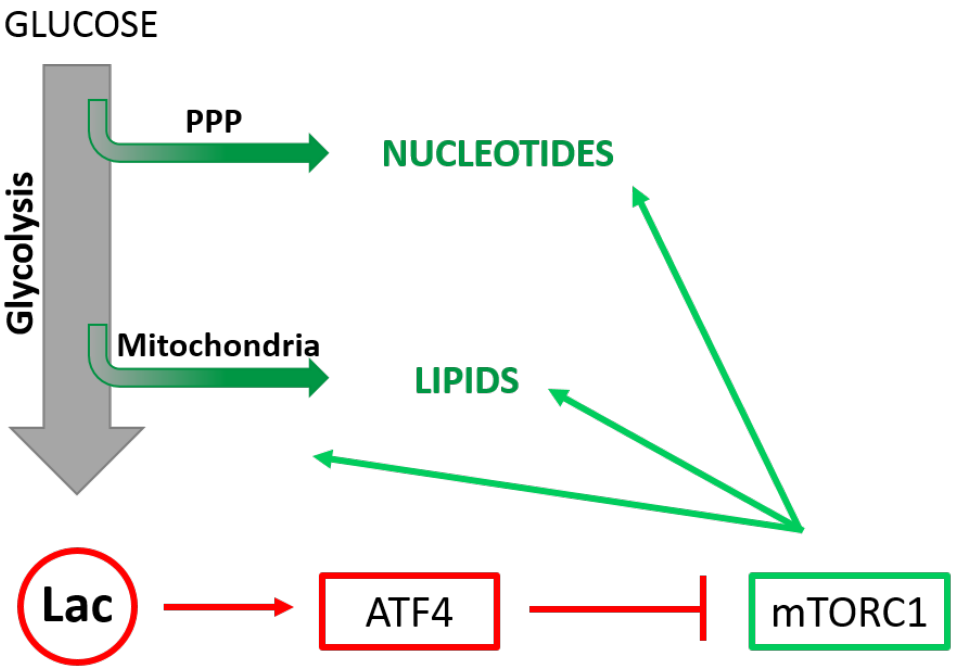

Figure 4-20. **Lactate is a negative feedback signal.** Schematic depicting lactate, the end product of glycolysis, acting as a negative feedback signal through ATF4-mediated mTORC1 inhibition.

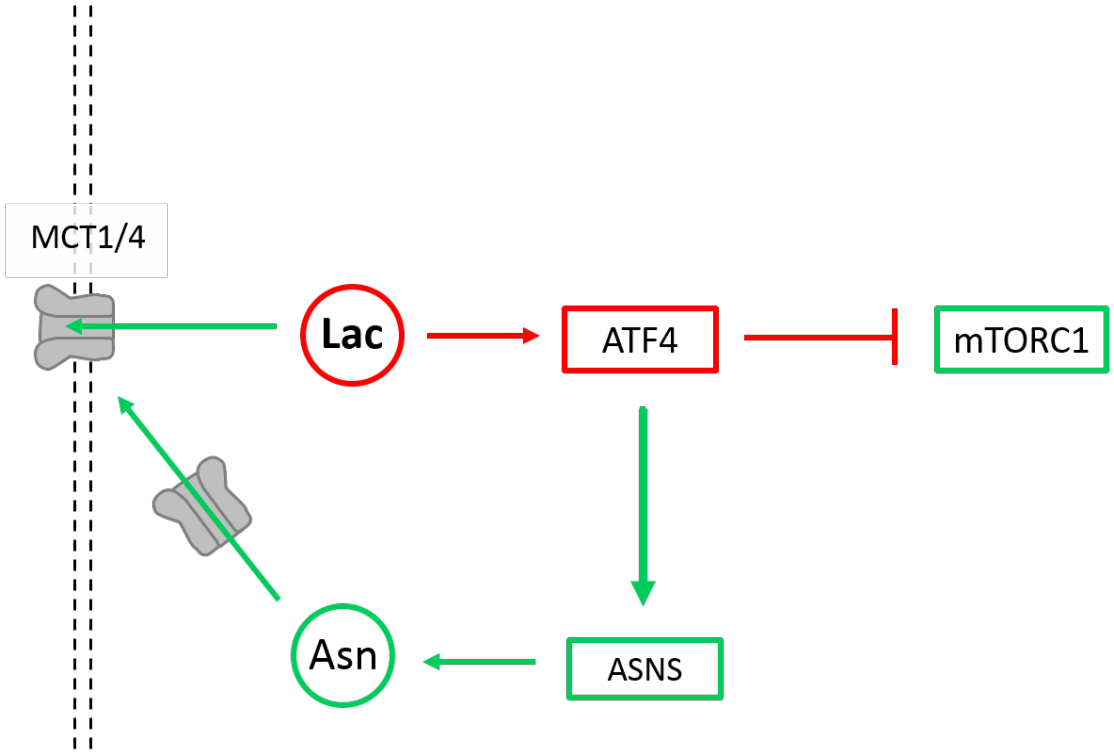

Figure 4-21. **Model depicting asparagine-lactate homeostasis.** Asparagine depletion is sensed through accumulation of intracellular lactate, which promotes ATF4-mediated ASNS expression and restoration of intracellular asparagine. Newly synthesized asparagine, in turn, leads to increased lactate export to turn down ATF4 activity and asparagine synthesis. The lactate-ATF4-mTORC1 axis results in inhibited anabolism upon asparagine depletion and requires asparagine restoration to be reactivated (via asparagine-mediated lactate expulsion).

A

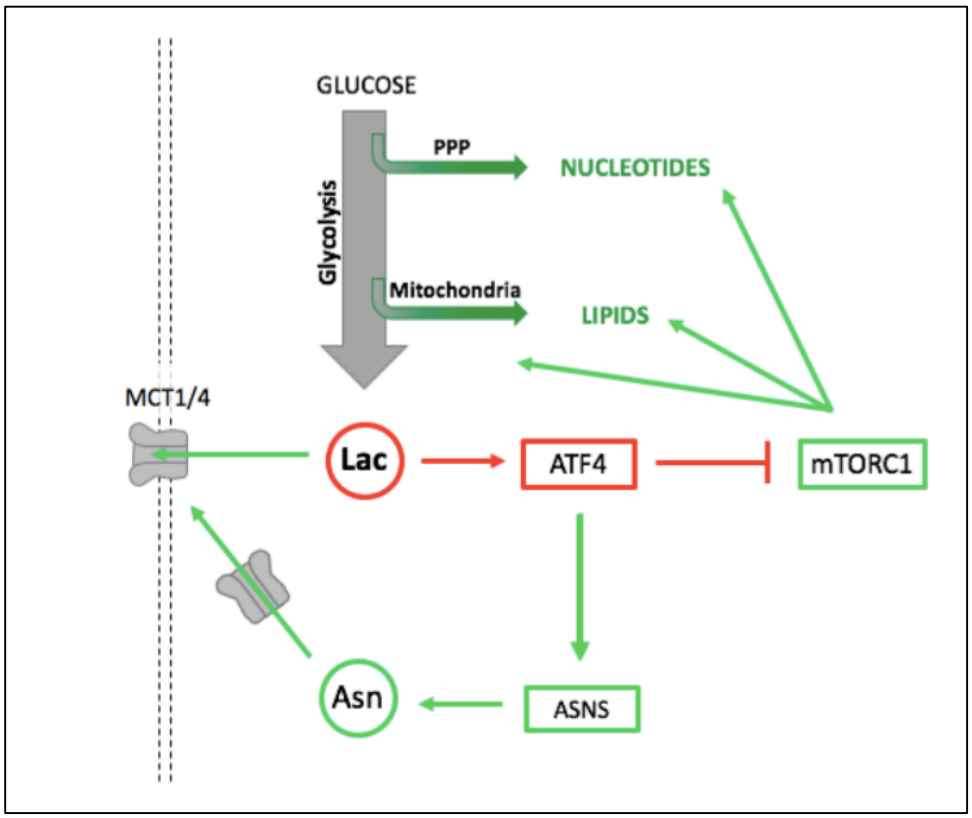
GLUCOSE
PPP
NUCLEOTIDES
Glycolysis
Mitochondria
LIPIDS
MCT1/4
Lac
ATF4
mTORC1
Asn
ASNS

B

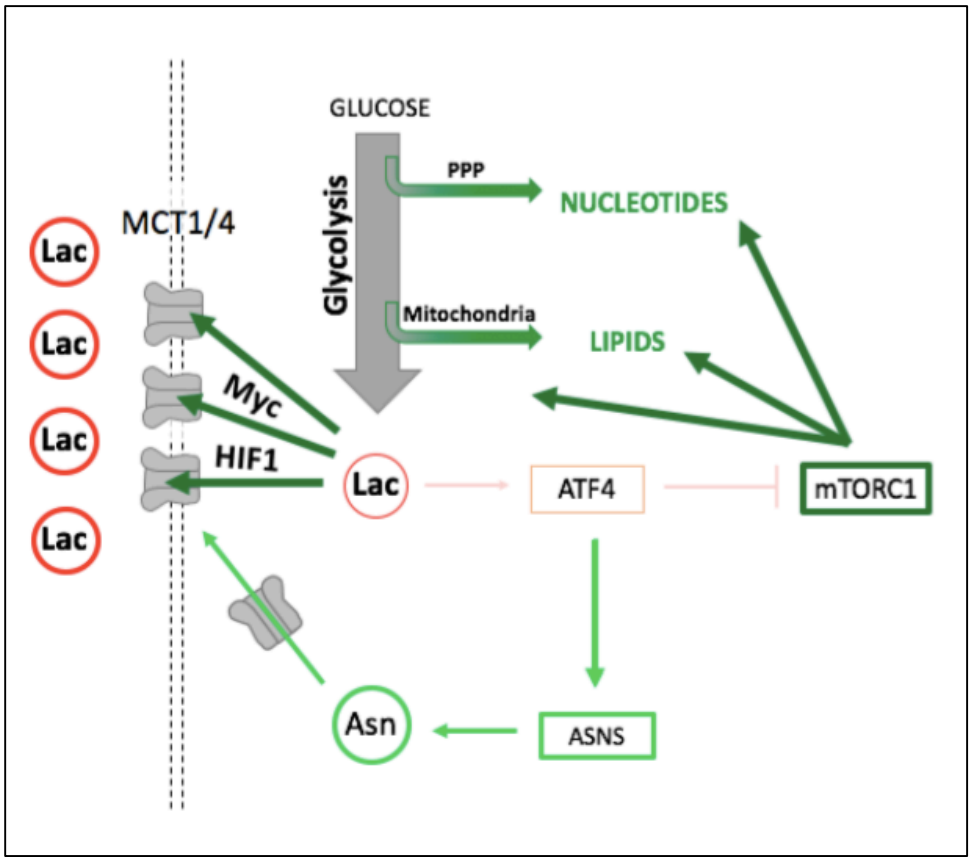
GLUCOSE
PPP
NUCLEOTIDES
MCT1/4
Glycolysis
Mitochondria
LIPIDS
Lac
Lac
Lac
Lac
Myc
HIF1
Lac
ATF4
mTORC1
Asn
ASNS

Figure 4-22. **Model depicting lactate regulation of cellular homeostasis and homeostatic break down during malignant transformation. (A)** Hypothesis: Lactate promotes metabolic and cellular homeostasis by downregulating anabolism through ATF4-mediated mTORC1 inhibition while simultaneously preventing its own accumulation through ATF4-mediated asparagine synthesis and downstream lactate transporter trafficking. **(B)** Hypothesis: Cancer cells break this homeostatic loop though Myc- and HIF1α-driven MCT1 and MCT4 upregulation and lactate export. Increased lactate export relieves ATF4-mediated mTORC1 inhibition and permits unrestricted anabolism and proliferation.

Figure 4-23. **βTrCP recognition motif is conserved in C. *elegans* ATFS-1 but is not present in yeast GCN4.** Amino acid sequence alignment of the human ATF4 βTrCP motif w with C. *elegans* ATFS-1 (left) and Saccharomyces *cerevisiae* GCN4 (right). The motif is conserved in C. *elegans* (highlighted in blue), but does not align with any portion of the Saccharomyces *cerevisiae* GCN4 amino acid sequence (the closest match is highlighted in grey).

REFERENCES

1. Faubert B, Li KY, Cai L, Hensley CT, Kim J, Zacharias LG, Yang C, Do QN, Doucette S, Burguete D, Li H, Huet G, Yuan Q, Wigal T, Butt Y, Ni M, Torrealba J, Oliver D, Lenkinski RE, Malloy CR, Wachsmann JW, Young JD, Kernstine K, DeBerardinis RJ. Lactate Metabolism in Human Lung Tumors. Cell. 2017;171(2):358-71 e9. doi: 10.1016/j.cell.2017.09.019. PubMed PMID: 28985563; PMCID: PMC5684706.

2. Hui S, Ghergurovich JM, Morscher RJ, Jang C, Teng X, Lu W, Esparza LA, Reya T, Le Z, Yanxiang Guo J, White E, Rabinowitz JD. Glucose feeds the TCA cycle via circulating lactate. Nature. 2017;551(7678):115-8. doi: 10.1038/nature24057. PubMed PMID: 29045397.

3. Sonveaux P, Vegran F, Schroeder T, Wergin MC, Verrax J, Rabbani ZN, De Saedeleer CJ, Kennedy KM, Diepart C, Jordan BF, Kelley MJ, Gallez B, Wahl ML, Feron O, Dewhirst MW. Targeting lactate-fueled respiration selectively kills hypoxic tumor cells in mice. J Clin Invest. 2008;118(12):3930-42. doi: 10.1172/JCI36843. PubMed PMID: 19033663; PMCID: PMC2582933.

4. Fiaschi T, Marini A, Giannoni E, Taddei ML, Gandellini P, De Donatis A, Lanciotti M, Serni S, Cirri P, Chiarugi P. Reciprocal metabolic reprogramming through lactate shuttle coordinately influences tumor-stroma interplay. Cancer Res. 2012;72(19):5130-40. doi: 10.1158/0008-5472.CAN-12-1949. PubMed PMID: 22850421.

5. DeBerardinis RJ, Mancuso A, Daikhin E, Nissim I, Yudkoff M, Wehrli S, Thompson CB. Beyond aerobic glycolysis: transformed cells can engage in glutamine metabolism that exceeds the requirement for protein and nucleotide synthesis. Proc Natl Acad Sci U S A. 2007;104(49):19345-50. doi: 10.1073/pnas.0709747104. PubMed PMID: 18032601; PMCID: 2148292.

6. Jain M, Nilsson R, Sharma S, Madhusudhan N, Kitami T, Souza AL, Kafri R, Kirschner MW, Clish CB, Mootha VK. Metabolite profiling identifies a key role for glycine in rapid cancer cell proliferation. Science. 2012;336(6084):1040-4. doi: 10.1126/science.1218595. PubMed PMID: 22628656; PMCID: 3526189.

7. Hosios AM, Vander Heiden MG. The redox requirements of proliferating mammalian cells. J Biol Chem. 2018. doi: 10.1074/jbc.TM117.000239. PubMed PMID: 29339555.

8. Ward PS, Thompson CB. Metabolic reprogramming: a cancer hallmark even warburg did not anticipate. Cancer Cell. 2012;21(3):297-308. doi: 10.1016/j.ccr.2012.02.014. PubMed PMID: 22439925; PMCID: PMC3311998.

9. Doherty JR, Yang C, Scott KE, Cameron MD, Fallahi M, Li W, Hall MA, Amelio AL, Mishra JK, Li F, Tortosa M, Genau HM, Rounbehler RJ, Lu Y, Dang CV, Kumar KG, Butler AA, Bannister TD, Hooper AT, Unsal-Kacmaz K, Roush WR, Cleveland JL. Blocking lactate export by inhibiting the

Myc target MCT1 Disables glycolysis and glutathione synthesis. Cancer Res. 2014;74(3):908-20. doi: 10.1158/0008-5472.CAN-13-2034. PubMed PMID: 24285728; PMCID: PMC3946415.

10. Guile SD, Bantick JR, Cheshire DR, Cooper ME, Davis AM, Donald DK, Evans R, Eyssade C, Ferguson DD, Hill S, Hutchinson R, Ingall AH, Kingston LP, Martin I, Martin BP, Mohammed RT, Murray C, Perry MW, Reynolds RH, Thorne PV, Wilkinson DJ, Withnall J. Potent blockers of the monocarboxylate transporter MCT1: novel immunomodulatory compounds. Bioorg Med Chem Lett. 2006;16(8):2260-5. doi: 10.1016/j.bmcl.2006.01.024. PubMed PMID: 16455256.

11. Murray CM, Hutchinson R, Bantick JR, Belfield GP, Benjamin AD, Brazma D, Bundick RV, Cook ID, Craggs RI, Edwards S, Evans LR, Harrison R, Holness E, Jackson AP, Jackson CG, Kingston LP, Perry MW, Ross AR, Rugman PA, Sidhu SS, Sullivan M, Taylor-Fishwick DA, Walker PC, Whitehead YM, Wilkinson DJ, Wright A, Donald DK. Monocarboxylate transporter MCT1 is a target for immunosuppression. Nat Chem Biol. 2005;1(7):371-6. PubMed PMID: 16370372.

12. Vattem KM, Wek RC. Reinitiation involving upstream ORFs regulates ATF4 mRNA translation in mammalian cells. Proc Natl Acad Sci U S A. 2004;101(31):11269-74. doi: 10.1073/pnas.0400541101. PubMed PMID: 15277680; PMCID: PMC509193.

13. Wek RC, Cavener DR. Translational control and the unfolded protein response. Antioxid Redox Signal. 2007;9(12):2357-71. doi: 10.1089/ars.2007.1764. PubMed PMID: 17760508.

14. Lomenick B, Hao R, Jonai N, Chin RM, Aghajan M, Warburton S, Wang J, Wu RP, Gomez F, Loo JA, Wohlschlegel JA, Vondriska TM, Pelletier J, Herschman HR, Clardy J, Clarke CF, Huang J. Target identification using drug affinity responsive target stability (DARTS). Proc Natl Acad Sci U S A. 2009;106(51):21984-9. doi: 10.1073/pnas.0910040106. PubMed PMID: 19995983; PMCID: 2789755.

15. Chin RM, Fu X, Pai MY, Vergnes L, Hwang H, Deng G, Diep S, Lomenick B, Meli VS, Monsalve GC, Hu E, Whelan SA, Wang JX, Jung G, Solis GM, Fazlollahi F, Kaweeteerawat C, Quach A, Nili M, Krall AS, Godwin HA, Chang HR, Faull KF, Guo F, Jiang M, Trauger SA, Saghatelian A, Braas D, Christofk HR, Clarke CF, Teitell MA, Petrascheck M, Reue K, Jung ME, Frand AR, Huang J. The metabolite alpha-ketoglutarate extends lifespan by inhibiting ATP synthase and TOR. Nature. 2014;510(7505):397-401. doi: 10.1038/nature13264. PubMed PMID: 24828042; PMCID: 4263271.

16. Lassot I, Segeral E, Berlioz-Torrent C, Durand H, Groussin L, Hai T, Benarous R, Margottin-Goguet F. ATF4 degradation relies on a phosphorylation-dependent interaction with the SCF(betaTrCP) ubiquitin ligase. Mol Cell Biol. 2001;21(6):2192-202. doi: 10.1128/MCB.21.6.2192-2202.2001. PubMed PMID: 11238952; PMCID: PMC86853.

17. Saxton RA, Sabatini DM. mTOR Signaling in Growth, Metabolism, and Disease. Cell. 2017;169(2):361-71. doi: 10.1016/j.cell.2017.03.035. PubMed PMID: 28388417.

18. Yang H, Rudge DG, Koos JD, Vaidialingam B, Yang HJ, Pavletich NP. mTOR kinase structure, mechanism and regulation. Nature. 2013;497(7448):217-23. doi: 10.1038/nature12122. PubMed PMID: 23636326; PMCID: PMC4512754.

19. Csibi A, Lee G, Yoon SO, Tong H, Ilter D, Elia I, Fendt SM, Roberts TM, Blenis J. The mTORC1/S6K1 pathway regulates glutamine metabolism through the eIF4B-dependent control of c-Myc translation. Curr Biol. 2014;24(19):2274-80. doi: 10.1016/j.cub.2014.08.007. PubMed PMID: 25220053; PMCID: PMC4190129.

20. Duvel K, Yecies JL, Menon S, Raman P, Lipovsky AI, Souza AL, Triantafellow E, Ma Q, Gorski R, Cleaver S, Vander Heiden MG, MacKeigan JP, Finan PM, Clish CB, Murphy LO, Manning BD. Activation of a metabolic gene regulatory network downstream of mTOR complex 1. Mol Cell. 2010;39(2):171-83. doi: 10.1016/j.molcel.2010.06.022. PubMed PMID: 20670887; PMCID: PMC2946786.

21. Ben-Sahra I, Manning BD. mTORC1 signaling and the metabolic control of cell growth. Curr Opin Cell Biol. 2017;45:72-82. doi: 10.1016/j.ceb.2017.02.012. PubMed PMID: 28411448; PMCID: PMC5545101.

22. Hitosugi T, Fan J, Chung TW, Lythgoe K, Wang X, Xie J, Ge Q, Gu TL, Polakiewicz RD, Roesel JL, Chen GZ, Boggon TJ, Lonial S, Fu H, Khuri FR, Kang S, Chen J. Tyrosine phosphorylation of mitochondrial pyruvate dehydrogenase kinase 1 is important for cancer metabolism. Mol Cell. 2011;44(6):864-77. doi: 10.1016/j.molcel.2011.10.015. PubMed PMID: 22195962; PMCID: PMC3246218.

23. Schell JC, Olson KA, Jiang L, Hawkins AJ, Van Vranken JG, Xie J, Egnatchik RA, Earl EG, DeBerardinis RJ, Rutter J. A role for the mitochondrial pyruvate carrier as a repressor of the Warburg effect and colon cancer cell growth. Mol Cell. 2014;56(3):400-13. doi: 10.1016/j.molcel.2014.09.026. PubMed PMID: 25458841; PMCID: PMC4268416.

24. Sprowl-Tanio S, Habowski AN, Pate KT, McQuade MM, Wang K, Edwards RA, Grun F, Lyou Y, Waterman ML. Lactate/pyruvate transporter MCT-1 is a direct Wnt target that confers sensitivity to 3-bromopyruvate in colon cancer. Cancer Metab. 2016;4:20. doi: 10.1186/s40170-016-0159-3. PubMed PMID: 27729975; PMCID: PMC5046889.

25. Liu Z, Sneve M, Haroldson TA, Smith JP, Drewes LR. Regulation of Monocarboxylic Acid Transporter 1 Trafficking by the Canonical Wnt/beta-Catenin Pathway in Rat Brain Endothelial Cells Requires Cross-talk with Notch Signaling. J Biol Chem. 2016;291(15):8059-69. doi: 10.1074/jbc.M115.710277. PubMed PMID: 26872974; PMCID: PMC4825010.

26. Elson DA, Ryan HE, Snow JW, Johnson R, Arbeit JM. Coordinate up-regulation of hypoxia inducible factor (HIF)-1alpha and HIF-1 target genes during multi-stage epidermal carcinogenesis and wound healing. Cancer Res. 2000;60(21):6189-95. PubMed PMID: 11085544.

27. Fischer K, Hoffmann P, Voelkl S, Meidenbauer N, Ammer J, Edinger M, Gottfried E, Schwarz S, Rothe G, Hoves S, Renner K, Timischl B, Mackensen A, Kunz-Schughart L, Andreesen R, Krause SW, Kreutz M. Inhibitory effect of tumor cell-derived lactic acid on human T cells. Blood. 2007;109(9):3812-9. doi: 10.1182/blood-2006-07-035972. PubMed PMID: 17255361.

28. Seth P, Csizmadia E, Hedblom A, Vuerich M, Xie H, Li M, Longhi MS, Wegiel B. Deletion of Lactate Dehydrogenase-A in Myeloid Cells Triggers Antitumor Immunity. Cancer Res. 2017;77(13):3632-43. doi: 10.1158/0008-5472.CAN-16-2938. PubMed PMID: 28446465; PMCID: PMC5505499.

29. Rzymski T, Milani M, Pike L, Buffa F, Mellor HR, Winchester L, Pires I, Hammond E, Ragoussis I, Harris AL. Regulation of autophagy by ATF4 in response to severe hypoxia. Oncogene. 2010;29(31):4424-35. doi: 10.1038/onc.2010.191. PubMed PMID: 20514020.

30. Pike LR, Singleton DC, Buffa F, Abramczyk O, Phadwal K, Li JL, Simon AK, Murray JT, Harris AL. Transcriptional up-regulation of ULK1 by ATF4 contributes to cancer cell survival. Biochem J. 2013;449(2):389-400. doi: 10.1042/BJ20120972. PubMed PMID: 23078367.

31. Sousa CM, Biancur DE, Wang X, Halbrook CJ, Sherman MH, Zhang L, Kremer D, Hwang RF, Witkiewicz AK, Ying H, Asara JM, Evans RM, Cantley LC, Lyssiotis CA, Kimmelman AC. Pancreatic stellate cells support tumour metabolism through autophagic alanine secretion. Nature. 2016;536(7617):479-83. doi: 10.1038/nature19084. PubMed PMID: 27509858; PMCID: PMC5228623.

32. Martinez-Outschoorn UE, Trimmer C, Lin Z, Whitaker-Menezes D, Chiavarina B, Zhou J, Wang C, Pavlides S, Martinez-Cantarin MP, Capozza F, Witkiewicz AK, Flomenberg N, Howell A, Pestell RG, Caro J, Lisanti MP, Sotgia F. Autophagy in cancer associated fibroblasts promotes tumor cell survival: Role of hypoxia, HIF1 induction and NFkappaB activation in the tumor stromal microenvironment. Cell Cycle. 2010;9(17):3515-33. doi: 10.4161/cc.9.17.12928. PubMed PMID: 20855962; PMCID: PMC3047617.

33. Kaelin WG, Jr., Ratcliffe PJ. Oxygen sensing by metazoans: the central role of the HIF hydroxylase pathway. Mol Cell. 2008;30(4):393-402. doi: 10.1016/j.molcel.2008.04.009. PubMed PMID: 18498744.

34. Oskolkova OV, Afonyushkin T, Leitner A, von Schlieffen E, Gargalovic PS, Lusis AJ, Binder BR, Bochkov VN. ATF4-dependent transcription is a key mechanism in VEGF up-regulation by oxidized phospholipids: critical role of oxidized sn-2 residues in activation of unfolded protein response. Blood. 2008;112(2):330-9. doi: 10.1182/blood-2007-09-112870. PubMed PMID: 18451308; PMCID: PMC2442744.

35. Wang Y, Alam GN, Ning Y, Visioli F, Dong Z, Nor JE, Polverini PJ. The unfolded protein response induces the angiogenic switch in human tumor cells through the PERK/ATF4 pathway.

Cancer Res. 2012;72(20):5396-406. doi: 10.1158/0008-5472.CAN-12-0474. PubMed PMID: 22915762; PMCID: PMC3743425.

36. Easwaran V, Lee SH, Inge L, Guo L, Goldbeck C, Garrett E, Wiesmann M, Garcia PD, Fuller JH, Chan V, Randazzo F, Gundel R, Warren RS, Escobedo J, Aukerman SL, Taylor RN, Fantl WJ. beta-Catenin regulates vascular endothelial growth factor expression in colon cancer. Cancer Res. 2003;63(12):3145-53. PubMed PMID: 12810642.

37. Hanahan D, Weinberg RA. Hallmarks of cancer: the next generation. Cell. 2011;144(5):646-74. doi: 10.1016/j.cell.2011.02.013. PubMed PMID: 21376230.

38. Basile KJ, Abel EV, Dadpey N, Hartsough EJ, Fortina P, Aplin AE. In vivo MAPK reporting reveals the heterogeneity in tumoral selection of resistance to RAF inhibitors. Cancer Res. 2013;73(23):7101-10. doi: 10.1158/0008-5472.CAN-13-1628. PubMed PMID: 24121492; PMCID: 3851924.

39. Abel EV, Basile KJ, Kugel CH, 3rd, Witkiewicz AK, Le K, Amaravadi RK, Karakousis GC, Xu X, Xu W, Schuchter LM, Lee JB, Ertel A, Fortina P, Aplin AE. Melanoma adapts to RAF/MEK inhibitors through FOXD3-mediated upregulation of ERBB3. J Clin Invest. 2013;123(5):2155-68. doi: 10.1172/JCI65780. PubMed PMID: 23543055; PMCID: 3635724.

Chapter 5

Future Directions

The work described in this dissertation identifies novel signaling roles for two metabolites: asparagine and lactate. We demonstrate that asparagine is used as an amino acid exchange factor for uptake of amino acids from the microenvironment. This exchange function of asparagine enables mTORC1 activation and downstream promotion of anabolic metabolism. In addition, we provide evidence that lactate, the end product of glycolysis, binds to and stabilizes ATF4. We further show that mTORC1 may be subject to feedback inhibition by lactate, downstream of lactate-ATF4 binding. Notably, asparagine and lactate levels are linked: asparagine depletion results in reduced lactate export. Lactate accumulation upon asparagine depletion allows the cell to both restore intracellular asparagine levels through ATF4 transcriptional activity and coordinate anabolism with amino acid availability through mTORC1 inhibition. Our findings have raised numerous additional questions. Here we discuss continuing work on the lactate-ATF4-mTORC1 axis.

Structural analysis of ATF4 in complex with L-lactate

Exogenous lactate treatment and lactate dehydrogenase knockdown indicate that lactate positively regulates ATF4 activity by increasing ATF4 protein levels (Figures 4-5 and 4-6). In addition, cell-free binding assays strongly suggest that L-lactate directly binds to ATF4 (Figures 4-7 and 4-9). Neither pyruvate nor D-lactate appear to share this ATF4 binding capability, suggesting a remarkably specific protein-metabolite interaction. Binding is dependent on ATF4 serine 219 (Figure 4-9), phosphorylation of which is required for βTrCP-mediated ATF4 proteasomal degradation(1). A crystal structure of full-length ATF4 has yet to be determined. A structure of ATF4 in complex with lactate would confirm ATF4-lactate binding. Moreover, a structure would reveal the mechanism of lactate sensing by ATF4 in atomic detail and resolve the specificity of the interaction.

MCT4 as a candidate ATF4 target gene

Lactate transport in proliferating cells is thought to be primarily mediated by MCT1 and MCT4 (2, 3). Our homeostatic model dictates that an increase in intracellular lactate triggers a cellular response designed to restore homeostatic levels of lactate (Figure 4-24). This response includes elevated ASNS expression downstream of lactate mediated ATF4 induction. Increased asparagine levels promote MCT1 and MCT4 plasma membrane localization (Figure 4-3). In addition to altered MCT1/4 localization, both ASNS depletion and exogenous lactate increase MCT1 and MCT4 protein levels (Figure 5-1). MCT1 is known to be regulated downstream of β-catenin(4-6). Therefore, our results indicating that lactate activates β-catenin, perhaps through direct binding, may explain increased MCT1 protein levels with elevated intracellular lactate. How MCT4 levels are regulated by increased intracellular lactate, however, is unclear. ATF4 binds to the DNA of many of its target genes through C/EBP-ATF4 response elements (CAREs). Analysis of the MCT4 gene reveals a canonical CARE element within the first intron (Figure 5-2A), raising the possibility that MCT4 is an ATF4 target gene. Consistent with this possibility, knockdown of ATF4 in HeLa cells results in reduced MCT4 mRNA levels (Figure 5-2B). Chromatin immunoprecipitation upon lactate treatment and ASNS knockdown will reveal whether MCT4 is in fact an ATF4 transcriptional target. It will also be interesting to see whether additional lactate transporters such as MCT2 and MCT3, which may be more highly expressed in non-proliferative tissues, are transcriptionally regulated by ATF4.

Cellular asparagine sensing

Intracellular asparagine levels modulate plasma membrane localization of MCT1 and MCT4, resulting in ATF4 activation through a non-eIF2α-dependent mechanism (Figures 4-2 and 4-3). Asparagine is therefore sensed indirectly through changes in intracellular lactate levels. However, the fact that asparagine regulates MCT1/4 localization upstream of altered lactate levels implies the existence of a direct asparagine sensing mechanism. An unbiased mass-

spectrometry-based DARTS approach to globally examine proteins protected by asparagine upon protease treatment revealed several β-catenin-related proteins as asparagine-binding candidates, including α-catenin, α-importin, and ɣ-catenin, which shares approximately 80% sequence homology with β-catenin. In addition, preliminary data indicate that asparagine and aspartate modestly protect *in vitro* translated β-catenin from protease digestion (Figure 5-3A). Consistent with positive regulation of β-catenin by asparagine, asparagine increases expression of canonical β-catenin target genes (Figure 5-3B-C). Given that β-catenin regulates MCT1 levels, it would be a fitting asparagine sensor. Further work is needed to determine whether β-catenin mediates asparagine regulation of lactate transporter trafficking.

Cell cycle regulator p53 may also be involved in asparagine sensing and signaling. Elevating intracellular asparagine with exogenous asparagine supplementation leads to increased p53 protein levels (Figure 5-3D). It has been shown that p53 binds to ATF4 target genes to negatively impact expression(7). Therefore, asparagine upregulation of p53 may be a negative feedback mechanism to limit ATF4 activity when asparagine is abundant. Notably, β-catenin promotes p53 protein stability(8). It remains to be determined whether asparagine regulation of p53 is downstream of β-catenin activation.

Regulation of cell cycle progression through cycling metabolite levels

Our homeostatic model proposes that non-proliferating cells restrict growth by stabilizing intracellular lactate at concentrations that limit anabolic metabolism to what is required for basic cellular processes. However, the signaling functions of asparagine and lactate suggest that the cell may manipulate asparagine synthesis or lactate export to acutely alter metabolism in certain contexts.

One context being explored is the cell cycle. The cell cycle has temporal metabolic needs, with certain phases benefiting from limited cellular metabolism and other phases requiring increased anabolism to duplicate nucleotides, lipids, and protein. For instance, it makes intuitive sense for G1 to be a phase of elevated anabolic metabolism in order to synthesize nucleotides prior to DNA replication in S phase. On the other hand, it has been argued that reduced oxidative metabolism would benefit the cell during S phase and mitosis(9). For instance, DNA replication in yeast in temporally restricted to the reductive phase of the metabolic cycle – when oxygen consumption is minimal(10, 11). This is thought to protect genome integrity by shielding replicating DNA from oxidative damage(12). Additionally, reducing biomass synthesis might conserve ATP for DNA replication and mitosis.

Asparagine and lactate both influence cell signaling and downstream anabolic metabolism: asparagine promotes amino acid acquisition and anabolism downstream of mTORC1 through its amino acid exchange function; lactate reduces anabolic metabolism downstream of mTORC1 through ATF4 stabilization. It will be interesting to see whether the cell takes advantage of these opposing signaling functions by temporally modulating asparagine and lactate levels in accordance with the metabolic demands of each cell cycle phase.

In addition, we have shown that intracellular asparagine and lactate levels are reciprocally regulated in a metabolite/signaling loop: 1) Lactate stabilizes ATF4, leading to asparagine synthesis downstream of ATF4 target ASNS. 2) Asparagine accumulation leads to lactate expulsion, reducing ATF4 activity and asparagine levels. 3) Reduced asparagine allows for lactate accumulation to renew the cycle. This natural lactate-asparagine cycling may also support temporal regulation of cell metabolism in accordance with the cell cycle.

Figure 5-4 proposes a hypothetical model whereby lactate-asparagine cycling promotes cycling of cellular processes. We are examining the following hypotheses for each cell cycle phase: G1/S: Intracellular asparagine depletion supports the G1/S transition due to asparagine upregulation of p53. S Phase: Intracellular asparagine reduction leads to intracellular lactate accumulation. G2/M: Lactate accumulation results in ATF4 stabilization, increased ATF4 transcriptional activity, and restored intracellular asparagine; intracellular asparagine exchanges with extracellular amino acids and promotes lactate export. G1: Reduced intracellular lactate relieves mTORC1 inhibition to promote anabolic metabolism; the amino acids acquired during G2/M amino acid exchange and ATF4-mediated *de novo* amino acid synthesis are used for protein synthesis; reduced intracellular lactate levels destabilize ATF4, reducing intracellular asparagine levels, and allowing for another G1/S transition.

Regulation of metabolic enzymes by cell cycle mediators is beginning to be explored(13). However, whether metabolites levels are sensed by cell cycle mediators to regulate cell cycle progression has not been addressed. For instance, are elevated intracellular asparagine levels sufficient to prevent the G1-S transition? Although cell cycle analysis of mammalian cellular respiration has not yet been performed, extrapolation from respiration cycling in yeast would suggest that the cell reduces respiration during S phase to promote genome stability. Given our data that asparagine is a primary purpose and product of cellular respiration (Chapter 3), asparagine itself may be a signal of active respiration that must be minimized to initiate S phase. It will also be interesting to determine whether elevated intracellular lactate prevents entry into G1. Lactate acutely decreases G1-specific cyclin D1 and c-Myc (which peaks in G1) protein levels (Figure 5-5), consistent with this possibility. These reductions are not observed at the mRNA level (Figure 4-17), suggesting that decreased cyclin D1 and c-Myc translation downstream of lactate-mediated mTORC1 inhibition may be responsible(14, 15). Elevated lactate may signal to the cell that intracellular asparagine has not been restored and that the cell

has not accumulated building blocks required for G1 biosynthetic processes. Mutual regulation between the cell cycle and metabolites would create a coordinated and efficient system whereby metabolite synthesis is directed during a particular cell cycle phase, with accumulation of that metabolite being required for transition into the metabolite-consuming phase of the cell cycle.

Lactate regulation of hair follicle activation

The hair follicle undergoes cycles of rest (telogen), regeneration (anagen), and degeneration (catagen). Entry into anagen requires activation of the hair follicle stem cells. In collaboration, we recently discovered that lactate dehydrogenase activity promotes hair follicle stem cell (HFSC) activation (Figure 5-6)(16). This work showed that genetic deletion of Ldha specifically in the HFSCs prevents hair follicle activation, whereas blocking pyruvate entry into the mitochondria with small molecule inhibitors of the mitochondrial pyruvate carrier (MPC) promotes HFSC activation and hair growth. These results suggest that pyruvate conversion to lactate is critical for HFSC activation.

Although LDHA activity is essential for HFSC activation, it is not yet clear whether lactate itself drives activation or whether pyruvate conversion to lactate creates a metabolic environment that benefits HFSC proliferation. For instance, blocking pyruvate mitochondrial entry has been shown to increase glycolytic flux(17, 18), which could promote HFSC proliferation because of increased flow of glucose carbons into biosynthetic pathways. Topical treatment of mouse epidermis with lactate is being performed to help distinguish between these possibilities. Increased HFSC activation and hair growth with topical lactate, independent of LDH activity, would suggest that lactate itself promotes HFSC activation. Although further experiments are needed for confirmation, our preliminary results are consistent with this possibility (data not shown). The work in this dissertation indicates that lactate is a signaling metabolite that

regulates ATF4, β-catenin, PFKFB3, and IkB levels in mouse epidermis (Figure 4-19). The importance of β-catenin activity in HFSC activation is well documented(19-21). It will be interesting to determine whether lactate regulation of these proteins is involved in LDHA-mediated HFSC activation.

HFSCs reside in a complex niche with many different types of cells, and signals from surrounding cells are critical for hair follicle cycling(22). An additional remaining question is whether HFSC-specific lactate production promotes hair follicle activation through cell-autonomous or non-cell-autonomous mechanisms. Examination of HFSC lactate transporter expression levels during telogen, anagen, and the telogen-anagen transition may help clarify whether lactate is signaling in a cell-autonomous manner. For instance, decreased HFSC lactate transporter expression with the initiation of anagen would suggest intracellular lactate accumulation promotes activation in a cell-autonomous manner. Conversely, increased HFSC lactate transporter expression upon anagen would suggest non-cell-autonomous lactate signaling, with HFSC export of lactate into the stem cell niche stimulating activation.

Immune cells in the skin influence hair follicle function. Anagen is a phase of immunosuppression relative to telogen, and it has been proposed that immune privilege at the hair follicle is required for hair follicle cycling(23). It was recently shown that regulatory T cells in the skin, which suppress inflammation, preferentially localize to the hair follicle(24), consistent with immune suppression benefiting HFSC activation. Given lactate suppression of immune cell function(25-28), these findings raise the possibility that immune cells are effectors of HFSC activation through non-cell-autonomous signaling: lactate exported by HFSCs at the telogen-anagen transition may promote entry into anagen by suppressing immunity in the hair follicle microenvironment. To examine this possibility, hair growth experiments are being performed on

immunocompetent versus immunodeficient mice. If immune cells are mechanistically involved, MPC inhibition and lactate treatment will not enhance hair growth on immunodeficient mice.

Lactate regulation of lifespan

Metabolism, inflammation, and aging are intimately linked. The influence of metabolism on aging is apparent from studies showing that dietary restriction increases longevity and decreases the occurrence of age-related diseases(29, 30). Moreover, several metabolites have recently been shown to influence lifespan(31-34). Metabolic regulation of longevity is frequently found to depend on changes in TORC1 signaling(31, 32, 35, 36), inhibition of which extends lifespan in several organisms(36). Chronic inflammation is also associated with aging and underlies many age-related-illnesses(37, 38). Aging-related inflammation is thought to be mediated in large part by NFkB, activity of which increases with age(39). Our results suggest that lactate may regulate both TORC1 signaling and inflammation. We show that lactates inhibits mTORC1 in a manner that is likely mediated by lactate-ATF4 binding. IkB, which inhibits NFkB activity through cytoplasmic sequestration, is an additional βTrCP substrate that is elevated upon lactate treatment (Figure 4-19). We hypothesize that lactate may promote lifespan extension through these signaling properties. This hypothesis is currently being examined by assessing *C. elegans* lifespan in the presence or absence of exogenous lactate.

Pyruvate/lactate streamlining by proliferating cells

Despite lactate inhibition of mTORC1 activity, cancer cell and other proliferating cells synthesize lactate, perhaps for use as a paracrine signal. Proliferating cells may therefore have mechanisms to streamline pyruvate metabolism and lactate export to avoid accumulation of cytoplasmic lactate.

We proposed that lactate may represent overflow pyruvate that cannot be metabolized when the oxidation/transamination pathways are saturated (Chapter 4). Most adult tissues express PKM1, a pyruvate kinase isoform with relatively high enzymatic activity. Cancer cells, however, have been shown to exclusively express the less active PKM2 isoform(40). Moreover, forced PKM1 expression in cancer cells reduces tumorigenicity(41). Modulating the kinetics of pyruvate synthesis may be a mechanism to prevent metabolic saturation by synthesizing pyruvate at a rate at which it can be immediately oxidized. In support of this hypothesis, we find that activating PKM2 in cancer cells with the small molecule TEPP-46 leads to increased levels of ATF4, ATF4 target genes, MCT1, and MCT4 (Figure 5-7), consistent with pyruvate synthesis kinetics influencing intracellular lactate levels.

In addition to streamlining pyruvate metabolism, proliferating cells may streamline lactate export through lactate channeling. Glycolytic enzymes have been shown to exist in complexes at the plasma membrane(42, 43). It has been proposed that glycolytic complexes support metabolite channeling to increase pathway efficiency. Future studies will examine whether proliferating cells form plasma membrane complexes consisting of lactate dehydrogenase and lactate transporters as a means of channeling lactate export and reducing cytoplasmic lactate.

Subcellular lactate pools

Subcellular locations often serve as platforms for molecular interactions for the purpose of coordinating cellular processes. An example is the lysosome, which colocalizes Rheb activation via growth factor signaling and amino acid sensing via lysosomal proteolysis/amino acid transport to coordinate mTORC1 activation(44). We are considering the possibility that lactate inhibition of mTORC1 may be similarly facilitated by lysosomal localized lactate generation. CRISPR/Cas9-mediated LDHA knockout abolishes ATF4 activation upon asparagine withdrawal in HeLa cells (Figure 5-8A), indicating that LDHA-mediated lactate generation, specifically, may

be responsible for ATF4 activation. Moreover, LDHA knockdown does not reduce the kinetics of glucose conversion to lactate (Figure 5-8B) or lactate export rates (Figure 5-8C), suggesting that LDHA knockdown affects ATF4 and mTORC1 activities without globally affecting lactate synthesis. These results raise the possibility that a subcellular lactate pool generated by LDHA is responsible for lactate regulatory functions.

We therefore examined LDHA localization by immunofluorescence. LDHA displays diffuse cytoplasmic staining. However, distinct LDHA puncta colocalize with lysosomal marker LAMP2 (Figure 5-9). Near complete LDHA depletion is required to affect ATF4 and mTORC1 activities: ~95% reduction in LDHA levels (shLDHA-1) has only minimal effects in comparison to near 100% knockdown (shLDHA-2) (Figure 5-9A-B). Staining of the residual LDHA in shLDHA-1 cells displays near complete overlap with LAMP2 staining (Figure 5-10). Our preliminary data are consistent with lactate channeling to an ATF4-mTORC1 complex through lysosomal surface-localized LDHA (Figure 5-11). Forster Resonance Energy Transfer (FRET)-based lactate sensors have been used to detect intracellular lactate(45). We expect that this FRET probe will enable the assessment of intracellular lactate distribution and, specifically, whether a subcellular lactate pool colocalizes with fluorophore-tagged LAMP2. The lysosomal surface may be a platform for efficient lactate-ATF4-mTORC1 signaling, similar to amino acid-mTORC1-Rheb signaling.

Additional lactate binding proteins

Because numerous proteins possess βTrCP recognition motifs (Figure 4-18), lactate may have several protein binding partners. DARTS binding assays indicate that lactate directly binds to ATF4 and β-catenin (Figures 4-9 and 4-21). Although cell lactate treatment increases PFKFB3 and IkBa protein levels, we have not yet confirmed lactate binding. Moreover, a complete list of candidate lactate binders has yet to be assembled. A more comprehensive candidates list will

be generated by globally analyzing lactate-sensitive BTrCP interactions through BTrCP immunoprecipitation followed by mass spectrometry.

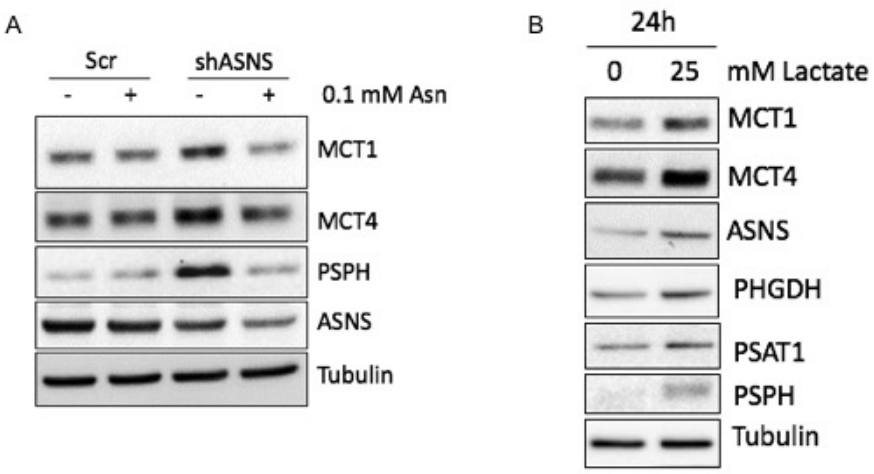

Figure 5-1. **Intracellular asparagine and lactate levels regulate MCT1 and MCT4 expression. (A)** Expression of ASNS shRNA results in increased MCT1 and MCT4 protein levels; increased MCT1 and MCT4 expression is rescued by exogenous asparagine supplementation. **(B)** Exogenous lactate treatment results in increased MCT1 and MCT4 protein levels.

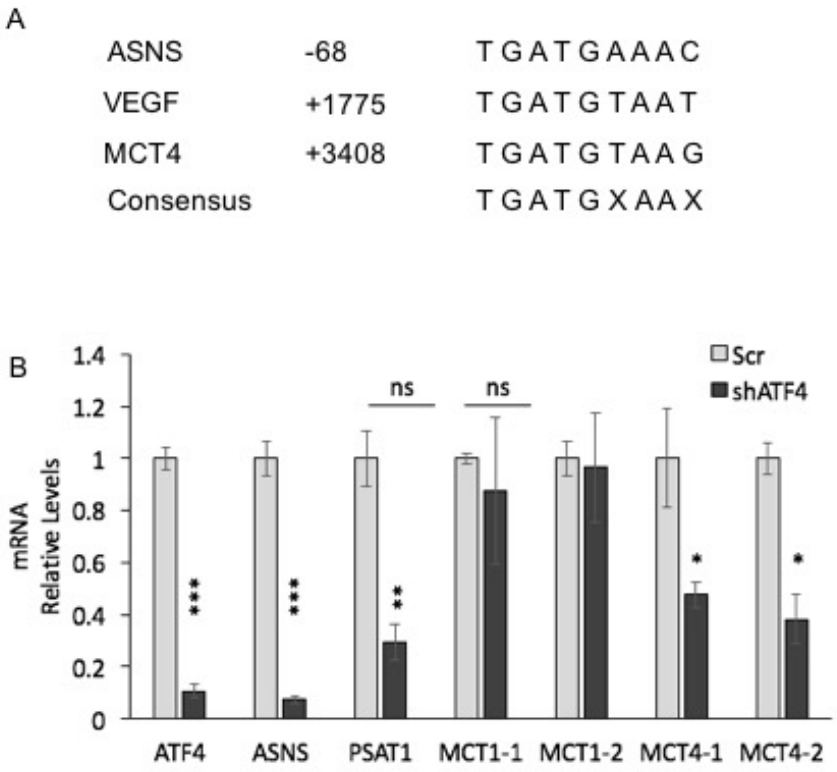

Figure 5-2. **Evidence that MCT4 may be an ATF4 transcriptional target gene. (A)** Intron 1 of human MCT4 contains a putative C/EBP-ATF4 response (CARE) element. Known ATF4 binding sites on ASNS and VEGF and the consensus CARE sequence are shown for comparison. **(B)** mRNA levels of MCT1, MCT4, and known ATF4 target genes ASNS and PSAT1 in HeLa cells expressing scrambled (Scr) or ATF4 shRNA. mRNA data generated with two separate primer pairs (-1 and -2) are shown for MCT1 and MCT4. Error bars denote standard deviation of the mean. *$p < 0.05$; **$p < 0.01$; ***$p < 0.001$; ns, not significant.

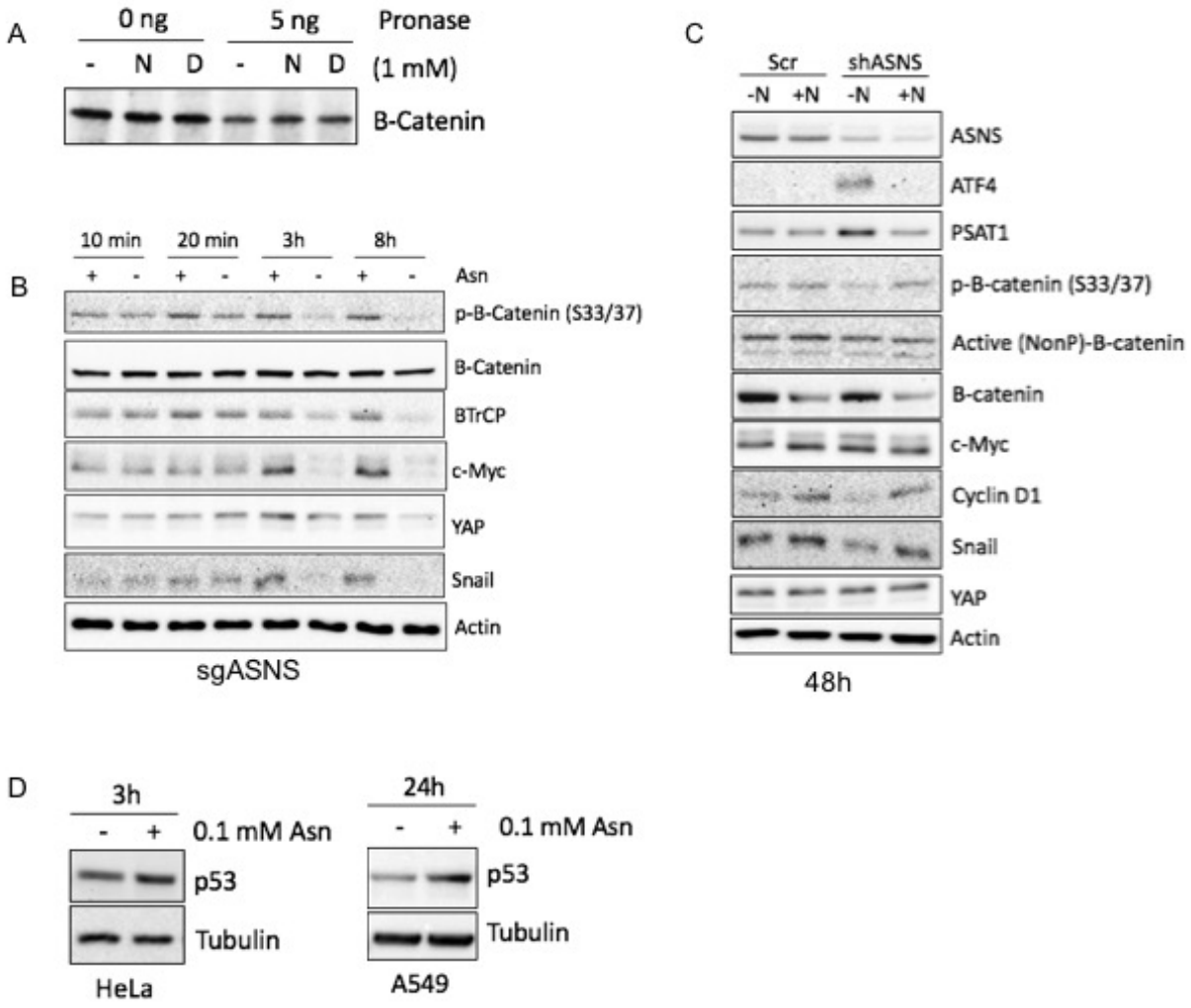

Figure 5-3. **Asparagine regulates β-catenin activity and p53 levels. (A)** DARTS: Protection of IVT β-catenin pronase digestion by 1 mM asparagine (N) and aspartate (D). **(B)** Immunoblot showing decreased expression of β-catenin target genes c-Myc, YAP, and Snail after asparagine withdrawal from HeLa ASNS knockout cells (sgASNS) for 3 hours and 8 hours. **(C)** Immunoblot showing increased expression of β-catenin target genes c-Myc, cyclin D1, and Snail in HeLa cells with 0.1 mM exogenous asparagine treatment for 48 hours; cyclin D1 and Snail expression are decreased with expression of ASNS shRNA. **(D)** Immunoblot showing increased p53 levels in HeLa and A549 cells with 0.1 mM exogenous asparagine treatment.

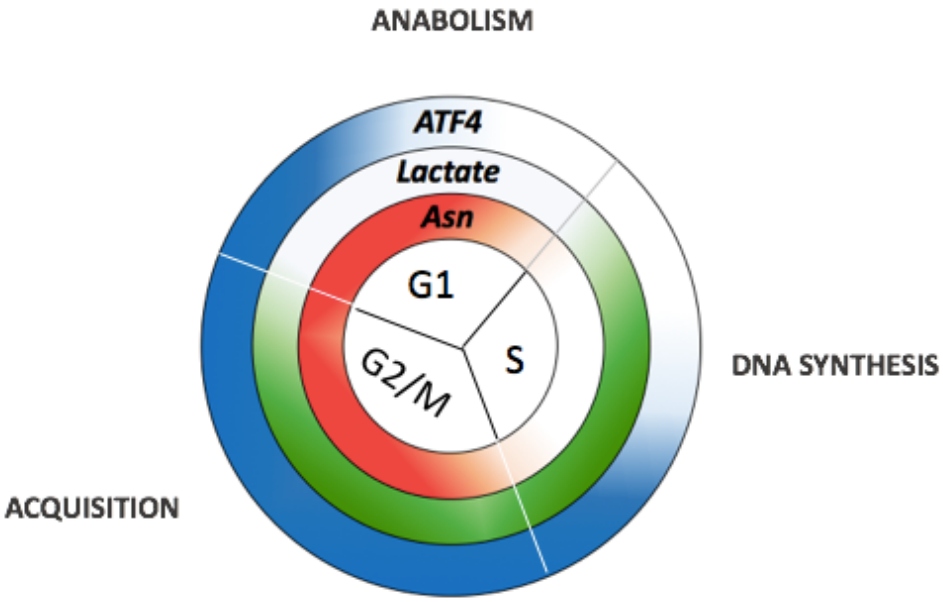

Figure 5-4. **Model depicting hypothetical regulation of cell cycle progression by metabolite cycling.** Color gradients represent relative levels of asparagine (red), lactate (green), and ATF4 (blue).

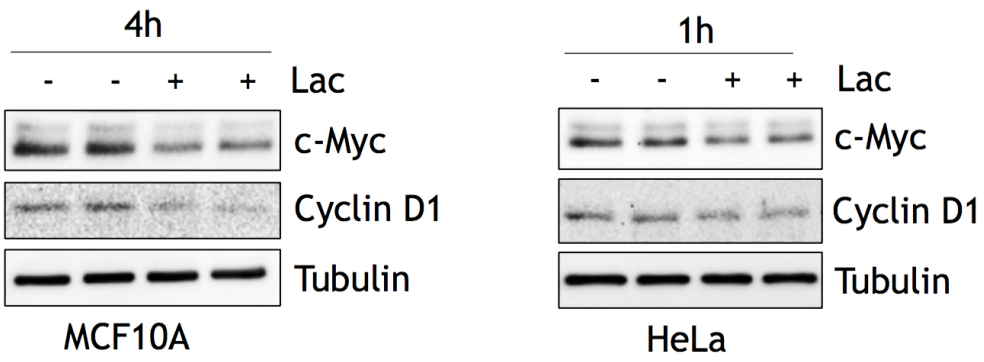

Figure 5-5. **Lactate acutely decreases c-Myc and cyclin D1 protein levels.** Immunoblots showing c-Myc and cyclin D1 levels after cell treatment with 25 mM lactate. Left, MCF10A cells, 4 hour treatment; right, HeLa cells, 1 hour treatment.

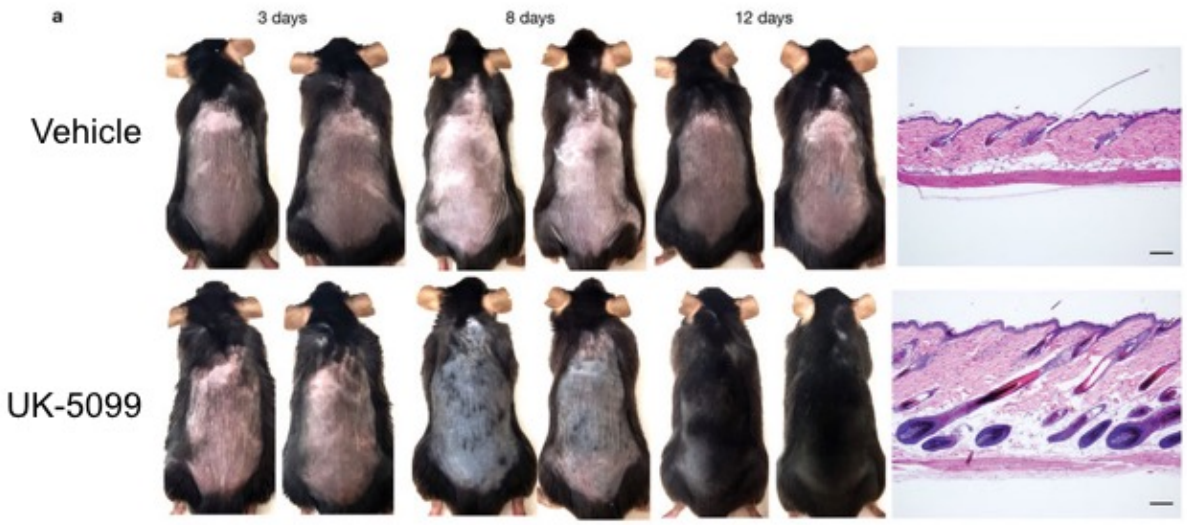

Figure 5-6. **Lactate dehydrogenase activity drives hair follicle stem cell activation.** Stimulation of lactate dehydrogenase activity with UK-5099, a small molecule that inhibit pyruvate entry into mitochondria, promotes hair follicle stem cell activation and hair growth. Figure from Flores et al. 2017.

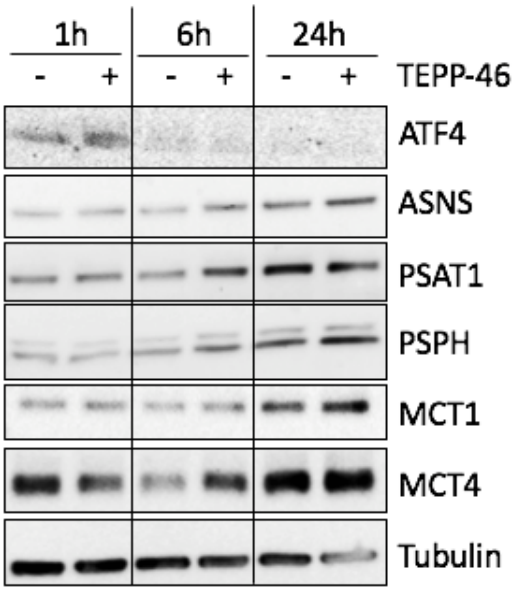

Figure 5-7. **PKM2 activation results in increased ATF4 activity**. Immunoblot showing levels of ATF4, ATF4 target genes (ASNS, PSAT1, and PSPH), and lactate transporters (MCT1 and MCT4) after HeLa cell treatment with PKM2 activator TEPP-46 (10 uM) for 1, 6, or 24 hours.

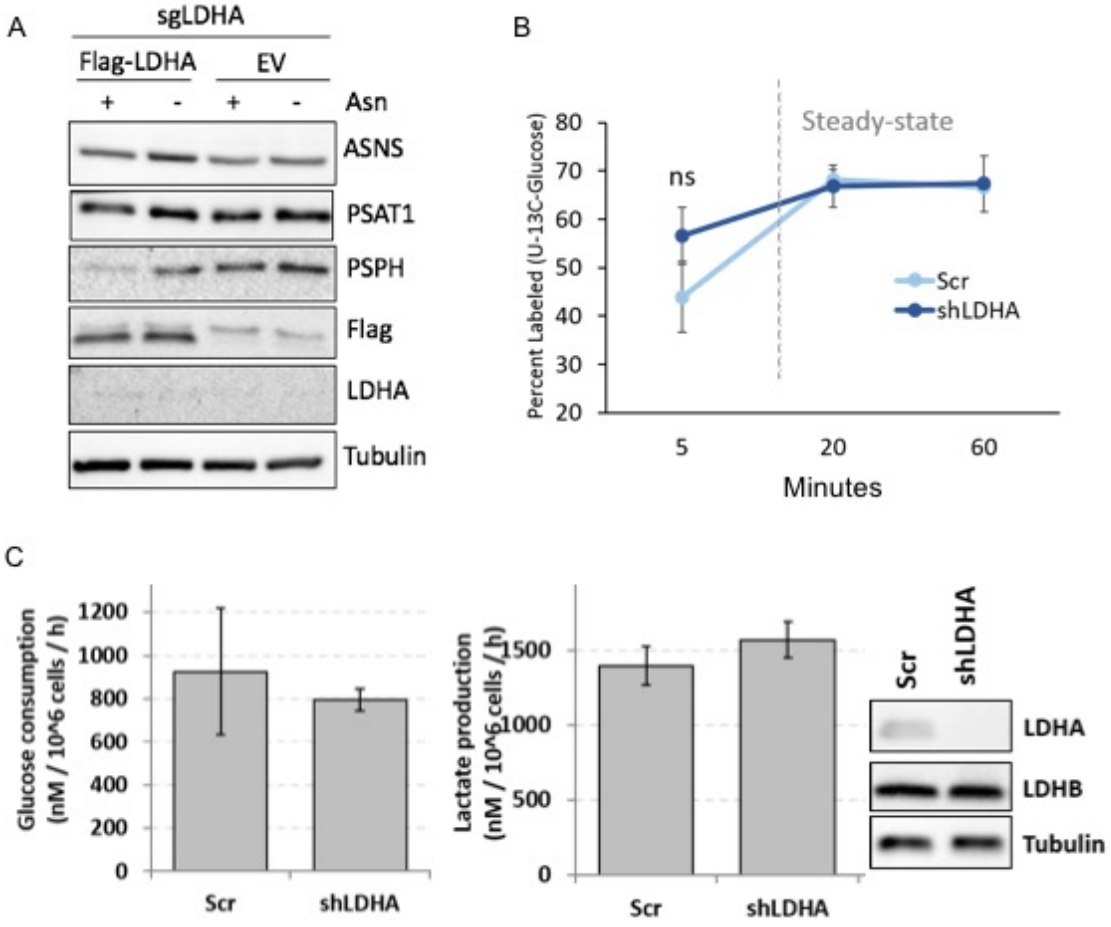

Figure 5-8. **Global LDHA reduction does not impact lactate production. (A)** LDHA knockout HeLa cells (sgLDHA) were rescued with flag-LDHA or empty vector (EV). In contrast to cells expressing flag-LDHA, asparagine depletion does not result in ATF4 activation in LDHA-null cells, as indicated by expression of ASNS, PSAT1, and PSPH. **(B)** The kinetics of glucose conversion to lactate, as indicated by lactate labeling by U-^{13}C-glucose prior to steady state labeling, is unaltered with expression of LDHA shRNA in HeLa cells. Relative lactate levels were also unchanged (data not shown). **(C)** HeLa cell expression of LDHA shRNA does not alter glucose consumption or lactate export rates.

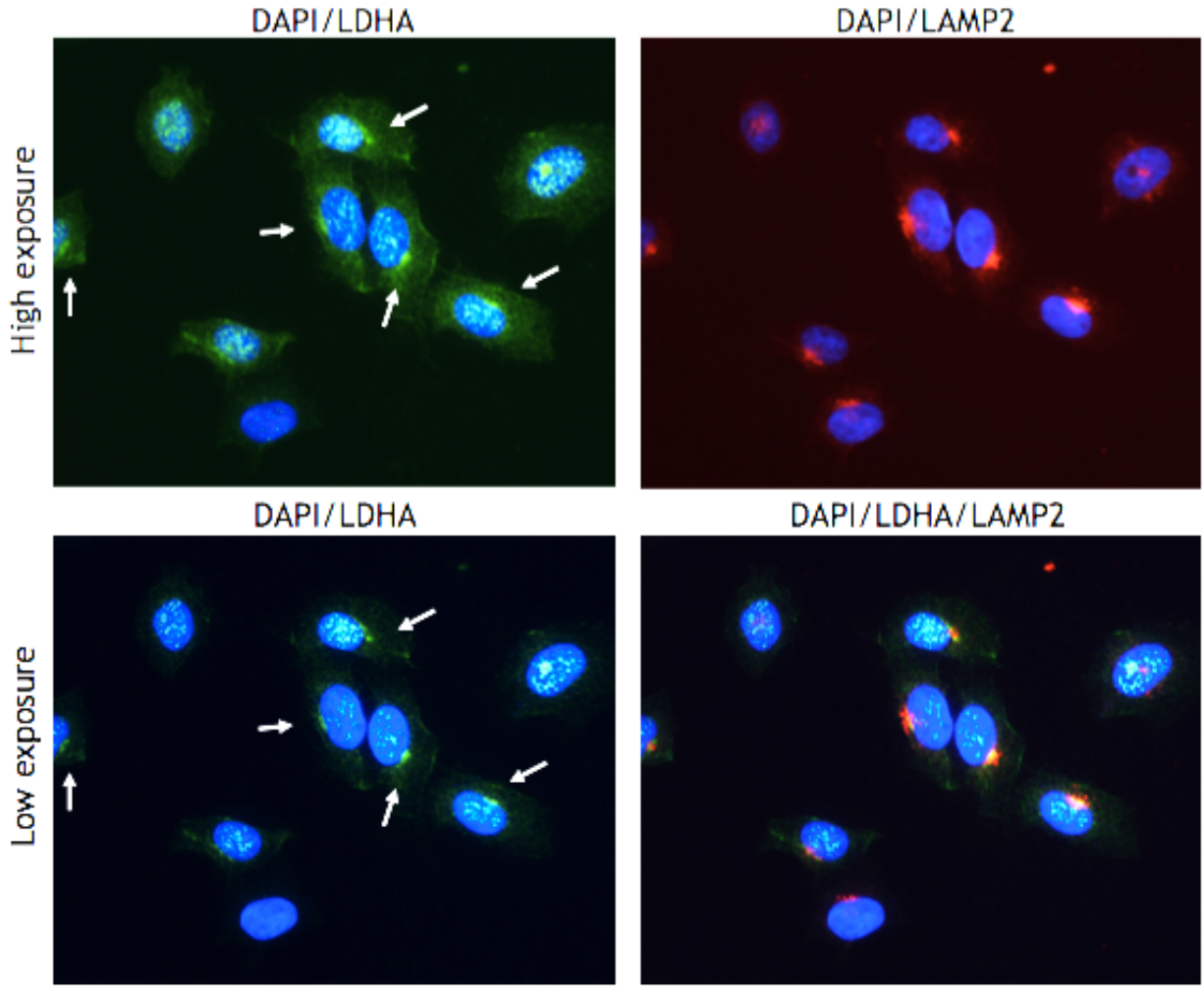

Figure 5-9. **Subcellular LDHA puncta colocalize with lysosome marker.** Immunofluorescence showing overlap between LDHA (green) and DAPI staining (left) or overlap between LDHA and lysosomal marker LAMP2 (red) (right) at long and short exposure times.

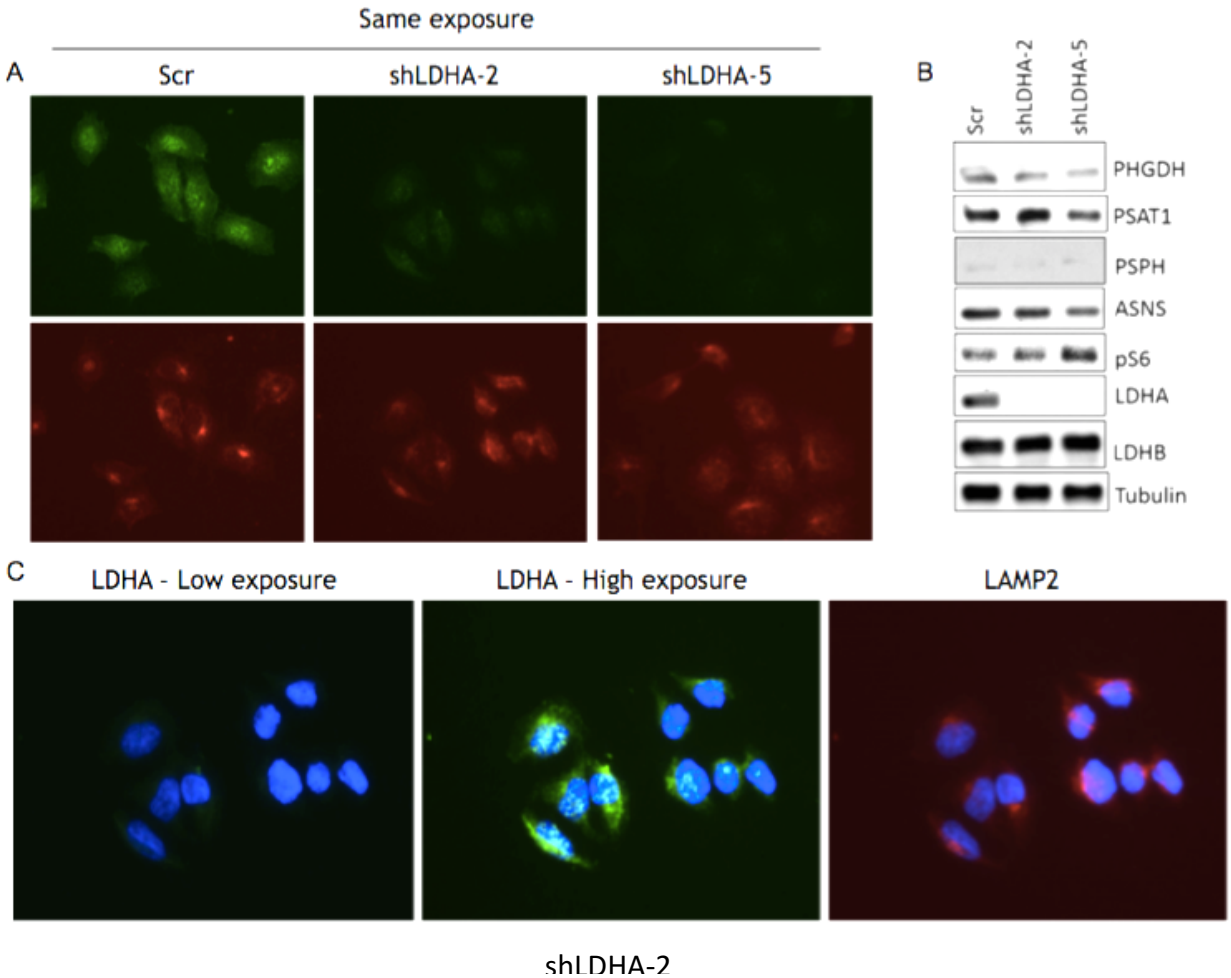

Figure 5-10. **Residual LDHA upon LDHA knockdown colocalizes with lysosome marker.** **(A-B)** Expression of shLDHA-2 and shLDHA-5 shRNA in HeLa cells results in partial or nearly complete depletion of LDHA, respectively. **(B)** Expression of shLDHA-5, but not expression of shLDHA-2, results in increased mTORC1 activity, as indicated by phosphorylation of S6 (S235/236). **(C)** Immunofluorescence of residual LDHA with expression of shLDHA-2 in HeLa cells at high and low exposure (left and middle panels); lysosome marker LAMP2 (right panel); all staining in overlayed with DAPI stain.

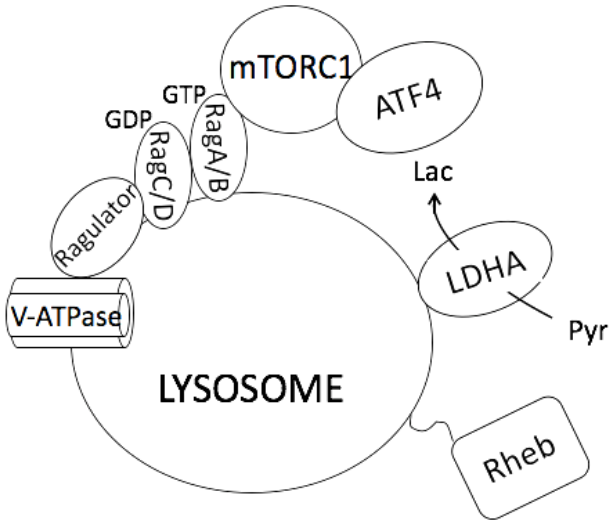

Figure 5-11. **Model depicting lysosome-localized lactate synthesis.** Lysosomal LDHA puncta (Figure 4-7 and 4-8) raise the possibility that a subcellular lactate pool generated at the lysosome is responsible for mTORC1 inhibition.

REFERENCES

1. Lassot I, Segeral E, Berlioz-Torrent C, Durand H, Groussin L, Hai T, Benarous R, Margottin-Goguet F. ATF4 degradation relies on a phosphorylation-dependent interaction with the SCF(betaTrCP) ubiquitin ligase. Mol Cell Biol. 2001;21(6):2192-202. doi: 10.1128/MCB.21.6.2192-2202.2001. PubMed PMID: 11238952; PMCID: PMC86853.

2. Halestrap AP, Meredith D. The SLC16 gene family-from monocarboxylate transporters (MCTs) to aromatic amino acid transporters and beyond. Pflugers Arch. 2004;447(5):619-28. doi: 10.1007/s00424-003-1067-2. PubMed PMID: 12739169.

3. Halestrap AP, Wilson MC. The monocarboxylate transporter family--role and regulation. IUBMB Life. 2012;64(2):109-19. doi: 10.1002/iub.572. PubMed PMID: 22162139.

4. Doherty JR, Yang C, Scott KE, Cameron MD, Fallahi M, Li W, Hall MA, Amelio AL, Mishra JK, Li F, Tortosa M, Genau HM, Rounbehler RJ, Lu Y, Dang CV, Kumar KG, Butler AA, Bannister TD, Hooper AT, Unsal-Kacmaz K, Roush WR, Cleveland JL. Blocking lactate export by inhibiting the Myc target MCT1 Disables glycolysis and glutathione synthesis. Cancer Res. 2014;74(3):908-20. doi: 10.1158/0008-5472.CAN-13-2034. PubMed PMID: 24285728; PMCID: PMC3946415.

5. Sprowl-Tanio S, Habowski AN, Pate KT, McQuade MM, Wang K, Edwards RA, Grun F, Lyou Y, Waterman ML. Lactate/pyruvate transporter MCT-1 is a direct Wnt target that confers sensitivity to 3-bromopyruvate in colon cancer. Cancer Metab. 2016;4:20. doi: 10.1186/s40170-016-0159-3. PubMed PMID: 27729975; PMCID: PMC5046889.

6. Liu Z, Sneve M, Haroldson TA, Smith JP, Drewes LR. Regulation of Monocarboxylic Acid Transporter 1 Trafficking by the Canonical Wnt/beta-Catenin Pathway in Rat Brain Endothelial Cells Requires Cross-talk with Notch Signaling. J Biol Chem. 2016;291(15):8059-69. doi: 10.1074/jbc.M115.710277. PubMed PMID: 26872974; PMCID: PMC4825010.

7. Ou Y, Wang SJ, Jiang L, Zheng B, Gu W. p53 Protein-mediated regulation of phosphoglycerate dehydrogenase (PHGDH) is crucial for the apoptotic response upon serine starvation. J Biol Chem. 2015;290(1):457-66. doi: 10.1074/jbc.M114.616359. PubMed PMID: 25404730; PMCID: PMC4281747.

8. Harris SL, Levine AJ. The p53 pathway: positive and negative feedback loops. Oncogene. 2005;24(17):2899-908. doi: 10.1038/sj.onc.1208615. PubMed PMID: 15838523.

9. Krall AS, Christofk HR. Cell cycle: Division enzyme regulates metabolism. Nature. 2017;546(7658):357-8. doi: 10.1038/nature22504. PubMed PMID: 28607481.

10. Tu BP, Kudlicki A, Rowicka M, McKnight SL. Logic of the yeast metabolic cycle: temporal compartmentalization of cellular processes. Science. 2005;310(5751):1152-8. doi: 10.1126/science.1120499. PubMed PMID: 16254148.

11. Tu BP, McKnight SL. Metabolic cycles as an underlying basis of biological oscillations. Nat Rev Mol Cell Biol. 2006;7(9):696-701. doi: 10.1038/nrm1980. PubMed PMID: 16823381.

12. Chen Z, Odstrcil EA, Tu BP, McKnight SL. Restriction of DNA replication to the reductive phase of the metabolic cycle protects genome integrity. Science. 2007;316(5833):1916-9. doi: 10.1126/science.1140958. PubMed PMID: 17600220.

13. Wang H, Nicolay BN, Chick JM, Gao X, Geng Y, Ren H, Gao H, Yang G, Williams JA, Suski JM, Keibler MA, Sicinska E, Gerdemann U, Haining WN, Roberts TM, Polyak K, Gygi SP, Dyson NJ, Sicinski P. The metabolic function of cyclin D3-CDK6 kinase in cancer cell survival. Nature. 2017;546(7658):426-30. doi: 10.1038/nature22797. PubMed PMID: 28607489; PMCID: PMC5516959.

14. Averous J, Fonseca BD, Proud CG. Regulation of cyclin D1 expression by mTORC1 signaling requires eukaryotic initiation factor 4E-binding protein 1. Oncogene. 2008;27(8):1106-13. doi: 10.1038/sj.onc.1210715. PubMed PMID: 17724476.

15. Dowling RJ, Topisirovic I, Alain T, Bidinosti M, Fonseca BD, Petroulakis E, Wang X, Larsson O, Selvaraj A, Liu Y, Kozma SC, Thomas G, Sonenberg N. mTORC1-mediated cell proliferation, but not cell growth, controlled by the 4E-BPs. Science. 2010;328(5982):1172-6. doi: 10.1126/science.1187532. PubMed PMID: 20508131; PMCID: PMC2893390.

16. Flores A, Schell J, Krall AS, Jelinek D, Miranda M, Grigorian M, Braas D, White AC, Zhou JL, Graham NA, Graeber T, Seth P, Evseenko D, Coller HA, Rutter J, Christofk HR, Lowry WE. Lactate dehydrogenase activity drives hair follicle stem cell activation. Nat Cell Biol. 2017;19(9):1017-26. doi: 10.1038/ncb3575. PubMed PMID: 28812580; PMCID: PMC5657543.

17. Schell JC, Olson KA, Jiang L, Hawkins AJ, Van Vranken JG, Xie J, Egnatchik RA, Earl EG, DeBerardinis RJ, Rutter J. A role for the mitochondrial pyruvate carrier as a repressor of the Warburg effect and colon cancer cell growth. Mol Cell. 2014;56(3):400-13. doi: 10.1016/j.molcel.2014.09.026. PubMed PMID: 25458841; PMCID: PMC4268416.

18. Vacanti NM, Divakaruni AS, Green CR, Parker SJ, Henry RR, Ciaraldi TP, Murphy AN, Metallo CM. Regulation of substrate utilization by the mitochondrial pyruvate carrier. Mol Cell. 2014;56(3):425-35. doi: 10.1016/j.molcel.2014.09.024. PubMed PMID: 25458843; PMCID: PMC4267523.

19. Lowry WE, Blanpain C, Nowak JA, Guasch G, Lewis L, Fuchs E. Defining the impact of beta-catenin/Tcf transactivation on epithelial stem cells. Genes Dev. 2005;19(13):1596-611. doi: 10.1101/gad.1324905. PubMed PMID: 15961525; PMCID: PMC1172065.

20. Huelsken J, Vogel R, Erdmann B, Cotsarelis G, Birchmeier W. beta-Catenin controls hair follicle morphogenesis and stem cell differentiation in the skin. Cell. 2001;105(4):533-45. PubMed PMID: 11371349.

21. Lo Celso C, Prowse DM, Watt FM. Transient activation of beta-catenin signalling in adult mouse epidermis is sufficient to induce new hair follicles but continuous activation is required to maintain hair follicle tumours. Development. 2004;131(8):1787-99. doi: 10.1242/dev.01052. PubMed PMID: 15084463.

22. Hsu YC, Pasolli HA, Fuchs E. Dynamics between stem cells, niche, and progeny in the hair follicle. Cell. 2011;144(1):92-105. doi: 10.1016/j.cell.2010.11.049. PubMed PMID: 21215372; PMCID: PMC3050564.

23. Paus R, Ito N, Takigawa M, Ito T. The hair follicle and immune privilege. J Investig Dermatol Symp Proc. 2003;8(2):188-94. doi: 10.1046/j.1087-0024.2003.00807.x. PubMed PMID: 14582671.

24. Ali N, Zirak B, Rodriguez RS, Pauli ML, Truong HA, Lai K, Ahn R, Corbin K, Lowe MM, Scharschmidt TC, Taravati K, Tan MR, Ricardo-Gonzalez RR, Nosbaum A, Bertolini M, Liao W, Nestle FO, Paus R, Cotsarelis G, Abbas AK, Rosenblum MD. Regulatory T Cells in Skin Facilitate Epithelial Stem Cell Differentiation. Cell. 2017;169(6):1119-29 e11. doi: 10.1016/j.cell.2017.05.002. PubMed PMID: 28552347; PMCID: PMC5504703.

25. Fischer K, Hoffmann P, Voelkl S, Meidenbauer N, Ammer J, Edinger M, Gottfried E, Schwarz S, Rothe G, Hoves S, Renner K, Timischl B, Mackensen A, Kunz-Schughart L, Andreesen R, Krause SW, Kreutz M. Inhibitory effect of tumor cell-derived lactic acid on human T cells. Blood. 2007;109(9):3812-9. doi: 10.1182/blood-2006-07-035972. PubMed PMID: 17255361.

26. Seth P, Csizmadia E, Hedblom A, Vuerich M, Xie H, Li M, Longhi MS, Wegiel B. Deletion of Lactate Dehydrogenase-A in Myeloid Cells Triggers Antitumor Immunity. Cancer Res. 2017;77(13):3632-43. doi: 10.1158/0008-5472.CAN-16-2938. PubMed PMID: 28446465; PMCID: PMC5505499.

27. Guile SD, Bantick JR, Cheshire DR, Cooper ME, Davis AM, Donald DK, Evans R, Eyssade C, Ferguson DD, Hill S, Hutchinson R, Ingall AH, Kingston LP, Martin I, Martin BP, Mohammed RT, Murray C, Perry MW, Reynolds RH, Thorne PV, Wilkinson DJ, Withnall J. Potent blockers of the monocarboxylate transporter MCT1: novel immunomodulatory compounds. Bioorg Med Chem Lett. 2006;16(8):2260-5. doi: 10.1016/j.bmcl.2006.01.024. PubMed PMID: 16455256.

28. Murray CM, Hutchinson R, Bantick JR, Belfield GP, Benjamin AD, Brazma D, Bundick RV, Cook ID, Craggs RI, Edwards S, Evans LR, Harrison R, Holness E, Jackson AP, Jackson CG, Kingston LP, Perry MW, Ross AR, Rugman PA, Sidhu SS, Sullivan M, Taylor-Fishwick DA, Walker PC, Whitehead YM, Wilkinson DJ, Wright A, Donald DK. Monocarboxylate transporter MCT1 is a target for immunosuppression. Nat Chem Biol. 2005;1(7):371-6. PubMed PMID: 16370372.

29. Colman RJ, Anderson RM, Johnson SC, Kastman EK, Kosmatka KJ, Beasley TM, Allison DB, Cruzen C, Simmons HA, Kemnitz JW, Weindruch R. Caloric restriction delays disease onset and mortality in rhesus monkeys. Science. 2009;325(5937):201-4. doi: 10.1126/science.1173635. PubMed PMID: 19590001; PMCID: PMC2812811.

30. Mattison JA, Roth GS, Beasley TM, Tilmont EM, Handy AM, Herbert RL, Longo DL, Allison DB, Young JE, Bryant M, Barnard D, Ward WF, Qi W, Ingram DK, de Cabo R. Impact of caloric restriction on health and survival in rhesus monkeys from the NIA study. Nature. 2012;489(7415):318-21. doi: 10.1038/nature11432. PubMed PMID: 22932268; PMCID: PMC3832985.

31. Chin RM, Fu X, Pai MY, Vergnes L, Hwang H, Deng G, Diep S, Lomenick B, Meli VS, Monsalve GC, Hu E, Whelan SA, Wang JX, Jung G, Solis GM, Fazlollahi F, Kaweeteerawat C, Quach A, Nili M, Krall AS, Godwin HA, Chang HR, Faull KF, Guo F, Jiang M, Trauger SA, Saghatelian A, Braas D, Christofk HR, Clarke CF, Teitell MA, Petrascheck M, Reue K, Jung ME, Frand AR, Huang J. The metabolite alpha-ketoglutarate extends lifespan by inhibiting ATP synthase and TOR. Nature. 2014;510(7505):397-401. doi: 10.1038/nature13264. PubMed PMID: 24828042; PMCID: 4263271.

32. Fu X, Chin RM, Vergnes L, Hwang H, Deng G, Xing Y, Pai MY, Li S, Ta L, Fazlollahi F, Chen C, Prins RM, Teitell MA, Nathanson DA, Lai A, Faull KF, Jiang M, Clarke SG, Cloughesy TF, Graeber TG, Braas D, Christofk HR, Jung ME, Reue K, Huang J. 2-Hydroxyglutarate Inhibits ATP Synthase and mTOR Signaling. Cell Metab. 2015;22(3):508-15. doi: 10.1016/j.cmet.2015.06.009. PubMed PMID: 26190651; PMCID: PMC4663076.

33. Lucanic M, Held JM, Vantipalli MC, Klang IM, Graham JB, Gibson BW, Lithgow GJ, Gill MS. N-acylethanolamine signalling mediates the effect of diet on lifespan in Caenorhabditis elegans. Nature. 2011;473(7346):226-9. doi: 10.1038/nature10007. PubMed PMID: 21562563; PMCID: PMC3093655.

34. Williams DS, Cash A, Hamadani L, Diemer T. Oxaloacetate supplementation increases lifespan in Caenorhabditis elegans through an AMPK/FOXO-dependent pathway. Aging Cell. 2009;8(6):765-8. doi: 10.1111/j.1474-9726.2009.00527.x. PubMed PMID: 19793063; PMCID: PMC2988682.

35. Hansen M, Taubert S, Crawford D, Libina N, Lee SJ, Kenyon C. Lifespan extension by conditions that inhibit translation in Caenorhabditis elegans. Aging Cell. 2007;6(1):95-110. doi: 10.1111/j.1474-9726.2006.00267.x. PubMed PMID: 17266679.

36. Stanfel MN, Shamieh LS, Kaeberlein M, Kennedy BK. The TOR pathway comes of age. Biochim Biophys Acta. 2009;1790(10):1067-74. doi: 10.1016/j.bbagen.2009.06.007. PubMed PMID: 19539012; PMCID: PMC3981532.

37. Chung HY, Sung B, Jung KJ, Zou Y, Yu BP. The molecular inflammatory process in aging. Antioxid Redox Signal. 2006;8(3-4):572-81. doi: 10.1089/ars.2006.8.572. PubMed PMID: 16677101.

38. Chung HY, Cesari M, Anton S, Marzetti E, Giovannini S, Seo AY, Carter C, Yu BP, Leeuwenburgh C. Molecular inflammation: underpinnings of aging and age-related diseases. Ageing Res Rev. 2009;8(1):18-30. doi: 10.1016/j.arr.2008.07.002. PubMed PMID: 18692159; PMCID: PMC3782993.

39. Salminen A, Huuskonen J, Ojala J, Kauppinen A, Kaarniranta K, Suuronen T. Activation of innate immunity system during aging: NF-kB signaling is the molecular culprit of inflamm-aging. Ageing Res Rev. 2008;7(2):83-105. doi: 10.1016/j.arr.2007.09.002. PubMed PMID: 17964225.

40. Mazurek S, Boschek CB, Hugo F, Eigenbrodt E. Pyruvate kinase type M2 and its role in tumor growth and spreading. Semin Cancer Biol. 2005;15(4):300-8. doi: 10.1016/j.semcancer.2005.04.009. PubMed PMID: 15908230.

41. Christofk HR, Vander Heiden MG, Harris MH, Ramanathan A, Gerszten RE, Wei R, Fleming MD, Schreiber SL, Cantley LC. The M2 splice isoform of pyruvate kinase is important for cancer metabolism and tumour growth. Nature. 2008;452(7184):230-3. doi: 10.1038/nature06734. PubMed PMID: 18337823.

42. Campanella ME, Chu H, Low PS. Assembly and regulation of a glycolytic enzyme complex on the human erythrocyte membrane. Proc Natl Acad Sci U S A. 2005;102(7):2402-7. doi: 10.1073/pnas.0409741102. PubMed PMID: 15701694; PMCID: PMC549020.

43. Dhar-Chowdhury P, Harrell MD, Han SY, Jankowska D, Parachuru L, Morrissey A, Srivastava S, Liu W, Malester B, Yoshida H, Coetzee WA. The glycolytic enzymes, glyceraldehyde-3-phosphate dehydrogenase, triose-phosphate isomerase, and pyruvate kinase are components of the K(ATP) channel macromolecular complex and regulate its function. J Biol Chem. 2005;280(46):38464-70. doi: 10.1074/jbc.M508744200. PubMed PMID: 16170200; PMCID: PMC4667781.

44. Zoncu R, Bar-Peled L, Efeyan A, Wang S, Sancak Y, Sabatini DM. mTORC1 senses lysosomal amino acids through an inside-out mechanism that requires the vacuolar H(+)-ATPase. Science. 2011;334(6056):678-83. doi: 10.1126/science.1207056. PubMed PMID: 22053050; PMCID: PMC3211112.

45. San Martin A, Ceballo S, Ruminot I, Lerchundi R, Frommer WB, Barros LF. A genetically encoded FRET lactate sensor and its use to detect the Warburg effect in single cancer cells. PLoS One. 2013;8(2):e57712. doi: 10.1371/journal.pone.0057712. PubMed PMID: 23469056; PMCID: PMC3582500.